[redacted]

NASA Conference Publication 2208

Advanced Aerodynamics

STAR (1+6)

Selected NASA Research

Presentations made at the Fifth Annual Status Review of the NASA Aircraft Energy Efficiency (ACEE) Energy Efficient Transport Program held at Dryden Flight Research Center, Edwards, California September 14-15, 1981

NASA

NASA Conference Publication 2208

Advanced Aerodynamics

Selected NASA Research

Presentations made at the Fifth Annual Status Review
of the NASA Aircraft Energy Efficiency (ACEE)
Energy Efficient Transport Program held at
Dryden Flight Research Center, Edwards, California
September 14-15, 1981

NASA
National Aeronautics
and Space Administration

**Scientific and Technical
Information Branch**

1981

FOREWORD

The fifth annual status review of the NASA Aircraft Energy Efficiency (ACEE) Energy Efficient Transport (EET) Program was held September 14-15, 1981, at the NASA Dryden Flight Research Center in Edwards, California. The conference included comprehensive reviews of major contracts by the ACEE EET contractors: Boeing Commercial Airplane Company, Douglas Aircraft Company, and Lockheed-California Company. In addition, a session included selected papers describing some of NASA's in-house sponsored research in advanced aerodynamics. The papers from this latter session are collected in this NASA Conference Publication. The papers from two similar sessions at last year's status review are published in NASA CP-2172.

Use of trade names or names of manufacturers in this report does not constitute an official endorsement of such products or manufacturers, either expressed or implied, by the National Aeronautics and Space Administration.

Dennis W. Bartlett
Session Chairman
Langley Research Center

CONTENTS

D1

N84 27661

ACOUSTIC FLIGHT TESTING OF ADVANCED DESIGN PROPELLERS ON A JETSTAR AIRCRAFT

Paul Lasagna and Karen Mackall
NASA Dryden Flight Research Center
Edwards, CA

ABSTRACT

Studies have established that advanced turboprop-powered aircraft have the potential to reduce fuel consumption by 15 to 30 percent as compared with an equivalent technology turbofan-powered aircraft. An important obstacle to the use of advanced design propellers is the cabin noise generated at Mach numbers up to .8 and at altitudes up to 35 000 feet.

As part of the NASA Aircraft Energy Efficiency Program, a joint Dryden Flight Research Center/Lewis Research Center research effort is being conducted to investigate the near-field acoustic characteristics on a series of advanced design propellers. Currently, Dryden Flight Research Center is flight testing a series of propellers on a JetStar airplane. The propellers used in the flight test were previously tested in wind tunnels at the Lewis Research Center.

The test propeller is mounted on a pylon above the fuselage. The propellers are two feet in diameter with the number of blades varying from two to ten and aerodynamic blade sweep angles varying from 0° to 34°. The propeller is driven by an air turbine drive motor, which is supplied with bleed air from the JetStar engines.

Instrumentation was installed to provide near-field acoustic data as well as propeller performance data. Twenty-eight microphones are installed on the fuselage below the propeller. The SR-3 propeller has been flown on six flights.

Data are presented showing the narrow band spectra, acoustic wave form, and acoustic contours on the fuselage surface. Additional flights with the SR-3 propeller and other advanced propellers are planned in the future.

Advanced Design Propellers Acoustic Flight Tests

Dryden Flight Research Center is flight testing a series of advanced design propellers on a JetStar airplane. The objective of the tests is to determine the near-field acoustic characteristics of the propellers at Mach numbers up to 0.8 and altitudes up to 30 000 feet. These propellers have been previously tested in the 8 x 6 foot wind tunnel at NASA Lewis.

Propeller Air Drive System

The advanced propellers are driven by an air turbine drive system. Low pressure (40 to 50 lb/in^2) bleed air from the four JetStar engines is collected by a manifold, fed to a five-inch diameter duct, and routed to the air drive motor. The quick-acting normally closed shut-off valve aft of the cabin pressure bulkhead is installed to isolate bleed air from the cabin in event of a duct rupture and to shut off air to the air drive motor if overspeed of the propeller occurs. The speed control valve in the cabin is an electrically operated valve which is used to control the rotational speed of the air drive motor.

PROPELLER AIR DRIVE SYSTEM INSTALLED ON THE NASA JETSTAR AIRPLANE

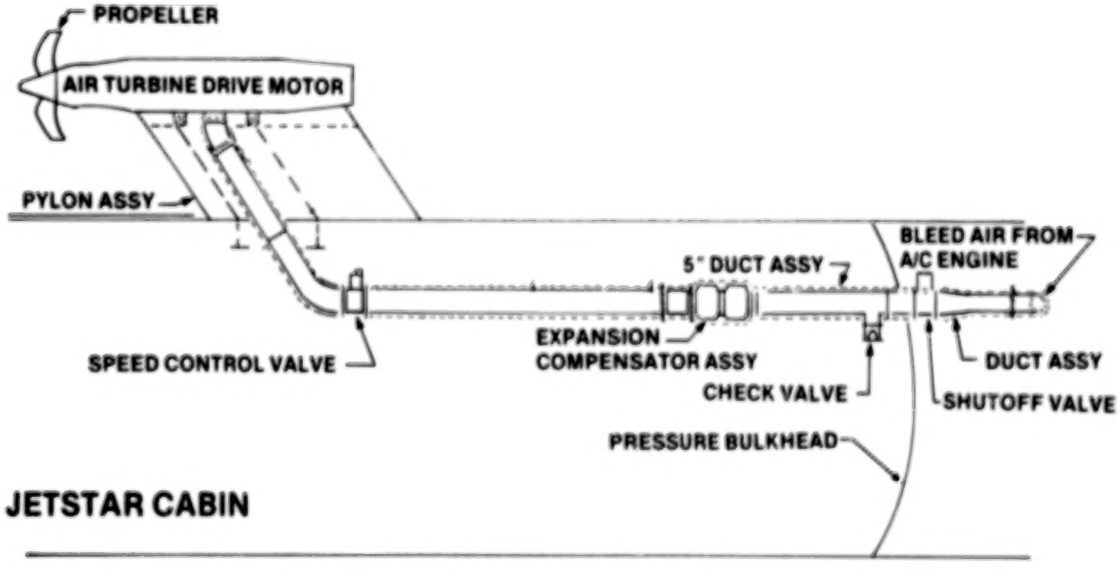

Air Turbine Drive Motor

The scale model of the advanced propellers tested on the JetStar airplane are driven by an air turbine drive motor. It is a three-stage motor which produces 210 shaft horsepower at an altitude of 30 000 feet and at RPM's up to 8 200. The motor has a disc type brake to be used only in an emergency. The slip-ring assembly is used when monitoring propeller blade strain-gage outputs. Cooling air, which is humidified, is supplied to the slip-ring assembly to increase the longevity of the brush surfaces.

AIR TURBINE DRIVE MOTOR

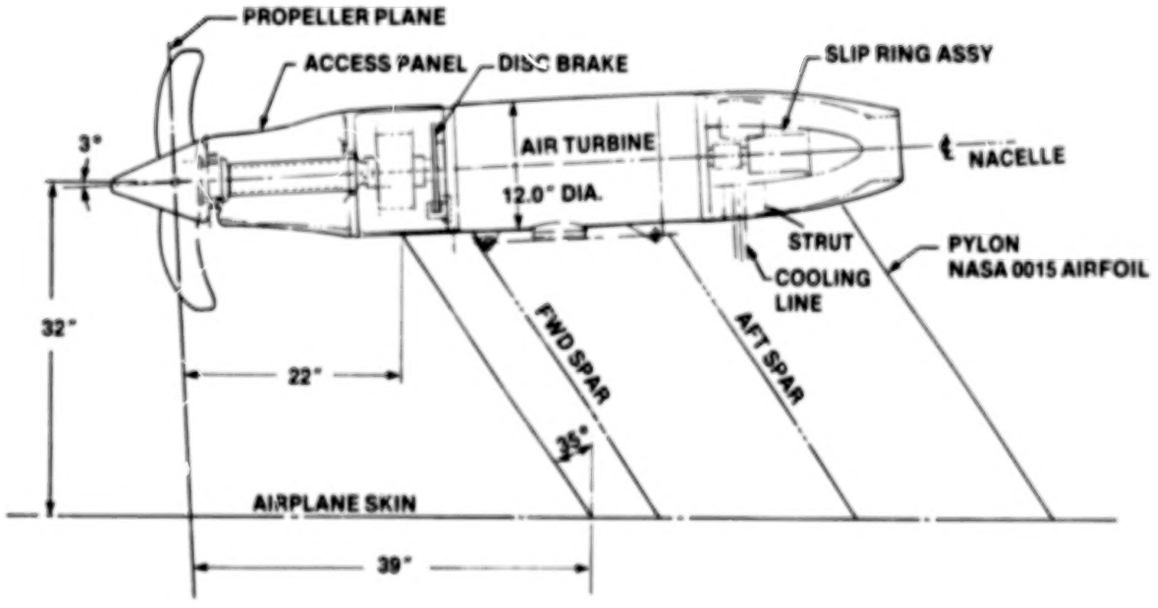

Advanced Propeller Installation on the JetStar

An eight-bladed advanced propeller, designated SR-3, is currently being flight tested at Dryden. The propeller has a two-foot diameter and an aerodynamic blade sweep angle of 34 degrees.

During the initial flight period of this propeller, strain gage signals were monitored to ensure that the vibratory stress limits of the blades were not exceeded. At the conclusions of these blade-stress flutter clearance flights, the strain gages were removed and flights for acoustic data collection were flown.

In the figure below, the strain gages and some of the flush mounted microphones are identified.

Propeller Flow Field Survey

The flow field at the propeller location was surveyed with the probes shown below. Flow angularity vanes with total pressure probes in the tips were mounted with the upper one on the propeller centerline location and the lower one at the tip of the propeller location. A static pressure orifice was located on the fuselage just below the propeller plane.

The flow angularity measurements confirmed that the -3^0 incidence of the propeller with respect to the fuselage is correct, and that no large flow angularity gradients exist. The local Mach number is within 0.05 of the free-stream Mach number.

Plans are being developed to measure the boundary-layer characteristics on the fuselage under the propeller. This may be important for detailed analysis of the acoustic results.

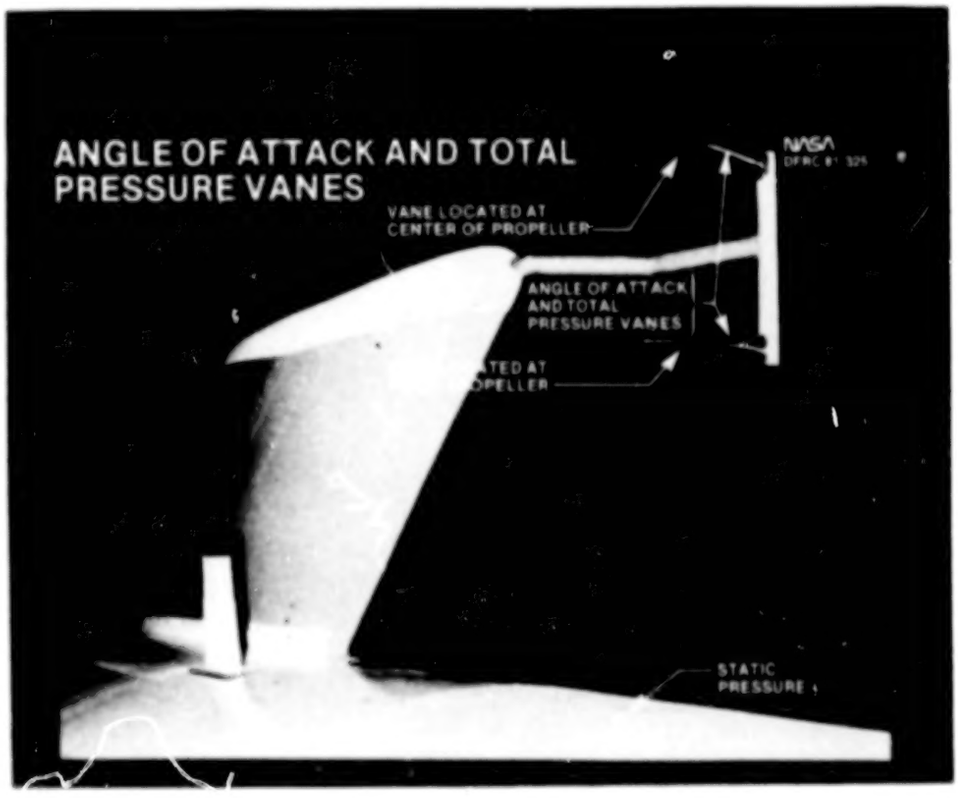

Spectral Analysis Facility

NASA Dryden Flight Research Center has a narrow-band 12-channel spectral analysis system capable of simultaneously acquiring, processing, and time-averaging acoustical and vibration data. To ensure quality data, the system is used for postflight analysis of acoustical data and noise trends during the previous flight before proceeding to the next flight. The analyzed data can be stored on a mangnetic disk for later processing.

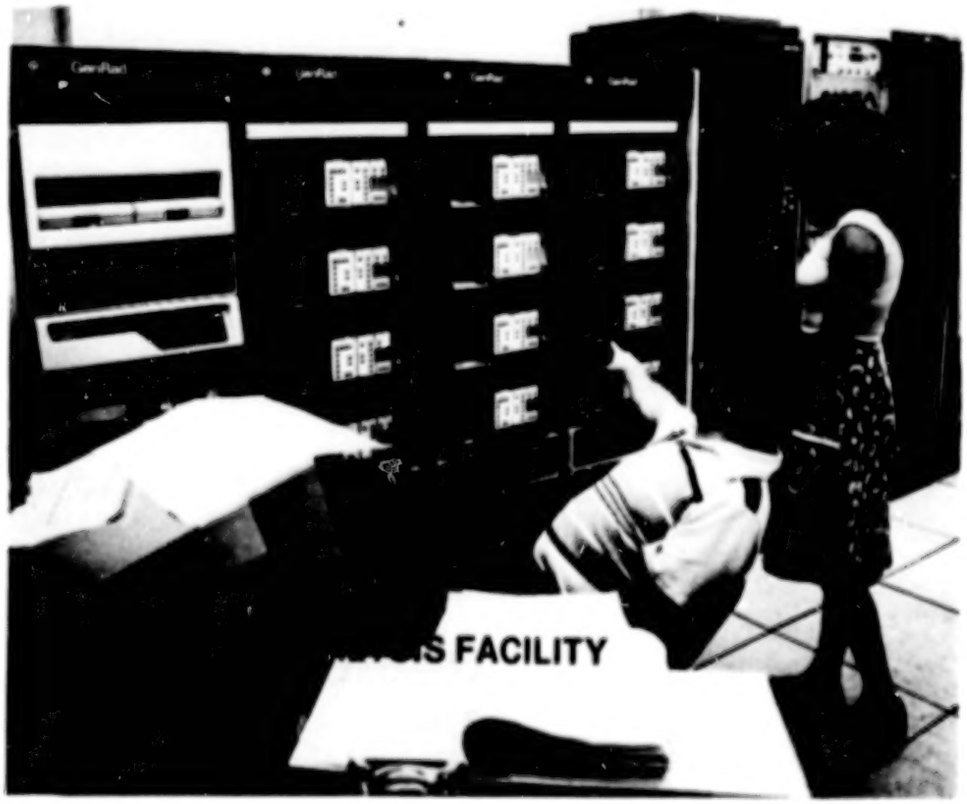

Acoustic Instrumentation

The near-field acoustic characteristics are being measured by an array of 28 microphones flush mounted to the airplane's skin in the area near the propeller. The microphones are 1/8-inch condenser type microphones and are vented to the atmosphere. Signal conditioning amplifiers that are used in conjunction with the microphones enable an operator onboard the airplane to adjust the microphone signals to optimum recording level. Frequency response of the microphone systems including the tape recorder and amplifiers, is flat to 20 000 hertz.

MICROPHONE ARRAY FOR NEAR-FIELD ACOUSTIC SURVEY OF ADVANCED DESIGN PROPELLERS ON THE JETSTAR

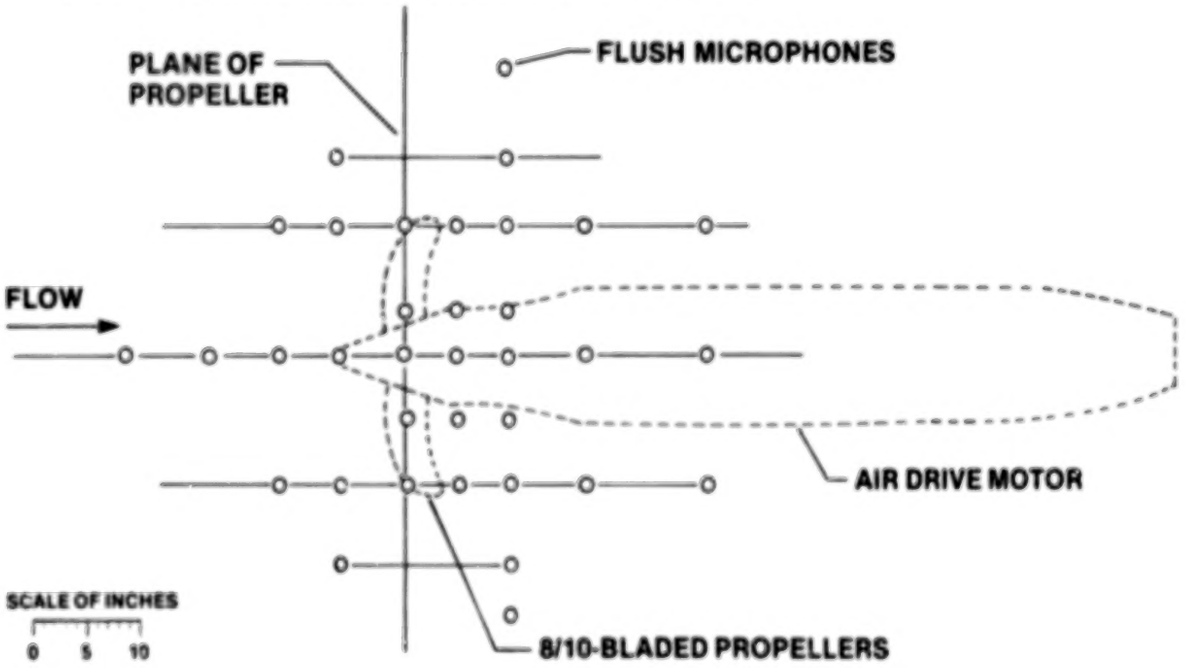

Acoustic Results From SR-3 Propeller

In-flight acoustic measurements were obtained on the SR-3 propeller. Preliminary data are shown for an airplane Mach number of 0.802 and an altitude of 29 130 feet. The propeller blade angle was set at 59 degrees (as referenced to the 75 percent propeller radius line). The propeller helical Mach number is 1.15 at 7750 revolutions per minute.

The maximum sound pressure level of 139 dB was measured at the microphone located 5 inches aft of the propeller plane. Baseline data flown without the propeller is well below the peak blade-passage frequencies.

The blade-passage-frequency sound-pressure-level contours on the JetStar fuselage shows the sound pressure level decreases rapidly forward of the propeller plane of rotation and decreases slowly aft of the plane of rotation. Levels to the side of the propeller gradually decrease.

PRELIMINARY SR3 ACOUSTIC RESULTS

M = .807, ALT = 29130 FT, RPM = 7750
HELICAL TIP MACH NUMBER = 1.15

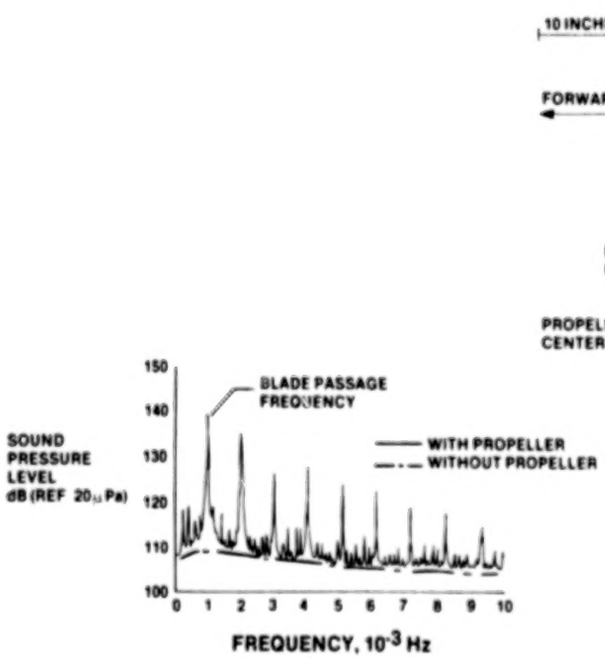

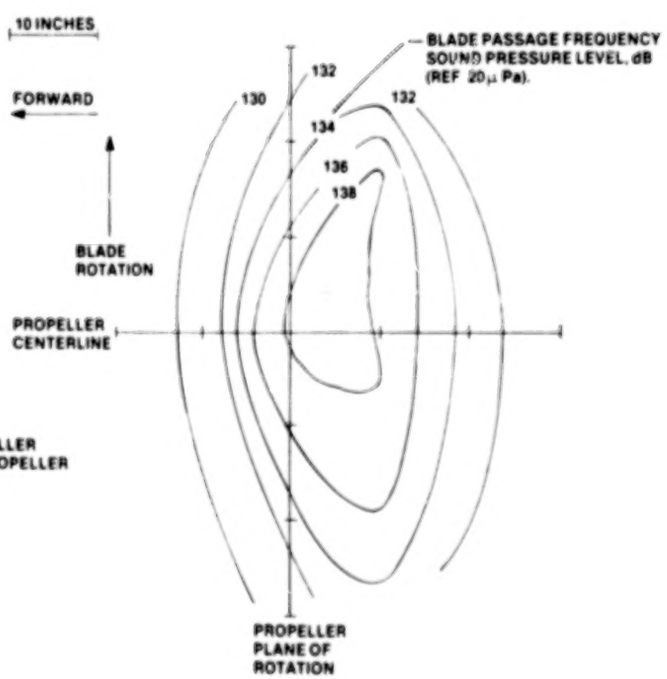

Future Plans For JetStar Tests

During the early fall of 1981, the acoustic tests on the SR-3 propeller will be completed. The ten-bladed SR-6 propeller will then be tested up to the end of 1981. In early 1982, it is planned to test SR-2, an eight-bladed propeller with unswept blades. Following that test, it is planned to do further testing on SR-3, both in the eight-bladed configuration, and in a 2-bladed configuration. It is also planned to make some additional flow-field measurements. The fuselage boundary-layer characteristics will be surveyed and the local Mach number at the propeller location will be more accurately determined.

FUTURE PLANS FOR JETSTAR TESTS

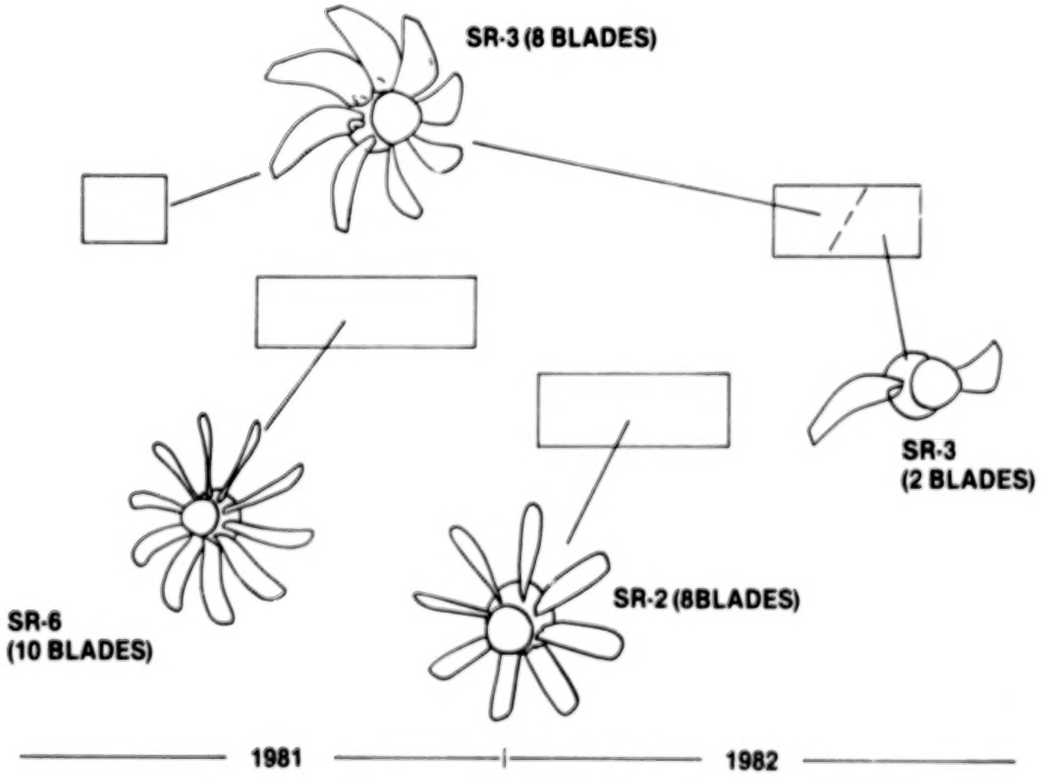

F-111 TACT NATURAL LAMINAR FLOW GLOVE FLIGHT RESULTS

Lawrence C. Montoya
Louis L. Steers
David Christopher
Bianca Trujillo
NASA Dryden Flight Research Center

ABSTRACT

In the early 1970's, the OPEC oil embargo resulted in a sharp esculation in the price of fuel. This in turn led to major concerns about aircraft fuel consumption. In response to this situation the National Aeronautics and Space Administration initiated a multiphased program to develop technology for more energy efficient transport aircraft. This program, identified as the Aircraft Energy Efficiency Program (ACEE), included within its scope laminar flow.

Improvements in cruise efficiency on the order of 15 - 40% can be obtained by increasing the extent of laminar flow over lifting surfaces. Two methods of achieving laminar flow are being considered, natural laminar flow and laminar flow control. Natural laminar flow (NLF) relies primarily on airfoil shape while laminar flow control involves boundary-layer suction or blowing with mechanical devices.

Previous flight tests have been conducted using the laminar flow concept. Limitations of these previous tests were low Reynolds number, unswept wings, and boundary-layer suction through slots in the wing surface. To obtain data for NLF at high Mach numbers and Reynolds numbers, a joint Dryden Flight Research Center (DFRC)/Langley Research Center (LaRC) effort was initiated under NASA's Energy Efficient Transport element of the ACEE program. The objective of the experiment was to evaluate the extent of natural laminar flow that could be achieved with consistency in a real flight environment at chord Reynolds numbers in the range of 30×10^6.

The experiment consisted of 19 flights conducted on the F-111 TACT airplane having a NLF airfoil glove section. The section consisted of a supercritical airfoil providing favorable pressure gradients over extensive portions of the upper and lower surfaces of the wing. Boundary-layer measurements were obtained over a range of wing-leading-edge sweep angles at Mach numbers from 0.80 to 0.85. Data were obtained for natural transition and for a range of forced transition locations over the test airfoil.

Prior to modifying the F-111 TACT airplane for the flight experiment, supporting wind-tunnel tests were conducted on a 1/24-scale model in the LaRC 8-Foot Transonic Pressure Tunnel. These model tests were conducted to assess the stability and control characteristics of the configuration

as modified for the NLF experiment. These tests also included pressure measurements at wind-tunnel Reynolds numbers and determined the wing glove fairing geometry for the flight article.

This paper will present the preliminary pressure distribution and boundary-layer analysis of the flight data. The analysis indicated that significant amounts of laminar flow were achieved in flight.

EXPERIMENT OBJECTIVES

The objective of the F-111 TACT NLF glove experiment was to determine the extent of laminar flow achievable at flight Reynolds numbers of 25 to 30 million using an airfoil section designed to provide the favorable pressure gradients. The extent of laminar flow was derived by pressure distribution and boundary-layer measurements augmented by "oil flow" photographs. These measurement techniques were applied to the "clean" natural-transition condition as well as a range of forced transition locations for a range of leading-edge sweeps and Mach numbers from 0.80 to 0.85.

GLOVE CHARACTERISTICS

The NLF experiment was conducted on the F-111 TACT airplane. The NLF section consisted of a supercritical airfoil designed to provide favorable pressure gradients over 65% of the upper surface and 50% of the lower surface. The wing glove fairing geometry for the test article, as well as pressure measurements and stability and control characteristics, were determined by the use of a 1/24-scale model within the LaRC 8 foot wind-tunnel. The glove section was designed to provide a near-optimum pressure distribution at a free stream Mach number of 0.82 for a wing-leading-edge sweep angle of 10^{o}.

COMPARISON OF NLF AND TACT AIRFOIL SPAN STATION 251

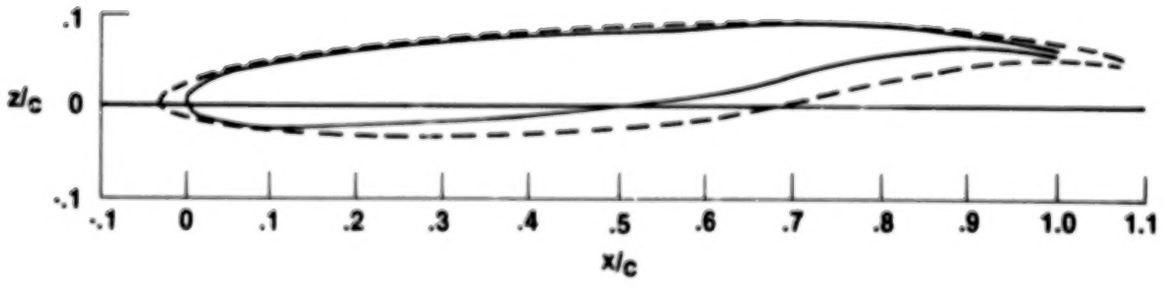

INSTRUMENTATION

The NLF glove sections were fitted on each wing of the F-111 tact airplane. The right wing glove section was fully instrumented, and the left wing glove section was added for symmetry. The test section had a span of 1.829 m with a test chord of 3.057 m. The edges of the test section were faired to reduce the effects of the TACT wing. A row of upper- and lower-surface pressure orifices were located at midspan of the glove. The upper-surface row consisted of 15 orifice locations and the lower-surface row consisted of 11 orifice locations. Boundary-layer rakes were located at 90% of the chord for the first 17 flights and at 60% chord for the last two. These boundary-layer rakes were 10.2 cm (4 in.) high and consisted of 18 pressure probes each. Both the boundary-layer rakes and the pressure orifice rows were alligned in a streamwise position relative to the flow for a wing sweep of 10^{0}. Transition strips were placed from 5% to 50% of the chord on the test section on some flights.

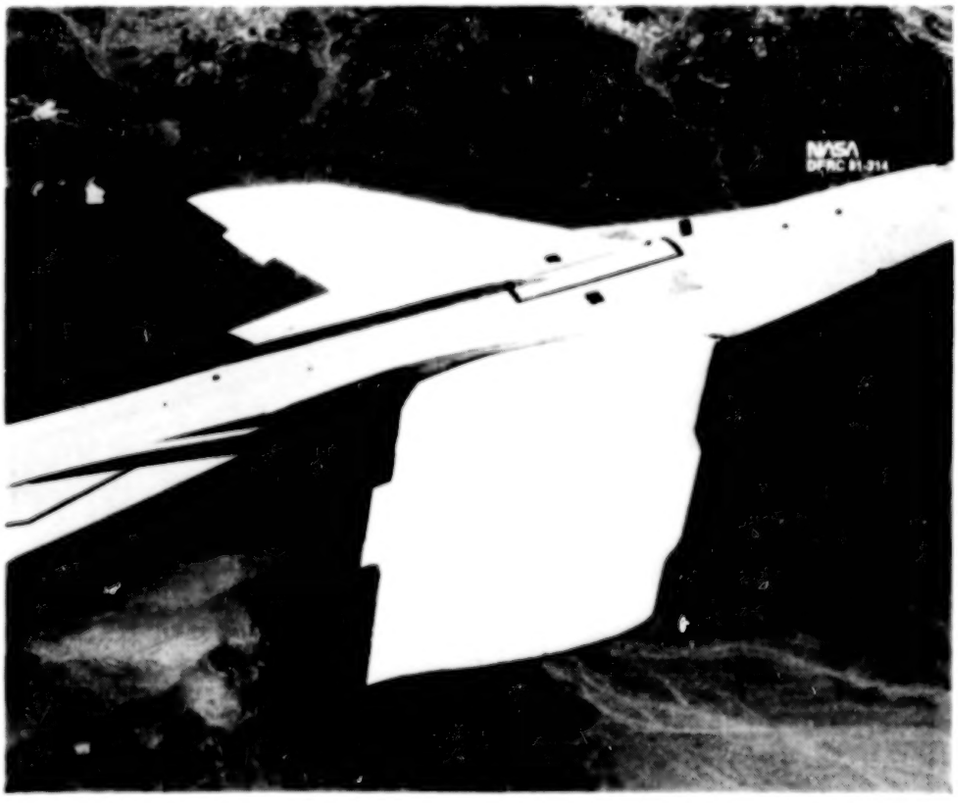

TYPICAL PRESSURE DISTRIBUTION AND BOUNDARY LAYER

In general the shapes of the flight and wind-tunnel pressure distribution data are similar at the design conditions of Mach 0.82 and leading-edge sweep of 10^0. The flight measured pressure distribution shows a favorable upper-surface pressure gradient to about .50 x/c while the wind-tunnel data continued on to about .70 x/c. The flight upper-surface boundary profile gives an idea of the shape and thickness as measured at the .90 x/c station for the corresponding pressure distribution presented.

PRELIMINARY NLF DATA

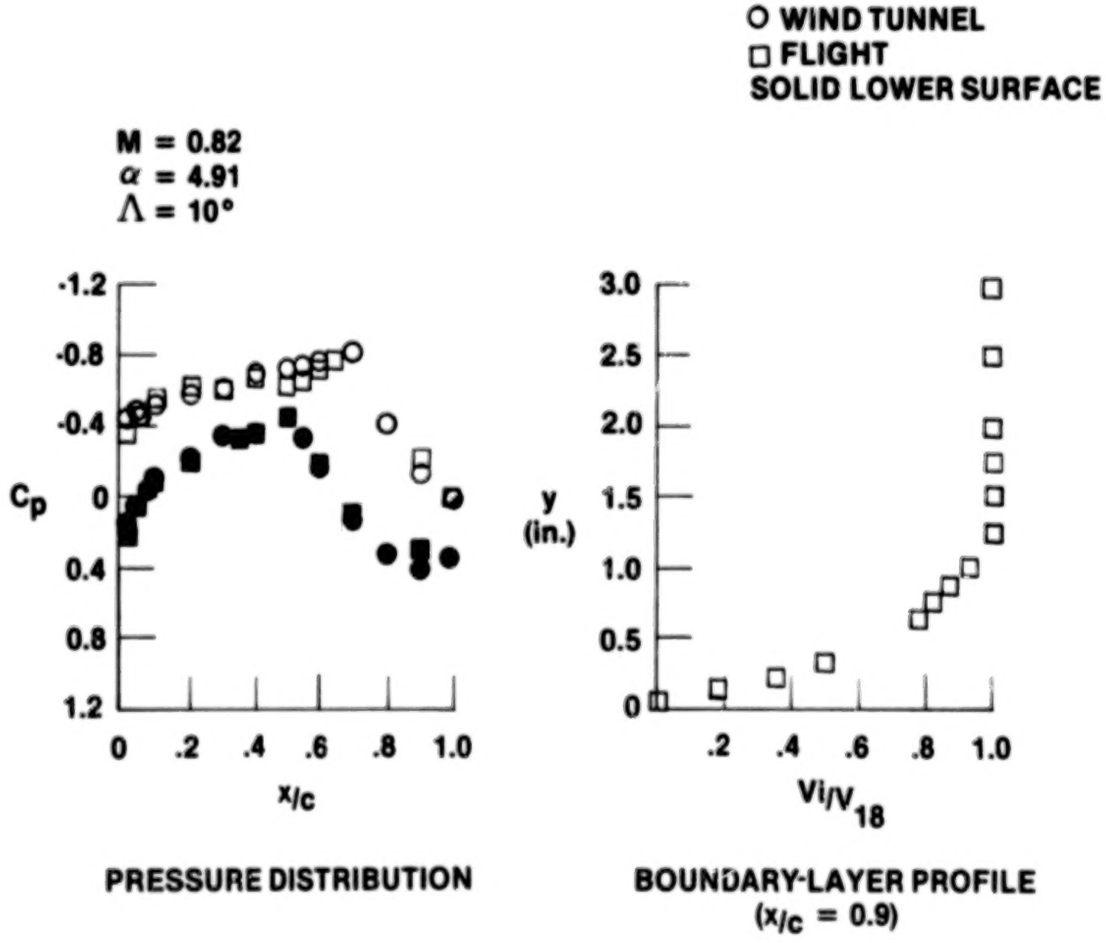

OIL FLOWS

The oil flow technique was used in an attempt to visualize the surface flow on both the model and full-scale tests. Upper-surface oil flows at the design conditions of Mach 0.82, sweep of 10^0, and angles of attack of 4^0 for the model and 5^0 for flight are shown below. As the pressure distributions indicated previously for these test conditions, the upper-surface flow is favorable to about 0.7 x/c where it terminates in a strong shock.

NATURAL AND FORCED TRANSITION RESULTS
($\Lambda = 10^{0}$)

Boundary-layer measurements were obtained to determine the extent of laminar flow achieved. Forced transition (transition strips placed at various chord locations) was used to "calibrate" the boundary-layer thickness measurements based on a known turbulent flow length, and to compare with the natural-transition boundary-layer measurements. The two pressure distributions presented are for natural transition (circle) and a 5%-chord forced transition. The data show that the boundary-layer thickness obtained for the natural transition in general agrees with the data obtained for forced transition at 40-50% chord. The natural-transition data also show that, at an angle of attack of about 4.6^{0}, there is a sudden thickening of the boundary (transition moves forward). This forward movement of transition resulted from an inboard TACT wing shock moving onto the test section causing an unfavorable gradient in the pressure distribution.

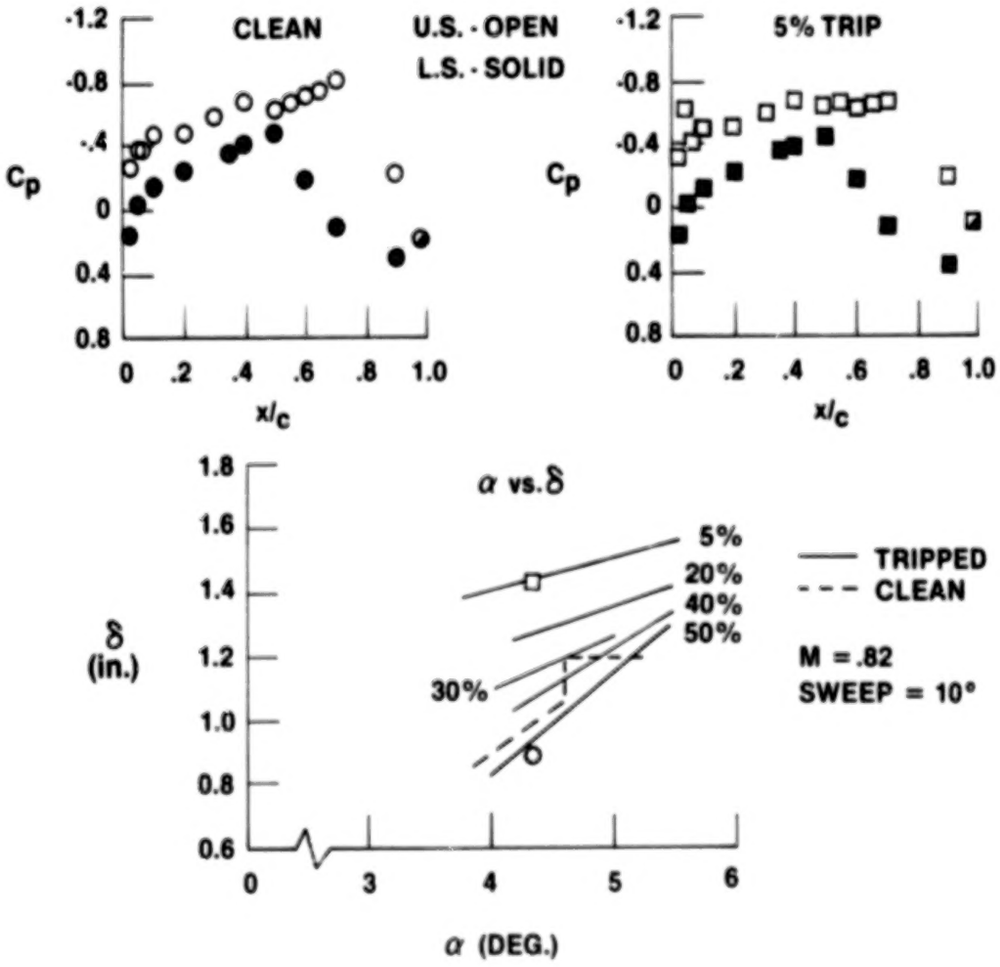

FORCED TRANSITION RESULTS
(Λ = 16° and 26°)

In addition to the data acquired at the design conditions (Mach 0.82 and a leading-edge sweep of 10°) points were also obtained at higher Mach numbers and larger leading-edge sweep angles. The data shown below are for 16° sweep at Mach 0.83 and 26° sweep and Mach 0.85. The boundary-layer thickness for both cases continues to decrease as the forced transition is moved aft indicating that laminar flow exists for these conditions. The airfoil section was designed for 10° of sweep; therefore, the adverse effect of the short span of the test section became more pronounced with increased sweep. These data are very encouraging in terms of the insensitivity of the concept to off-design conditions.

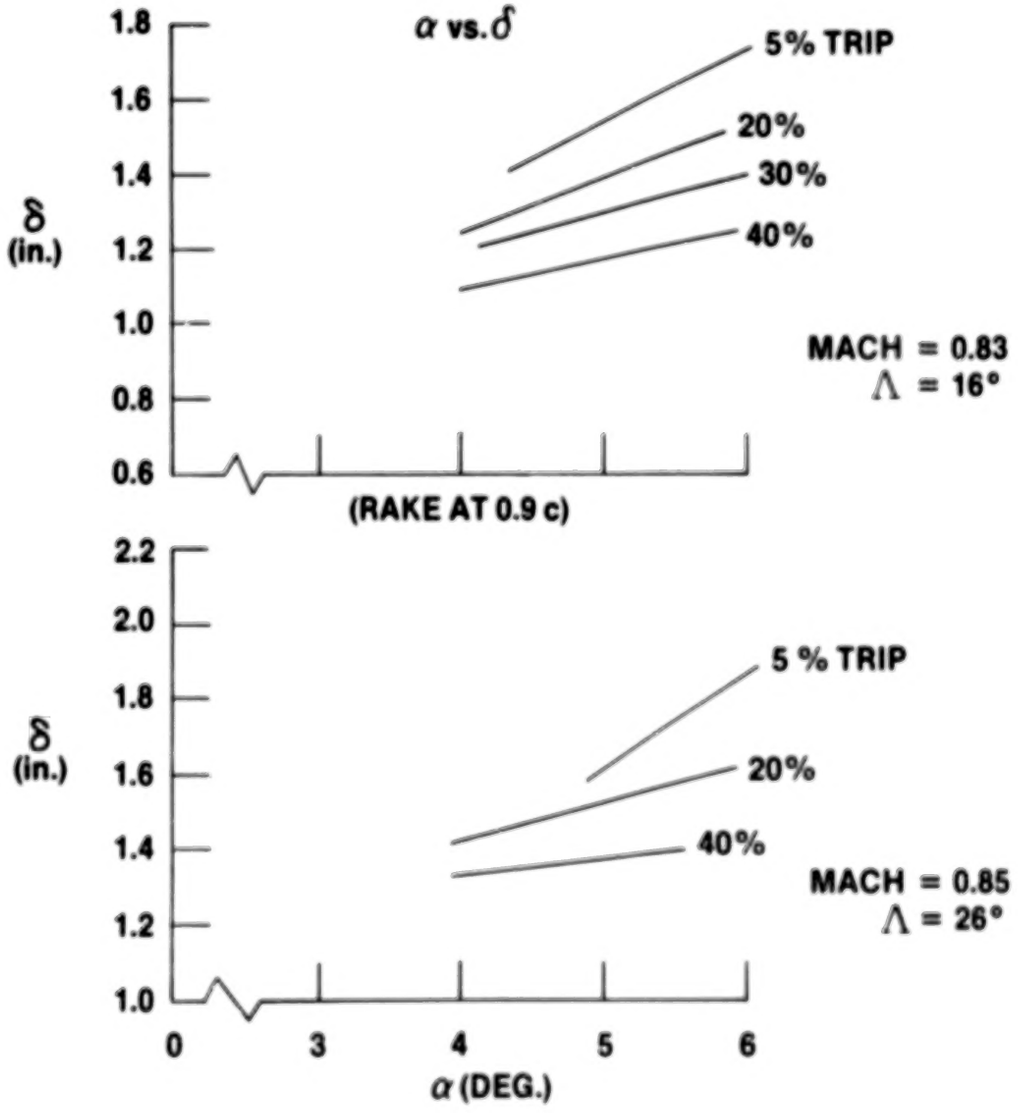

SUMMARY

The natural laminar flow experiment conducted on the F-111/TACT airplane has demonstrated that a significant amount of laminar flow can be achieved at flight Reynolds numbers up to 30 million. The experiment also showed that significant laminar flow could be achieved at off-design cruise conditions with a regard to Mach number and leading-edge sweep.

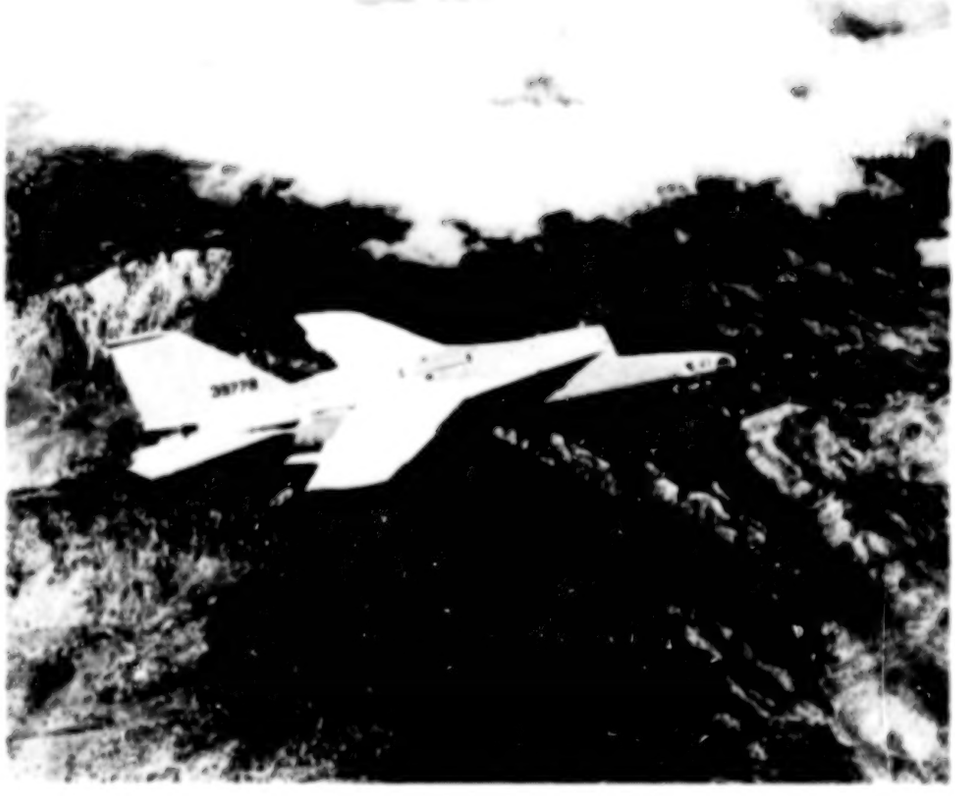

MEASURED TRANSONIC UNSTEADY PRESSURES ON AN ENERGY EFFICIENT TRANSPORT WING WITH OSCILLATING CONTROL SURFACES

F. W. Cazier, Jr.; Judith J. Watson; Robert V. Doggett, Jr.;
Maynard C. Sandford; and Rodney H. Ricketts
NASA Langley Research Center

EXPANDED ABSTRACT

Highlight results are presented from subsonic and transonic pressure measurement studies conducted in the Langley Transonic Dynamics Tunnel on a supercritical wing model representative of an energy efficient transport design. Steady- and unsteady-pressure data were acquired on the upper and lower wing surface at an off-design Mach number of 0.60 and at the design Mach number of 0.78, for a Reynolds number of 2.2×10^6 (based on the wing average chord). The model configuration consisted of a sidewall-mounted half-body fuselage and a semi-span wing with an aspect ratio of 10.76, a leading-edge sweepback angle of 28.8°, and supercritical airfoil sections. The wing is instrumented with 252 static pressure orifices and 164 dynamic pressure gages. It is equipped with 10 oscillating control surfaces, five along the leading edge and five along the trailing edge of the wing. Only three control surfaces were tested in the present study, namely, one inboard (trailing-edge) and two outboard (leading-edge and trailing-edge located in tandem) control surfaces, and only unsteady pressures of the outboard control surfaces are presented in this paper. Model test variables included wing angle of attack, control-surface mean deflection angle, control-surface oscillating deflection angle and frequency, and phasing between oscillating leading-edge and trailing-edge controls when used together. Results of a study are included establishing that the wing is very stiff and therefore the measured steady and unsteady pressures are not significantly affected by model flexibility.

INTRODUCTION

The design of active control systems for energy efficient transports with supercritical wings requires an understanding of both steady and unsteady transonic aerodynamics. Although considerable effort is being placed on developing methods for predicting unsteady transonic aerodynamics and significant progress has been made, no theoretical method has been developed to the point that it can be used to predict unsteady transonic loads reliably. Thus, a research program was initiated at the National Aeronautics and Space Administration (NASA) Langley Research Center to aid in understanding unsteady transonic flow phenomena by generating a comprehensive data base of measured steady and unsteady pressures on a three-dimensional, semispan wind-tunnel-model wing with both leading-edge and trailing-edge oscillating control surfaces.

Initial wind-tunnel tests included the use of only two trailing-edge control surfaces for generating steady and unsteady aerodynamics. One control surface was an inboard control located between 10 and 24 percent semispan, and the other was an outboard control surface located between 59 and 79 percent semispan. Highlight results from these initial tests are presented in reference 1, and a complete tabulation of all data is presented in reference 2.

A second series of tests has now been completed and highlight results are presented in this paper. For the sake of completeness a description of the model (following that given in references 1 and 2) is repeated herein. This second wind-tunnel test included the use of three control surfaces. One inboard control (trailing-edge) is located between 10 and 24 percent semispan and two outboard controls (leading-edge and trailing-edge in tandem) are located between 59 and 79 percent semispan. The two trailing-edge control surfaces are the same controls reported previously in references 1 and 2. The present results, however, are for different test conditions. Both series of tests were conducted in the Langley Transonic Dynamics Tunnel using Freon[1] as the test medium. Model parameters investigated included wing angle-of-attack, control surface mean deflection angle, control surface oscillating deflection angle and frequency, and phasing between oscillating leading-edge and trailing-edge controls when used together.

---

[1]Freon: Registered trademark of E. I. du Pont de Nemours and Co., Inc.

WIND-TUNNEL MODEL

A photograph of the model mounted in the Langley Transonic Dynamics Tunnel is shown in figure 1. The model consisted of a half-body fuselage similar to that of a "wide-body" transport and a stiff semispan wing having a planform representative of current energy efficient transport designs. The model was mounted on the tunnel sidewall on a turntable mechanism which allowed the angle of attack to be varied.

Figure 1

MODEL GEOMETRY

A sketch of the wing is presented in figure 2. The wing has a leading-edge sweepback angle of 28.8°, an aspect ratio of 10.76, and a semispan of 2.286 meters. The side of the half-body fuselage was located at wing station 0.219 m.

The wing is equipped with 10 oscillating control surfaces. Each control surface can be oscillated independently. Outlined in the figure are five leading-edge control surfaces hinged about the 15-percent chord and five trailing-edge control surfaces hinged about the 80-percent chord. Only the three control surfaces indicated by the cross hatched area were studied in the present investigation, namely, the inboard trailing edge and two outboard control surfaces (leading-edge and trailing-edge located in tandem).

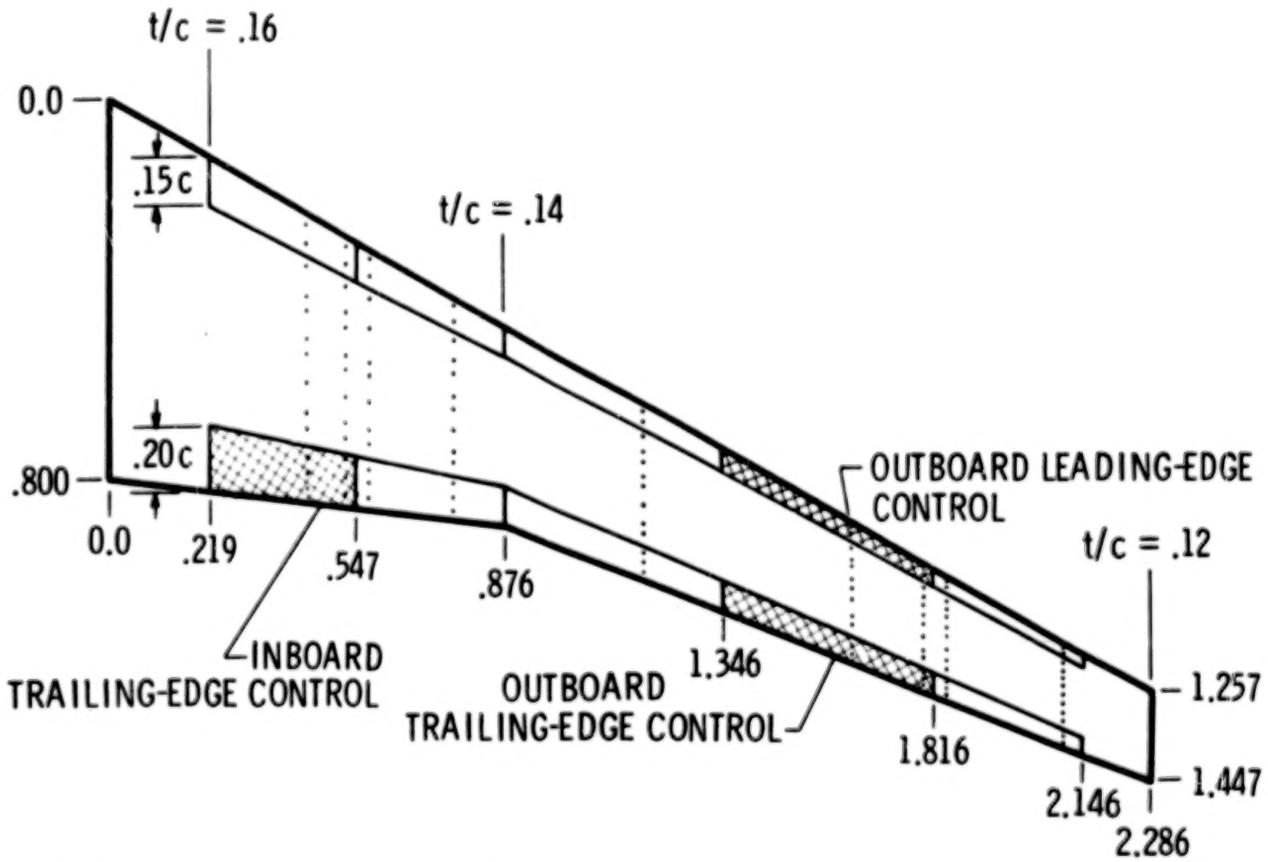

Figure 2

AIRFOIL SECTION

The design of the wing contour was based on three different supercritical airfoils. These airfoils were located at wing stations 0.219 m, 0.876m and 2.286 m and had thickness-to-chord ratios of 0.16, 0.14, and 0.12, respectively. The supercritical airfoil shapes are shown at the left in figure 3. Straight line interpolation along constant percent chords was used between adjacent airfoil sections. The section twist angles at each station, referenced to a horizontal reference plane, are also shown in the figure. A comparison of a typical design airfoil section at wing station 0.383 m and the corresponding measurements for the actual model airfoil section are shown at the right in the figure. These data show that the desired and actual airfoil sections are almost identical.

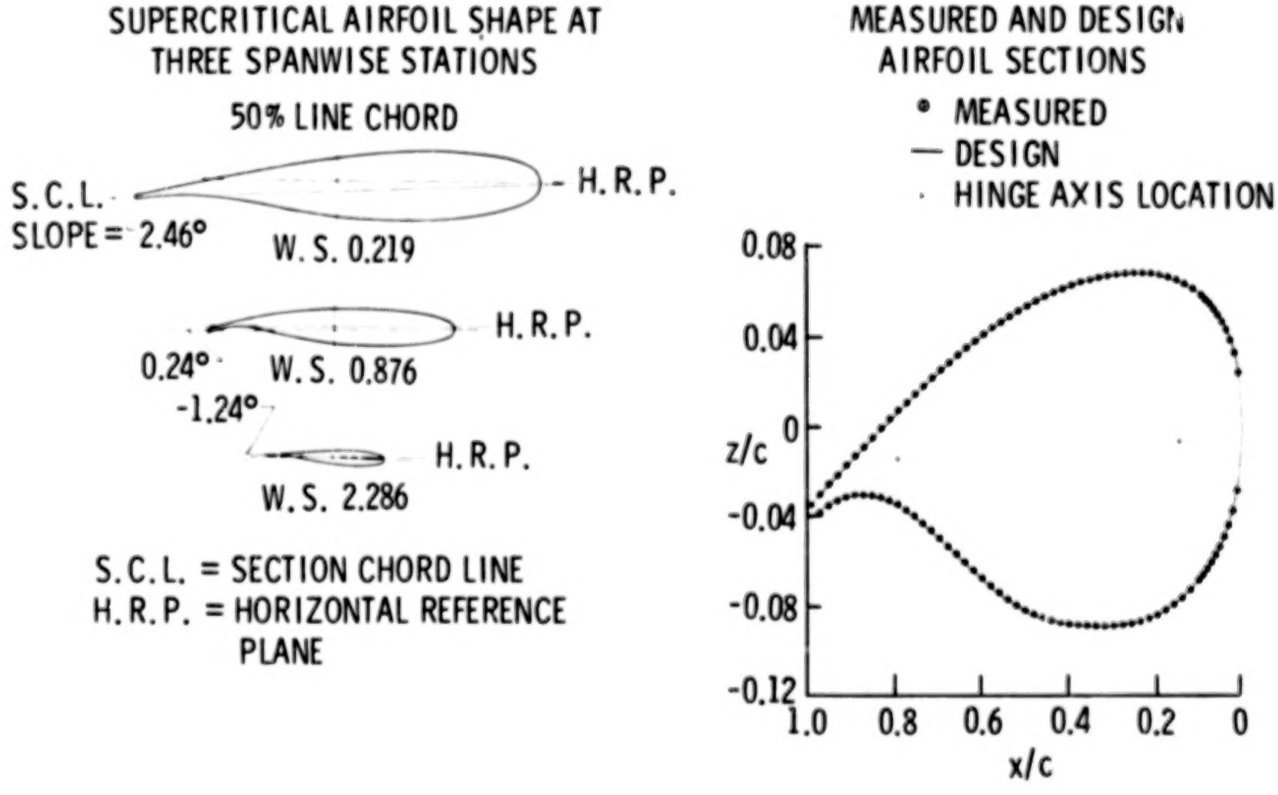

Figure 3

MODEL WING BOX CONSTRUCTION

The wing box was constructed from aluminum alloy and consisted of upper and lower sections. Each section was stiffened in bending by a boron filament insert bonded to the internal cutout area shown in figure 4. The sections were permanently bonded together to form a box cross section. This type of construction produced a stiff, lightweight wing structure whose fundamental frequency (23 Hz) was well above the maximum control surface excitation frequency used during the tests (15 Hz). These requirements for a stiff, high frequency wing structure were dictated by the need to minimize the dynamic and static deformations of the model due to aerodynamic loads.

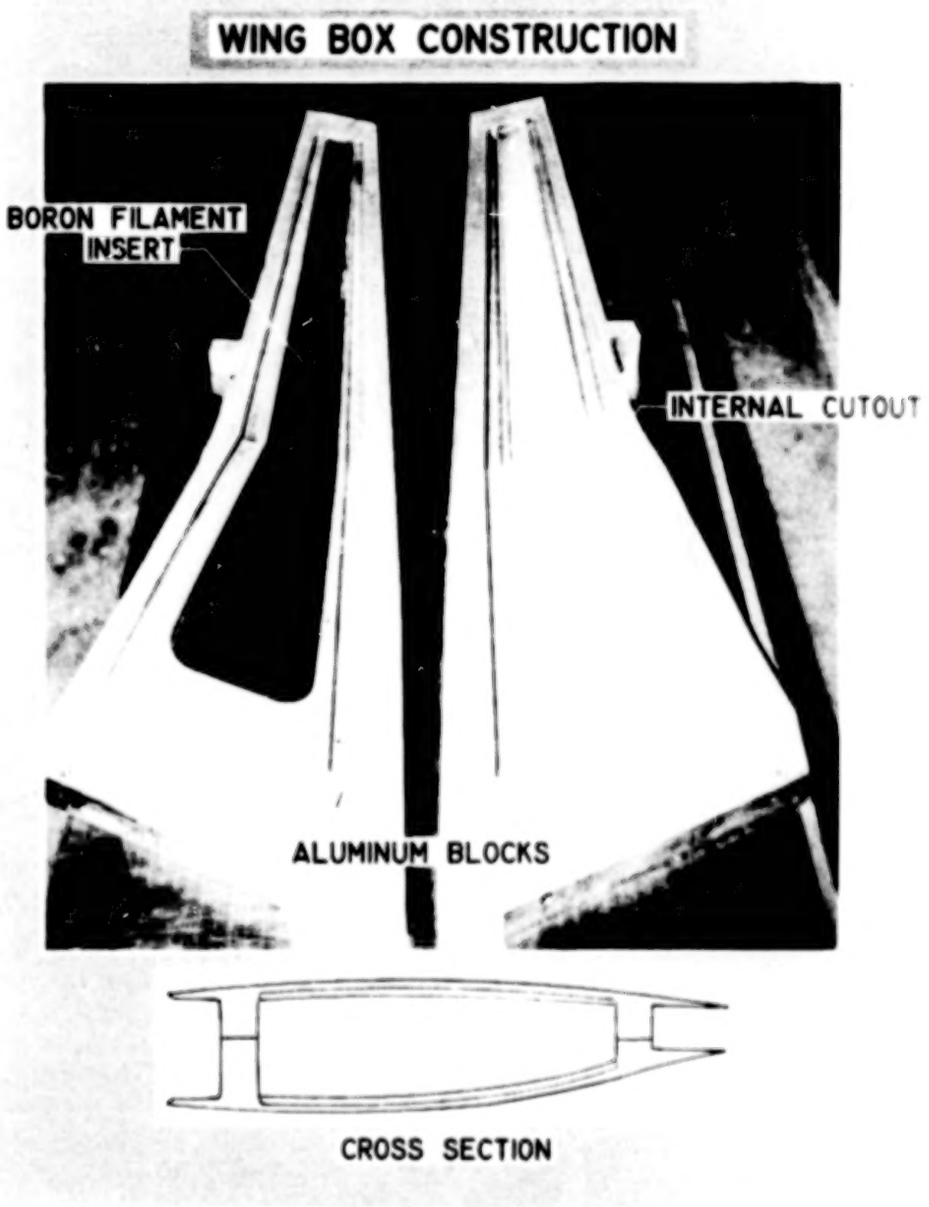

Figure 4

MODEL CONTROL SURFACES AND ACTUATOR CONSTRUCTION

Lightweight control surfaces were constructed using stiff Kevlar[2]-balsa sandwich material thereby minimizing the control surface inertia loads and deformations. Typical control surfaces are shown at the left in figure 5. Miniature hydraulic actuators of the rotating vane type were used both to position the control surfaces statically and to oscillate them at amplitudes up to $\pm 6^{0}$ over a frequency range from 5 to 15 Hertz. A typical actuator is shown at the right in the figure.

---

[2]Kevlar: Registered trademark of E. I. du Pont de Nemours and Co., Inc.

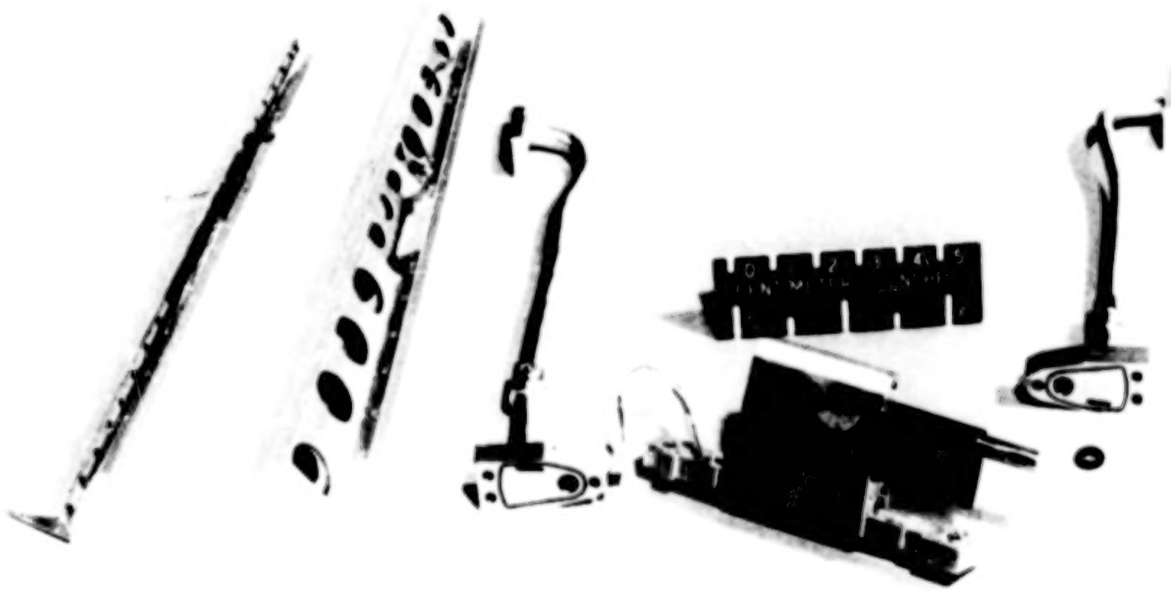

CONTROL SURFACES HYDRAULIC ACTUATOR

Figure 5

WING INSTRUMENTATION

The model was instrumented with 252 static pressure orifices and 164 in situ dynamic pressure transducers. Pressure measurements were made at nine different spanwise stations. Half of the orifices/transducers were located on the upper surface, and the other half were located at corresponding stations on the lower surface to facilitate obtaining lifting pressure distributions. The nine chordwise rows of dots shown on the sketch in figure 2 indicate the approximate locations of pressure measurement stations. Small precision potentiometers were used to measure directly the control-surface angular displacements. The model root angle of attack was measured by a digital encoder that was mechanically linked to the turntable in the wind-tunnel wall and also by an angle-of-attack accelerometer mounted in the fuselage at the wing root. The wing was mounted to a five-component balance which measured the wing static forces and moments. Six accelerometers were installed in the model to detect wing vibrations. The large amount of instrumentation installed in the model is evident in figure 6.

Figure 6

TEST CONDITIONS/PARAMETERS

The test conditions and model variables for the first two wind-tunnel entries are summarized in figure 7. In the first entry the model was tested at several subsonic Mach numbers, M, from M = 0.4 to M = 0.82 and two Reynolds numbers (based on wing average chord) of 2.2×10^6 and 4.7×10^6. The model was tested at two angles of attack ($\alpha = 0^0$ and α for design lift coefficient). In these initial tests (ref. 1,2), only two trailing-edge control surfaces were deflected, one inboard and one outboard (see fig. 2). These control surfaces were deflected statically and also oscillated at several amplitudes and frequencies. For the second entry, additional steady-state and oscillating control surface pressure data were obtained at M = 0.6 and M = 0.78 for these trailing-edge control surfaces. In addition, data were obtained by using an outboard leading-edge control surface (see fig. 2) that was deflected (steady-state data) and oscillated (dynamic data) independently and in conjunction with the outboard trailing-edge control surface. Tests were performed at one Reynolds number, RN = 2.2×10^6, for the second entry. The model was in the tunnel for its third series of tests as this status report was being written.

TUNNEL CONDITIONS AND WING CONFIGURATIONS TESTED
Entries 1 and 2

		M = .40	.60	.70	.75	.78	.80	.82
α	RN = 2.2×10^6	0^0, 3.83^0	0^0, 2.85^0	0^0, 2.66^0	0^0, 2.38^0	-3^0 to 4^0 0^0, 2.05^0	0^0, 2.25^0	0^0, 2.43^0
	RN = 4.7×10^6	0^0, 4.00^0	0^0, 3.42^0	0^0, 3.08^0	0^0, 2.75^0	0^0, 2.47^0	0^0, 2.21^0	0^0, 2.21^0
Inboard Trailing-edge Control	Static	0^0	-6^0 to 6^0	0^0	0^0	-6^0 to 12^0	0^0	0^0
	Dynamic		$\pm 4^0$			$\pm 2^0, \pm 4^0, \pm 6^0$		
Outboard Trailing-edge Control	Static	0^0	-6^0 to 6^0	0^0	0^0	-9^0 to 9^0	0^0	0^0
	Dynamic		$\pm 4^0$			$\pm 2^0, \pm 4^0, \pm 6^0$		
Outboard Leading-edge Control	Static	0^0	-6^0 to 6^0	0^0	0^0	-6^0 to 6^0	0^0	0^0
	Dynamic		$\pm 4^0$			$\pm 2^0, \pm 4^0, \pm 6^0$		
Outboard Tandem Leading-edge Trailing-edge Control	Static		-4^0, 4^0			-4^0, 4^0		
	Dynamic		$\pm 4^0$			$\pm 4^0$		

Figure 7

EFFECTS OF MODEL FLEXIBILITY ON AERODYNAMIC LOADS

A study was made to determine the stiffness of the model and assess whether or not elastic deformations of the model significantly affected the aerodynamic loading. This was accomplished by constructing a finite-element model (FEM) of the wind-tunnel model using stiffness data determined from laboratory measurements. Static loads were applied to the wind-tunnel model and resultant deflections and twist measured in laboratory tests. Then the experimentally measured shape was compared to the calculated shape determined by applying the same static loads to the FEM. The excellent agreement of the analytical and experimental deflections verified the FEM. Next, the aerodynamic loads were verified at M = 0.60. Shown on the left half of figure 8 are the analytical loads predicted by the aerodynamic theory of reference 3. The variation in lift coefficient with angle of attack is shown in the upper left and the location of the center of pressure in the lower left. The corresponding experimental loads were determined from wind-tunnel data by chordwise integration of the static pressure distribution at each of the nine instrumented chords on the wing. The correlation is very good. The experimentally measured and analytically predicted aerodynamic loads were applied to the finite-element model to predict the wing's deformed shape at M = 0.60. The bending deflection and twist about the 40 percent chord is given on the right half of figure 8. For an angle of attack of one degree a deflection of about 1 mm and a twist angle of about .015 degree are predicted for the tip of the wing. Similar studies were conducted for M = 0.78 aerodynamic loads and for deflected control surfaces. Each of these results indicates that the model can be considered rigid and that the pressure measurement results are not influenced to any significant degree by model flexibility.

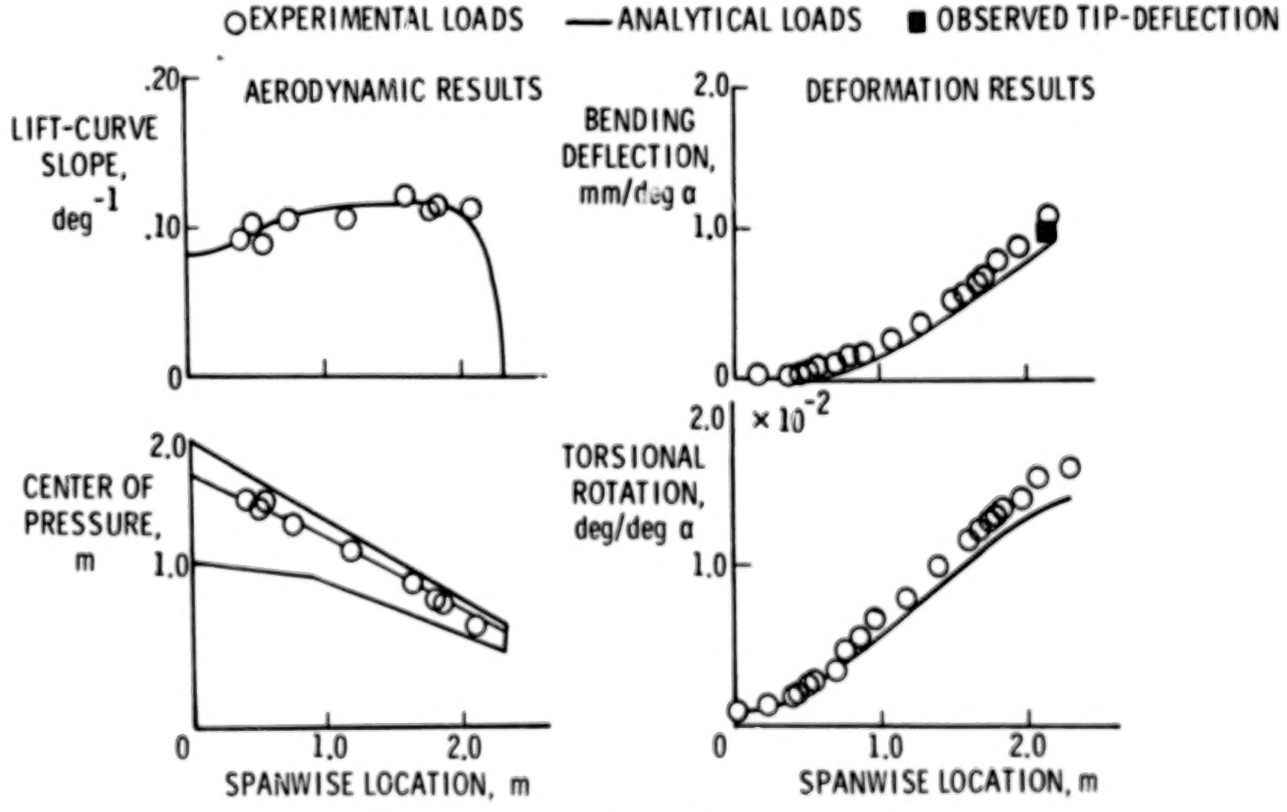

Figure 8

OUTBOARD LEADING-EDGE CONTROL AMPLITUDE EFFECTS

The chordwise distributions of lifting pressures due to oscillations of the leading edge control at 10 Hz are shown in figure 9 for wing station 1.629 m. Results are given in terms of pressure magnitude and phase relative to the surface displacement for three amplitudes of $\pm 2^0$, $\pm 4^0$, and $\pm 6^0$. The data are for M = .78 and RN = 2.2×10^6 for two angles of attack, $\alpha = 0^0$ and $\alpha = 2.06^0$. The $\alpha = 2.06^0$ case corresponds to the design cruise condition for the wing; the $\alpha = 0^0$ case is an off-design condition. Forward of the 50 percent chord, the amplitude varies in approximately a linear manner with input amplitude, with the maximum occurring near the leading edge, falling to a relative minimum near the leading-edge hingeline, and increasing to another relative maximum, before decreasing. Aft of the 50-percent chord, the oscillating pressure amplitude is small and approximately the same regardless of the input amplitude. Over most of the wing, the phase is not affected by the amplitude of the control surface. The oscillating pressure is in phase with the leading-edge control surface over the control surface and about 180^0 out of phase aft of the hinge line except near the mid-chord. For the $\alpha = 0^0$ and input amplitude = 2^0 case, the phase angle changes from near 180^0 at the 45 percent chord to near 0^0 at 60 percent chord and back to 180^0 at 75 percent chord. Phase shifts are observed in the same region for $\alpha = 2.06^0$ case. Results obtained for control surface oscillating angles of $\pm 4^0$ and $\pm 6^0$ are similar.

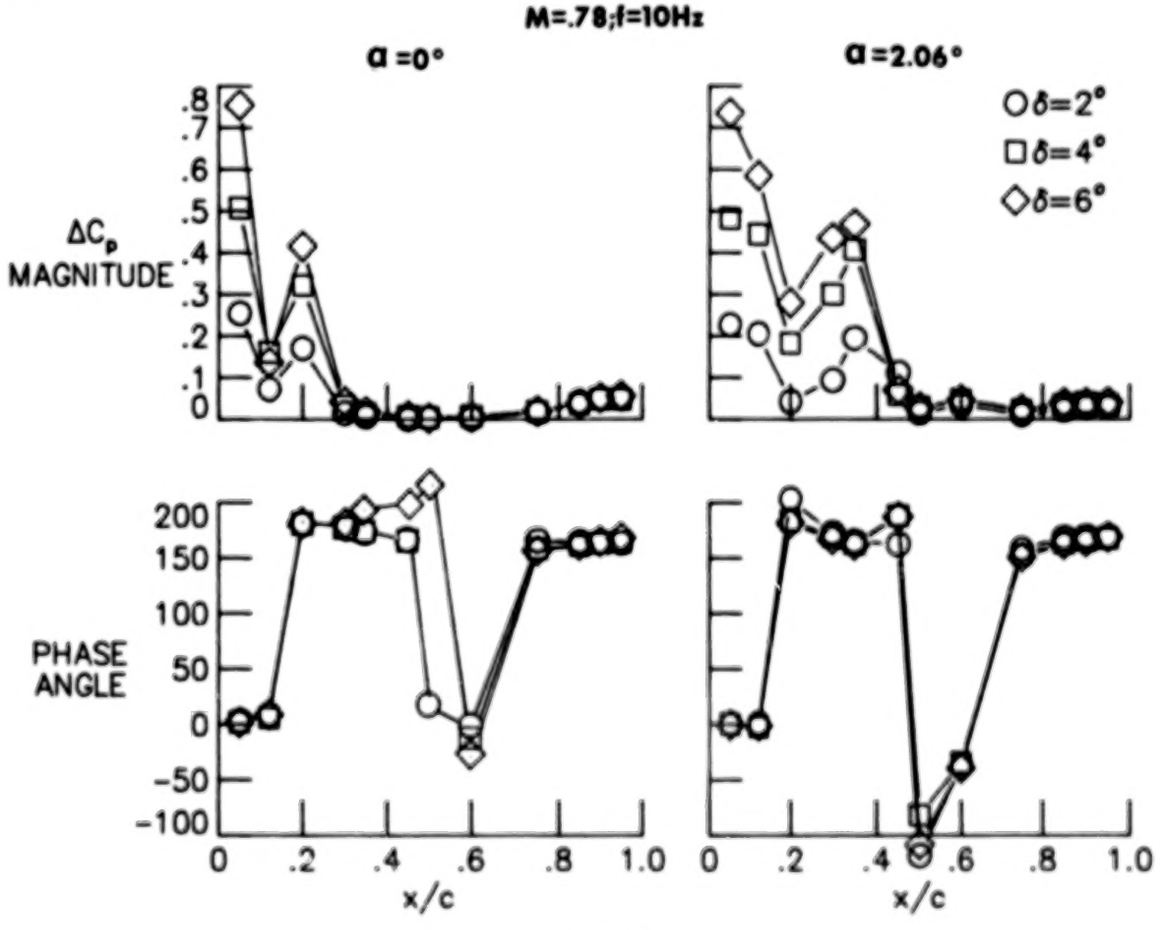

Figure 9

OUTBOARD LEADING-EDGE CONTROL FREQUENCY EFFECTS

Presented in figure 10 are the chordwise distributions of lifting pressure due to the oscillation of the outboard leading-edge control surface at $\pm 4^{0}$ for three frequencies: 5, 10, and 15 Hz, which at M = .78 correspond to reduced frequencies of .11, .21, and .32, respectively. Data are given in terms of lifting pressure magnitude and phase relative to control surface motion for Mach numbers .60 and .78 at angles of attack which gave the design cruise lift coefficient. The Reynolds number is 2.2×10^{6}. The chordwise distributions of pressure exhibit the same characteristics as discussed under amplitude effects and are quite similar for both Mach numbers. The M = .60 data show no effect of oscillating frequency on the pressure magnitude. The M = .60 phase angle results show the pressure being in phase with the motion over the control surface and 180^{0} out of phase downstream of the hinge line. The phase angles for the M = .78 are similar except in the vicinity of the mid-chord where the phase angle changes from a lead to a lag and then to a lead again. The reason for this abrupt change in phase is not known for certain but is believed to be due to the presence of a shock wave on the wing. There seems to be a small effect of oscillating frequency on the phase angles. This is shown clearly by the M = .60 results where the phase lead of the pressure aft of the hinge line is systematically reduced by increasing the frequency of oscillation. The M = .78 data show some differences in pressure near the 30-percent chord station. These differences may be due to the relatively coarse spacing of the pressure transducers in this region where sharp pressure gradients occur. Results similar to those presented in the figure were also obtained for $\alpha = 0^{0}$.

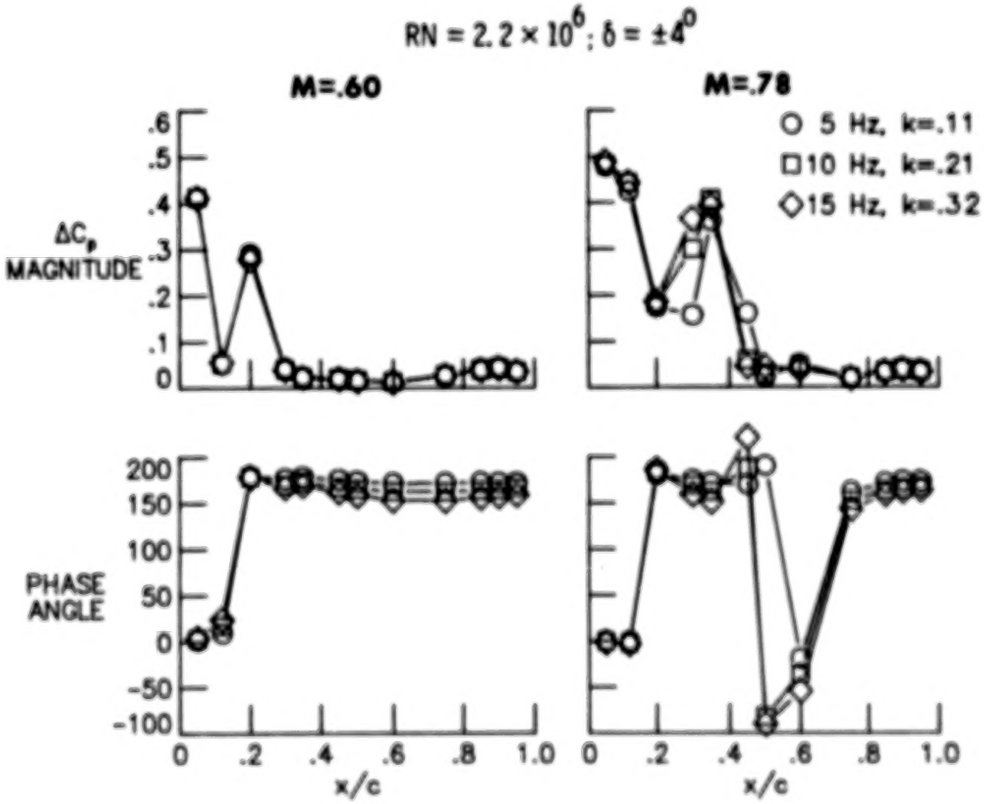

Figure 10

OUTBOARD LEADING-EDGE AND TRAILING-EDGE CONTROL SURFACES OSCILLATED SIMULTANEOUSLY

Chordwise distributions at wing station 1.629 of lifting pressure magnitude and phase angle are presented in figure 11 for simultaneous operation of the outboard leading-edge and outboard trailing-edge control surfaces. The phase angle is the angle between the pressure and position of the leading-edge control surface. Data are presented for the controls being oscillated in phase (at right in figure) and out of phase (at left in figure) at $+4^0$ for $M = .78$ and $RN = 2.2 \times 10^6$. The out-of-phase case results are presented for three frequencies, 5, 10, and 15 Hz ($k = .11$, .21, and 32, respectively). The in-phase case results are presented at two frequencies, 10 and 15 Hz. The chordwise distribution of pressure magnitude shows the same maximum and minimum pressure characteristics in the vicinity of the leading-edge control surface discussed previously. In general, the pressure magnitudes are not affected by frequency of oscillation. The most obvious exception to this observation is for the out-of-phase case at $x/c = 0.30$ where the $f = 5$ Hz and $f = 10$ Hz results agree but the $f = 15$ Hz value is considerably higher. The phase angle results are similar over the forward portion of the chord. The pressures on the leading-edge control for both cases are in phase with the motion (as would be expected) and lag the motion by about 180^0 aft of the leading-edge control surface hinge line. Over the rear portion of the chord the out-of-phase data show the pressures leading the motion whereas the in-phase data show a significant phase lag. A superposition of the independent leading-edge and trailing-edge results approximates these simultaneous operation results.

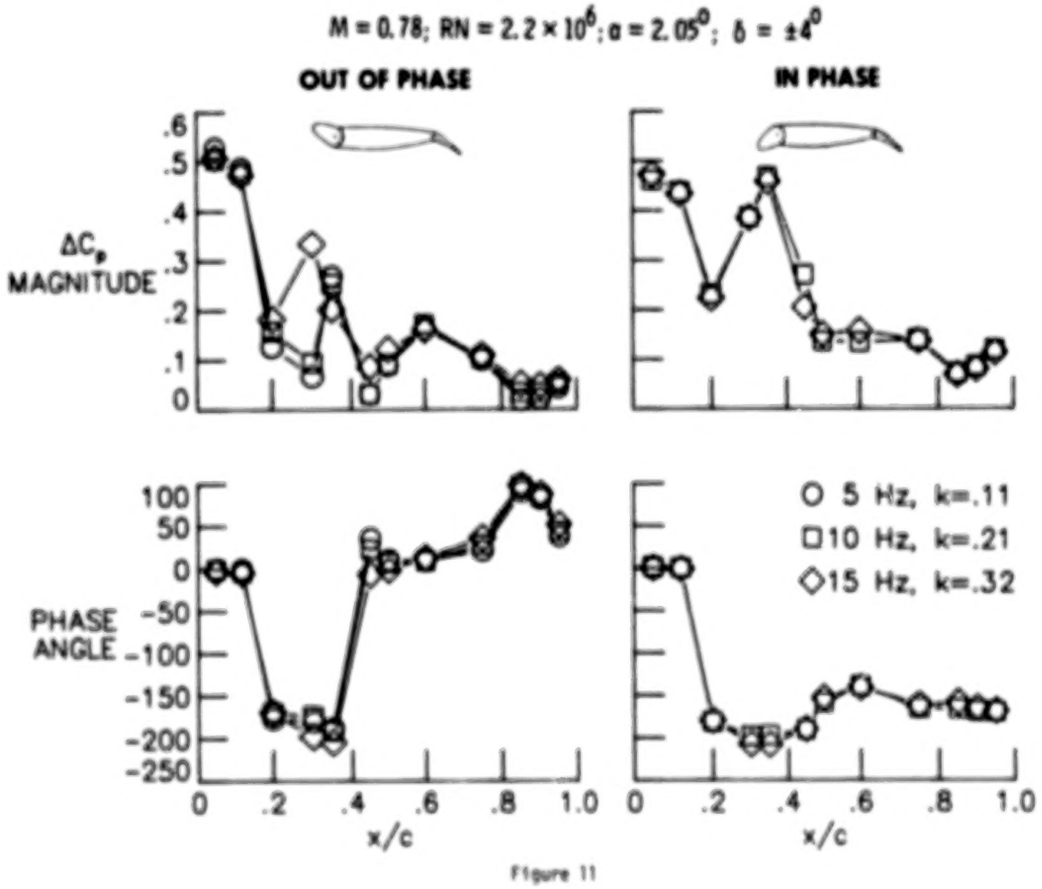

Figure 11

COMPARISON OF MEASURED AND CALCULATED RESULTS

A comparison of measured and calculated chordwise distribution of lifting pressure at wing station 1.629 is presented in figure 12 for both the outboard leading-edge and outboard trailing-edge control surfaces. These results are for M = 0.60 with the control surfaces oscillating at 10 Hz through an angle of +4°. The calculated results were obtained using linear subsonic lifting surface theory (ref. 3). This kernel function method accounts for control surface edge and hinge line singularities. Airfoil thickness effects are partially accounted for by modifying the local streamwise velocity. The data in the figure are presented as the variation with fraction of chord of the magnitude of lifting pressure and phase angle referenced to the control surface position. In general, the calculated data show the same trends as the experimental results and show reasonable agreement with the experimental results except in the region of the oscillating control surfaces. The disagreement is greater for the trailing-edge control surface where the theory overestimates the measured pressures and underestimates the measured phase.

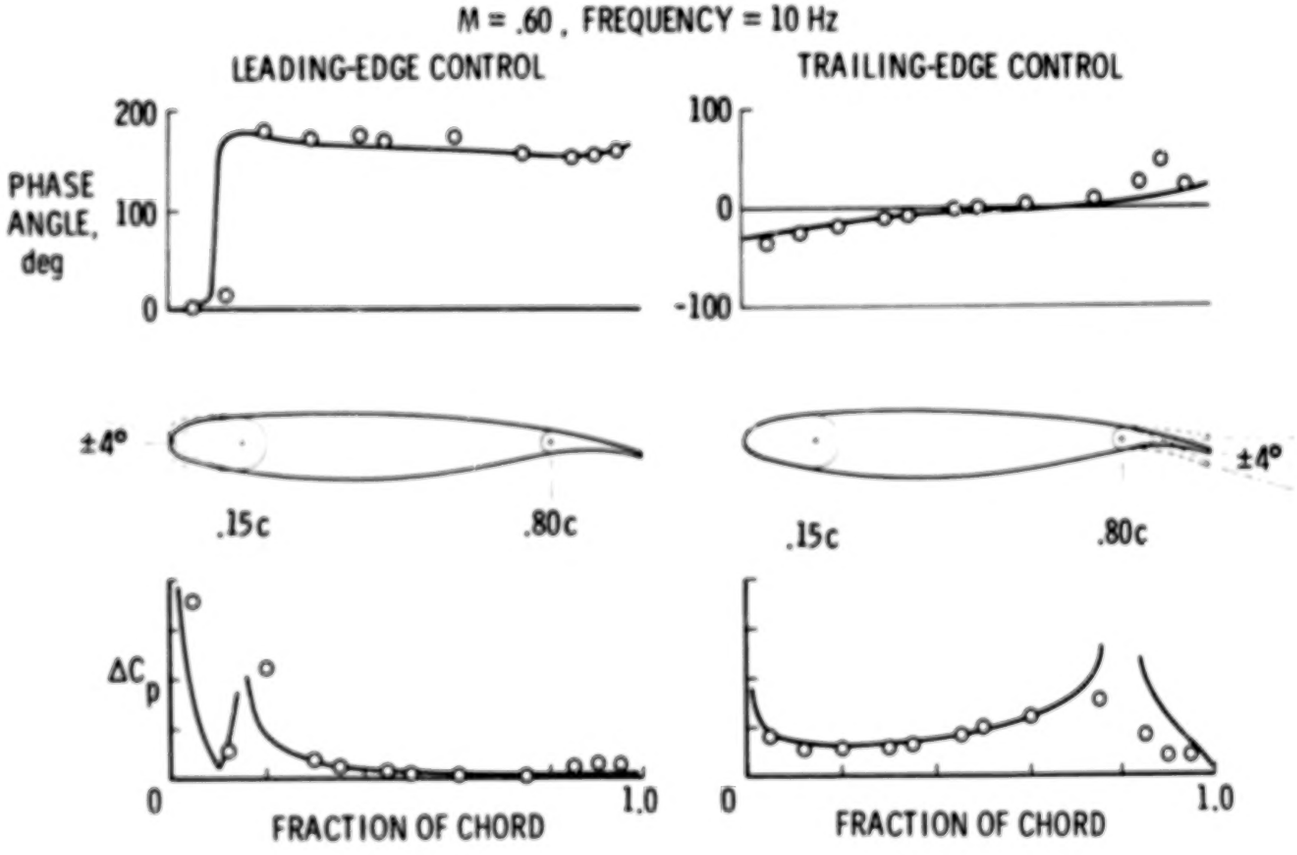

Figure 12

SUMMARY

An experimental investigation is being conducted on a supercritical wing model representative of an energy efficient transport with oscillating control surfaces. The purpose of this investigation is to obtain a comprehensive data base of measured transonic unsteady pressures for use in designing active control systems and for use in validating transonic unsteady aerodynamic theories. The model has been tested twice in the Langley Transonic Dynamics Tunnel and is currently being tested a third time. The matrix of wind-tunnel test conditions and model variables for which steady and unsteady pressure distributions are available is given. Selected measured unsteady results from the second test for an outboard leading-edge control surface and an outboard trailing-edge control surface are presented and discussed. Measured data for an oscillating leading-edge control surface and an oscillating trailing-edge control surface are compared with calculated results obtained from subsonic lifting surface theory.

REFERENCES

1. Sandford, M. C.; Ricketts, R. H.; Cazier, F. W., Jr.; and Cunningham, H. J.; Transonic Unsteady Airloads on an Energy Efficient Transport Wing with Oscillating Control Surfaces. Journal of Aircraft, vol. 18, no. 7, July 1981, pp. 557-561.

2. Sandford, Maynard C.; Ricketts, Rodney H.; and Cazier, F. W., Jr.: Transonic Steady- and Unsteady-Pressure Measurements on a High Aspect-Ratio Supercritical-Wing Model with Oscillating Control Surfaces. NASA TM-81888, December 1980.

3. Rowe, W. S.; Sebastian, J. D.; and Petrarca, J. R.: Reduction of Computer Usage Costs in Predicting Unsteady Aerodynamic Loadings Caused by Control Surface Motions - Analysis and Results. NASA CR-3009, March 1979.

STATUS OF ADVANCED AIRFOIL TESTS IN THE LANGLEY 0.3-METER TRANSONIC CRYOGENIC TUNNEL

Charles L. Ladson and Edward J. Ray
NASA Langley Research Center

ABSTRACT

A joint NASA/U.S. industry program to test advanced technology airfoils in the Langley 0.3-meter Transonic Cryogenic Tunnel (TCT) has been formulated under the Langley ACEE Project Office. The objectives of this program include providing U.S. industry an opportunity to compare their most advanced airfoils to the latest NASA designs by means of high Reynolds number tests in the same facility. At the same time, industry would gain experience in the design and construction of cryogenic models as well as experience in cryogenic test techniques.

This paper presents the status and details of the test program. Typical aerodynamic results obtained, to date, are presented at chord Reynolds number up to 45×10^6 and are compared to results from other facilities and theory. Details of a joint agreement between NASA and the Deutsche Forschungs- und Versuchsanstalt fur Luft- and Raumfahrt e.V. (DFVLR) for tests of two airfoils are also included. Results of these tests will be made available as soon as practical.

INTRODUCTION

Future U.S. commercial transports must be highly energy efficient to effectively compete in the increasingly competitive world marketplace. Areas in which improvements can be made to increase overall efficiency include structures, propulsion, controls, and aerodynamics. The Langley Research Center (LRC) has devoted considerable effort over the past several years to the application of supercritical airfoil technology to the design of a more efficient transport aircraft wing. This effort has been well documented and U.S. industry has similar efforts underway. To augment this area of research, the LRC ACEE Project Office in cooperation with the Transonic Aerodynamics Division initiated a joint NASA/U.S. industry program for testing advanced airfoils at high Reynolds numbers using the LRC 0.3-meter TCT as the basic facility for these tests.

The purpose of this paper is to present a status report on this joint NASA/industry test program, which is now in progress. The basic objectives of and approach to the program will be discussed as well as a brief description of the LRC 0.3-meter TCT and some recent experience in airfoil model fabrication methods. Typical aerodynamic results obtained, to date, are shown along with comparisons to data from other facilities and theory.

OBJECTIVES

During the initial stages of the development of the proposal for this joint NASA/industry test program, several primary objectives were agreed upon by representatives of the Langley ACEE Project Office and the Transonic Aerodynamics Division. These objectives are listed in figure 1. As shown, the first goal is to provide the U.S. transport industry an opportunity to test their most advanced airfoils at high Reynolds numbers in the Langley 0.3-meter TCT. An advanced NASA supercritical airfoil would also be tested in the same facility at similar test conditions and make the data available as soon as practical. In this manner, each company could make any comparisons desired to compare and evaluate their current levels of technology. No effort would be made on the part of NASA to compare any of the airfoils in regards to performance characteristics. As an outgrowth of this effort, each company would gain valuable experience in the design, fabrication, and testing of models to be used in a cryogenic wind tunnel. This experience should prove to be useful in future test programs involving use of the NTF. By means of publication of all of the results of the computer test program, the data base of high Reynolds number aerodynamic data will be enhanced.

The DFVLR of Germany has expressed a desire to test in this facility for the past several years. It was decided to pursue this interest and invite them to participate in a joint test program also. The direct benefit of this agreement would be an opportunity to evaluate current European advanced airfoil technology.

Other objectives could be explored if mutually agreed upon in pretest conferences with the participants in the program. These could involve such areas as determining the effectiveness of low Reynolds number fixed transition tests, methods of determining transition location, and flow visualization techniques.

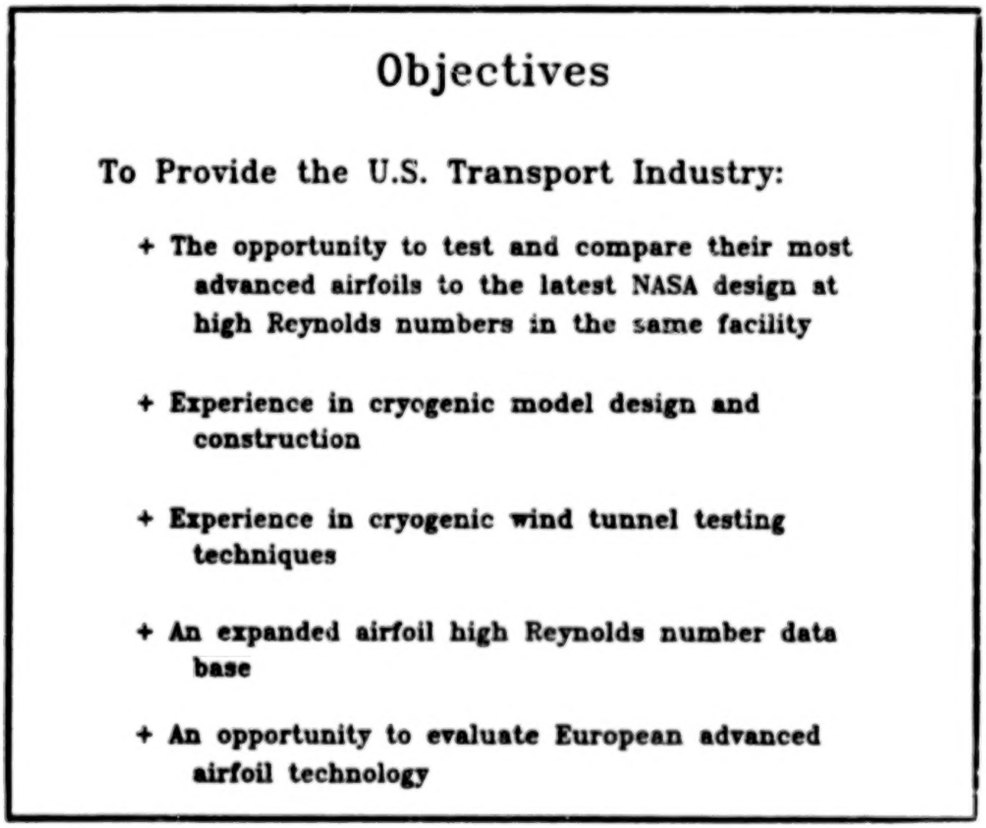

Figure 1

APPROACH

To achieve the objectives of this program, the approach, outlined in figure 2 was adopted. The approach includes testing of a basic series of NACA/NASA correlation airfoils to establish the relationship between data from the LRC 0.3-meter TCT and other facilities such as the LRC 8-Foot Transonic Pressure Tunnel (TPT), the LAC CFF, and the NAE 2-D insert for the 5-foot transonic tunnel. A formal proposal for the joint NASA/industry test program would be written, defining such items as the airfoil design conditions, NASA and company rights to final data, and details of any cost sharing. The industry models would then be tested by NASA in accordance with these agreements. A similar approach was to be used for the joint NASA/DFVLR program.

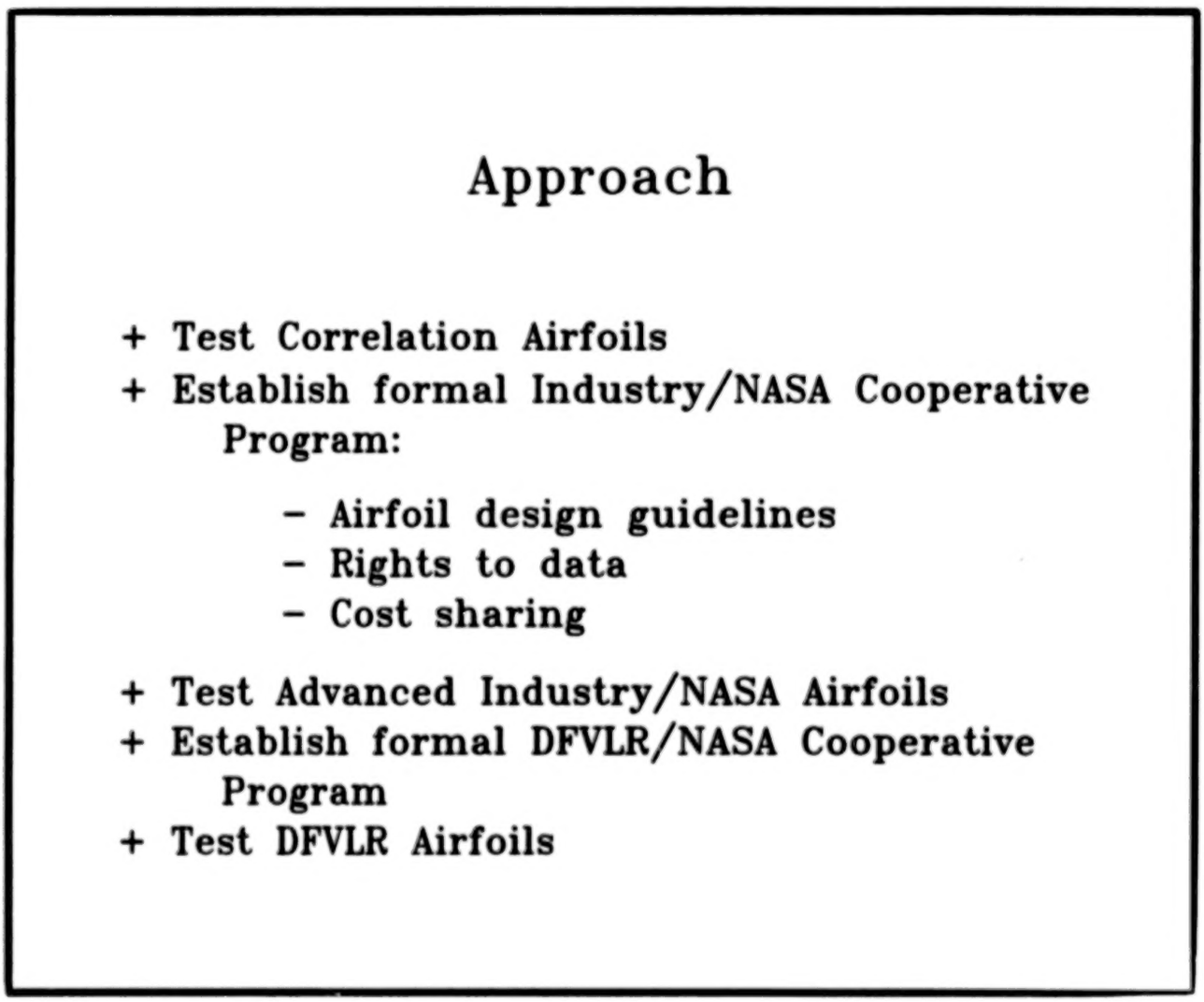

Figure 2

SCHEDULE OF EVENTS

The time schedule for the implementation of this program is presented in figure 3. The preliminary meetings between NASA personnel and the companies involved were held in February of 1980 and formal invitations to participate were sent out in June of the same year. The formal NASA/DFVLR agreement was signed in December. Although tests were begun last November, model tests are not scheduled for completion until mid 1982. Publication of all basic data should be complete within 6 months of the final test program. Detailed analysis of the correlation airfoils with comparisons to other data and theory will be conducted and appropriate results published at a later date.

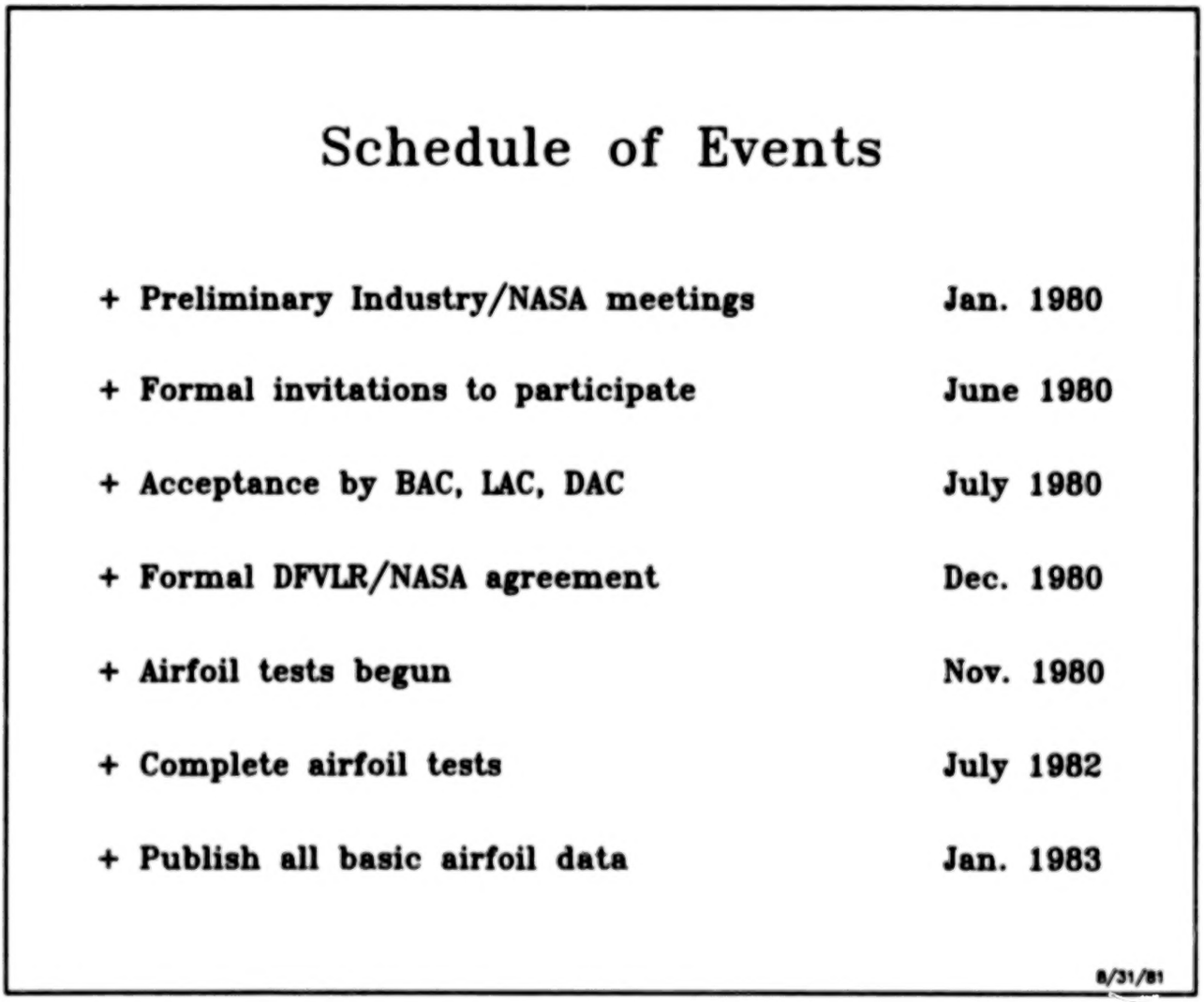

Figure 3

TEST PROGRAM STATUS

A list of each of the airfoil models to be tested in the program, the model status, and scheduled test date are presented in figure 4. Four airfoils are included in the correlation series, two conventional NACA airfoils and two NASA supercritical airfoils. Each of these was chosen since there are other data available, some from high Reynolds number facilities. Of these airfoils, only the NACA 0012 has been tested to date and the data are presently under analysis.

The advanced NASA supercritical airfoil was tested in December, but when removed from the tunnel after completion of the test series, the model was found to be slightly warped in a spanwise direction and a decambering of the trailing edge resulted. This model is being redesigned for future tests, but analysis of the existing data will continue.

Prior to the conception of this joint program, the Boeing Aircraft Company (BAC) had contacted LRC requesting a test program in the LRC 0.3-meter TCT. The model resulting from this earlier contact, designated as the BAC 1, was tested in June 1980 and is included in this program for convenience. The status of the other company models is indicated on figure 4.

Tests of the two models supplied by DFVLR have just been completed and final data plotting and analysis are in progress.

Airfoil Test Program Status

	Status	Test Date
Correlation		
NACA 0012	Complete	Nov. 80
NACA 65-213	Complete	Nov. 81
NASA SC(2)0510	Construction	Nov. 81
NASA SC(2)0714	Redesign	Mar. 82
Advanced NASA		
NASA SC(3)0712A	Available	Dec. 80
NASA SC(3)0712B	Redesign	Feb. 82
Industry Program		
BAC 1	Complete	June 80
BAC 2	Construction	Fall 81
DAC	Design	Spring 82
LAC 1	Construction	Sept. 81
LAC 2	Construction	Sept. 81
DFVLR Program		
Cast 10	Complete	Aug. 81
R-4	Complete	Aug. 81

Figure 4

THE 0.3-METER TRANSONIC CRYOGENIC TUNNEL

A photograph of the LRC 0.3-meter TCT, in which the test program is being undertaken, is shown in figure 5. This tunnel is a continuous flow fan driven transonic tunnel which uses nitrogen gas as the test medium. It is capable of operating at Mach numbers from about 0.2 to 0.85 and the maximum Reynolds number (at M = .85) based on a model chord of 15.24 cm (6.00 in) is about 50×10^6. The basic tunnel is described in reference 1 and a description of the 2-D test section is contained in reference 2. Additional information on instrumentation and calibration results are available in reference 3. Shown in figure 5 are the fan drive section, low speed diffuser, contraction and screen section, test section, and high speed diffuser. Liquid nitrogen injection ports and gaseous nitrogen exhaust ports for pressure control and sidewall boundary layer bleed are also visible. The 2.2 megawatt drive motor is located just off the lower right-hand corner of figure 5.

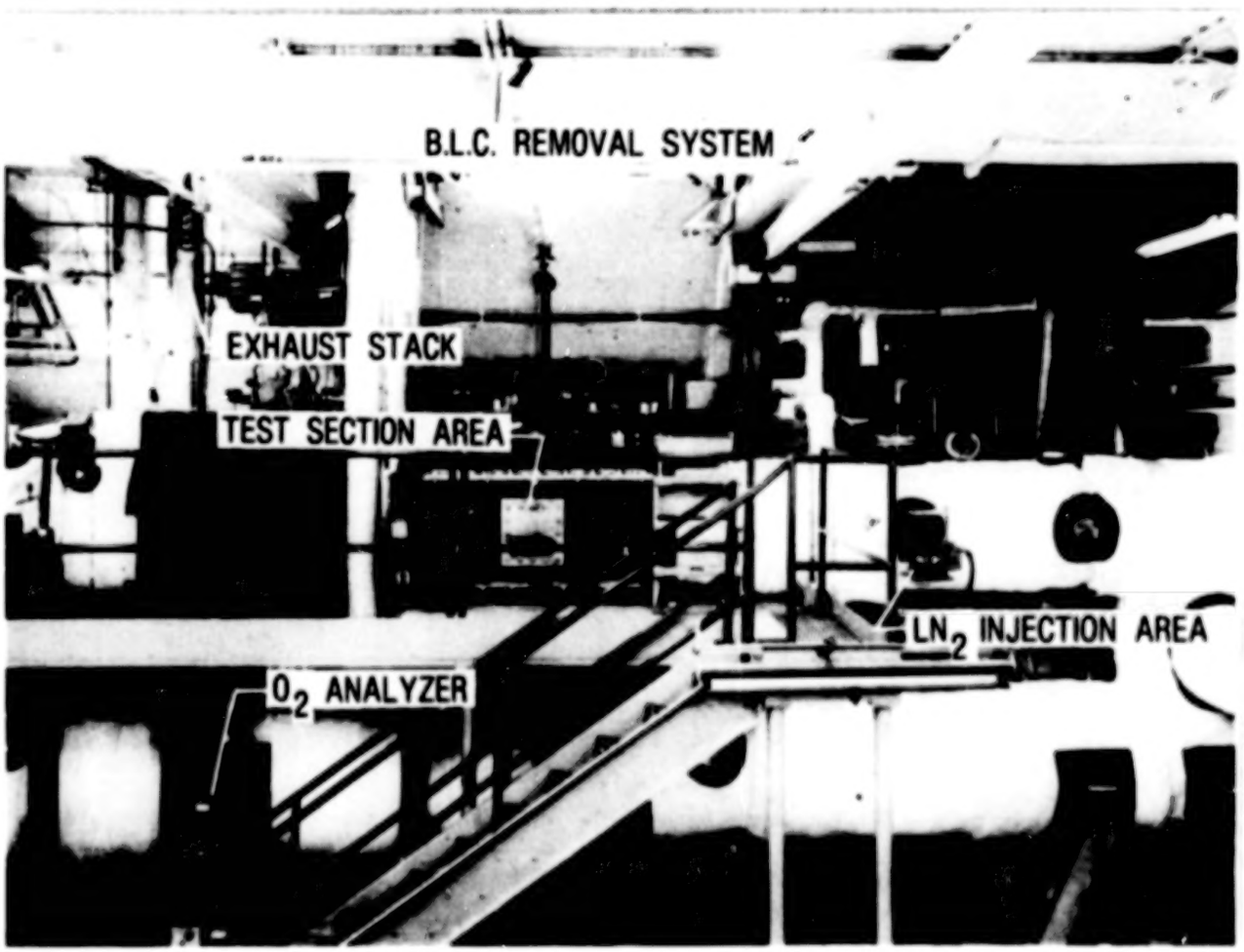

Figure 5

0.3-METER TCT TEST SECTION

A top view of the LRC 0.3-meter TCT test section is shown in figure 6. In this picture, the top of the plenum chamber and the top tunnel slotted wall have been removed. Visible in the photograph are the airfoil model, wake survey probe, angle of attack position encoder, boxes housing a schlieren system, and the bottom slotted wall. Both the top and bottom walls have two slots with an open area ratio of 0.05. The test section has removable sidewall inserts just upstream of the model location. The solid inserts can be removed and porous media installed for removal of the tunnel sidewall boundary layer. By use of this mechanism, the wall effects, due to sidewall boundary layer, can be investigated and reduced or possibly eliminated. At present, the capability of this system is still being investigated and only a very limited amount of data have been obtained.

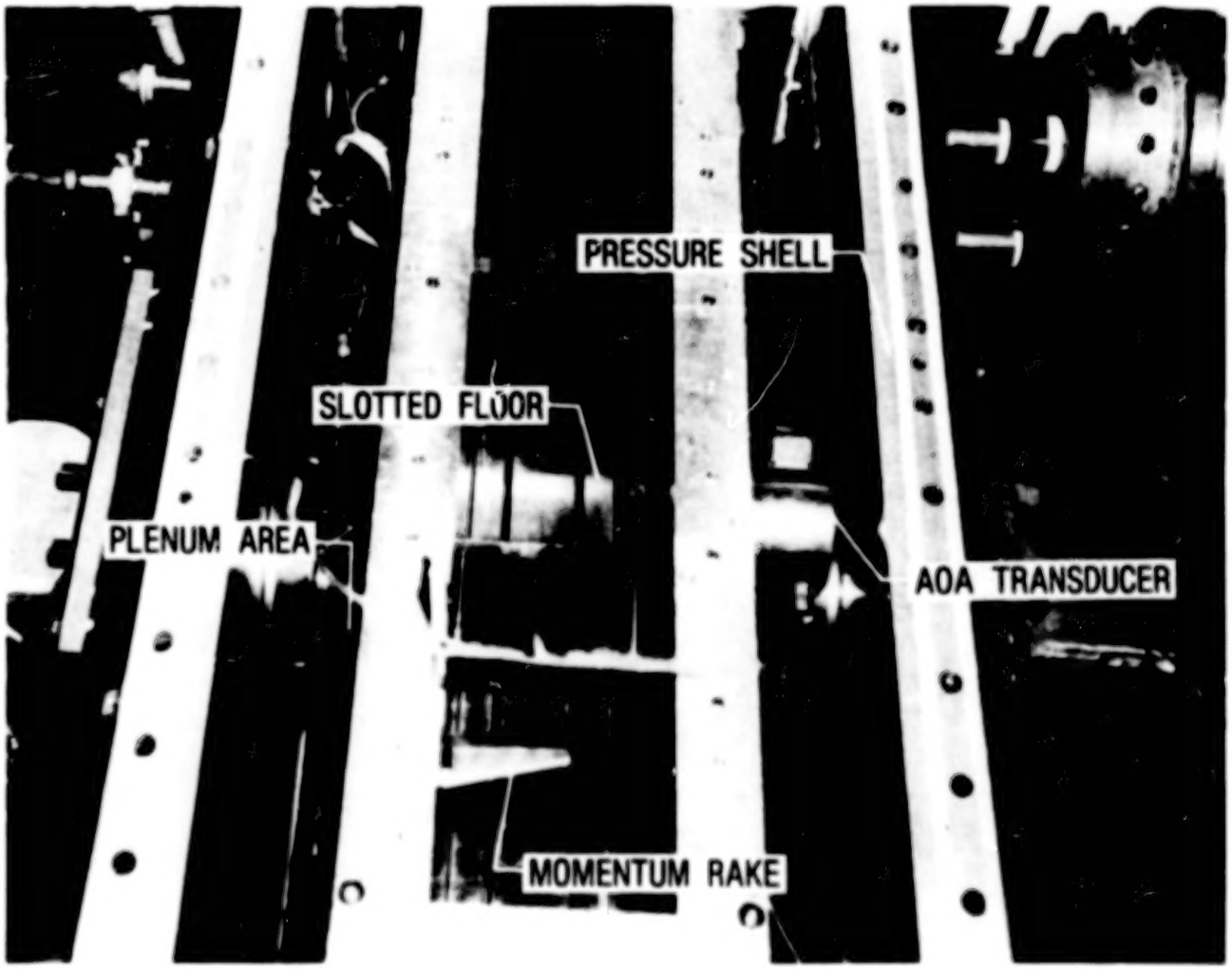

Figure 6

MODEL FABRICATION EXPERIENCE

A tabulation of several of the materials and fabrication methods used to construct airfoil models for the LRC 0.3-meter TCT by both LRC and industry are summarized in figure 7. In general, for the high Reynolds number testing, it was deemed necessary to have all orifice tubing installed interior to the model surface to avoid surface irregularities. The currently accepted approach requires the model being built in two pieces, all tubing installed and checked, and then the two model pieces assembled. Most of the models were machined on a numerical control milling machine to acquire the required surface contour accuracy and then assembled by one of the several techniques listed. Electron beam welding has proved to be successful in many cases, but when used with HP 9-4-20 alloy steel, the welds cracked several days later with no external stress applied. Brazing does not cause the local stresses associated with welding, but does require heating the model to braze temperatures. If tubes have already been brazed in place, care must be taken so that the remelt temperature is not reached during the second braze cycle. Bonding with epoxy as well as mechanical joints are other methods which have been used.

Some work is currently being done with travelling wire EDM techniques to reduce machining time. Another technique under development at LRC is a type of diffusion welding process in which grooves are cut in the model pieces before joining. These grooves then form the internal tubing system for the model, again reducing construction time. This method is described in reference 4. With the time required to design, build, and verify a model for testing taking well over 1 man-year, work on more simplified techniques is well justified.

The time(s) and cost(s) shown for sample 2-D airfoils will undoubtably increase substantially for more complex models (such as NTF series), further justifying additional fabrication research.

Model Fabrication Experience

	Material	Fab. Method	Assembly Technique	Man Hours	Comments
LRC	A-286	N.C. Mill	E.B. Weld	2500	Acceptable
	13-8 (H1150M)	↓	Braze	2000	Acceptable(marginal)
	HP 9-4-20		E.B. Weld	2000	Welds cracked
	15-5 (H1150M)		Epoxy	1000	Distorted during testing
	347		Braze	2000	Distorted-final heat treat
	Nitronic 40		E.B. Weld	2000	Welds cracked
BAC	A-286	N.C. Mill	E.B. Weld	3000	Acceptable
	A-286	EDM	E.B. Weld	2100	In construction
DAC	Nitronic 40	EDM	Braze	~1000	Technique in development
LAC	347	N.C. Mill	Epoxy	2800	Acceptable(marginal)
	347	N.C. Mill	Trench & Solder	900	Evaluate surface tubes
DFVLR	V2A 14301	N.C. Mill	Braze	2200	Acceptable

Figure 7

COMPARISON OF RESULTS

One of the purposes of the comparison airfoil series was to provide data from the LRC 0.3-meter TCT which could be compared to similar data obtained in other facilities. This type of comparison with data from the 8-Foot TPT for a NACA 0012 airfoil (from ref. 5) is presented in figure 8 for a Mach number of 0.3 and a Reynolds number of 3.0×10^6. Although the data generally show very good agreement, the maximum normal force coefficient is slightly lower in the LRC 0.3-meter TCT. Also, the LRC 0.3-meter TCT data show a slightly higher drag coefficient and a more negative pitching moment at the higher normal force coefficients. This is probably the result of a more forward location of the separation point, which, in turn, is caused by the tunnel sidewall boundary layer effects. A tunnel sidewall boundary layer removal system is being incorporated into the facility, but will not be fully operational until late 1982.

The normal force curve slopes are also different as would be expected for uncorrected data. At $c_n = 1.0$, the geometric angle of attack is about one degree higher for the LRC 0.3-meter TCT data. However, the difference in the angle-of-attack correction for the two sets of data is only about 0.2 degrees based on the method of reference 6. Thus, most data comparisons are made at constant normal force coefficients since, as will be discussed later, much improvement in the correlation techniques is needed.

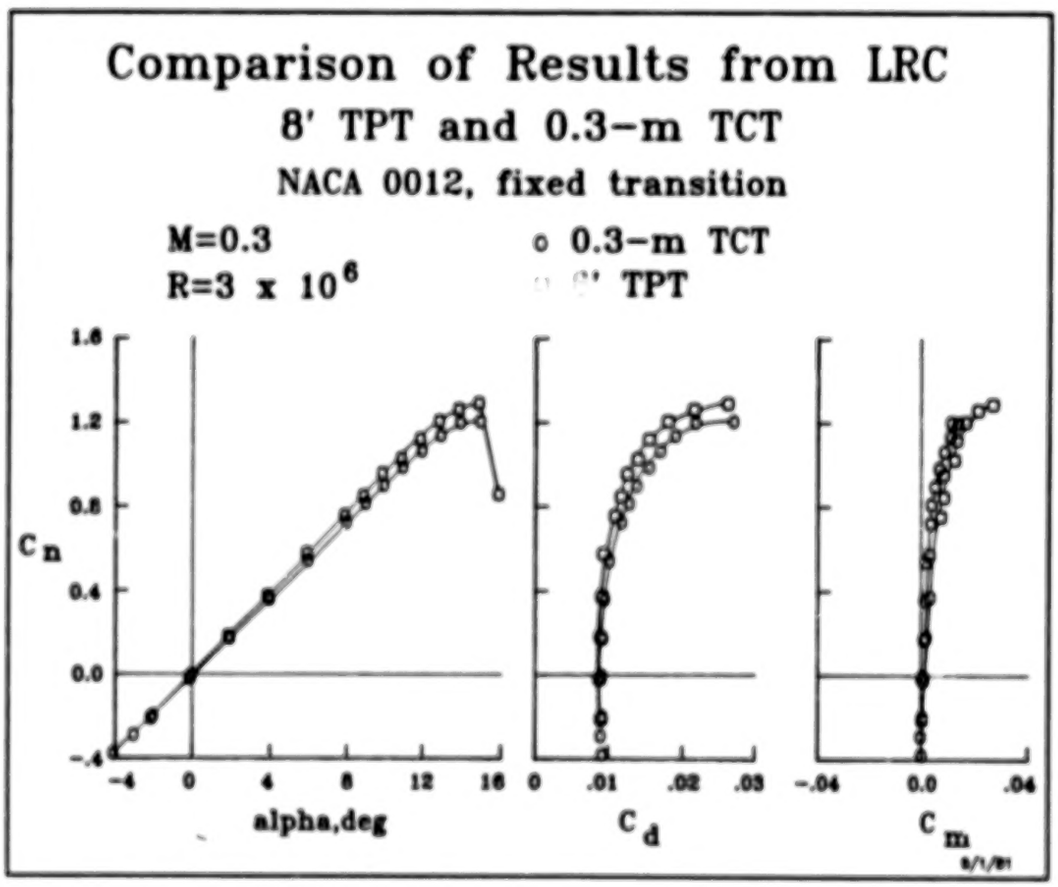

Figure 8

Additional comparisons between the LRC 0.3-meter TCT and the 8-Foot TPT for the NACA 0012 are presented in figure 9 for a Mach number of 0.7 and a Reynolds number of 9.0×10^6. At this higher Mach number supercritical condition, the agreement between the two facilities is essentially the same as was observed for the lower Mach number data shown in figure 8.

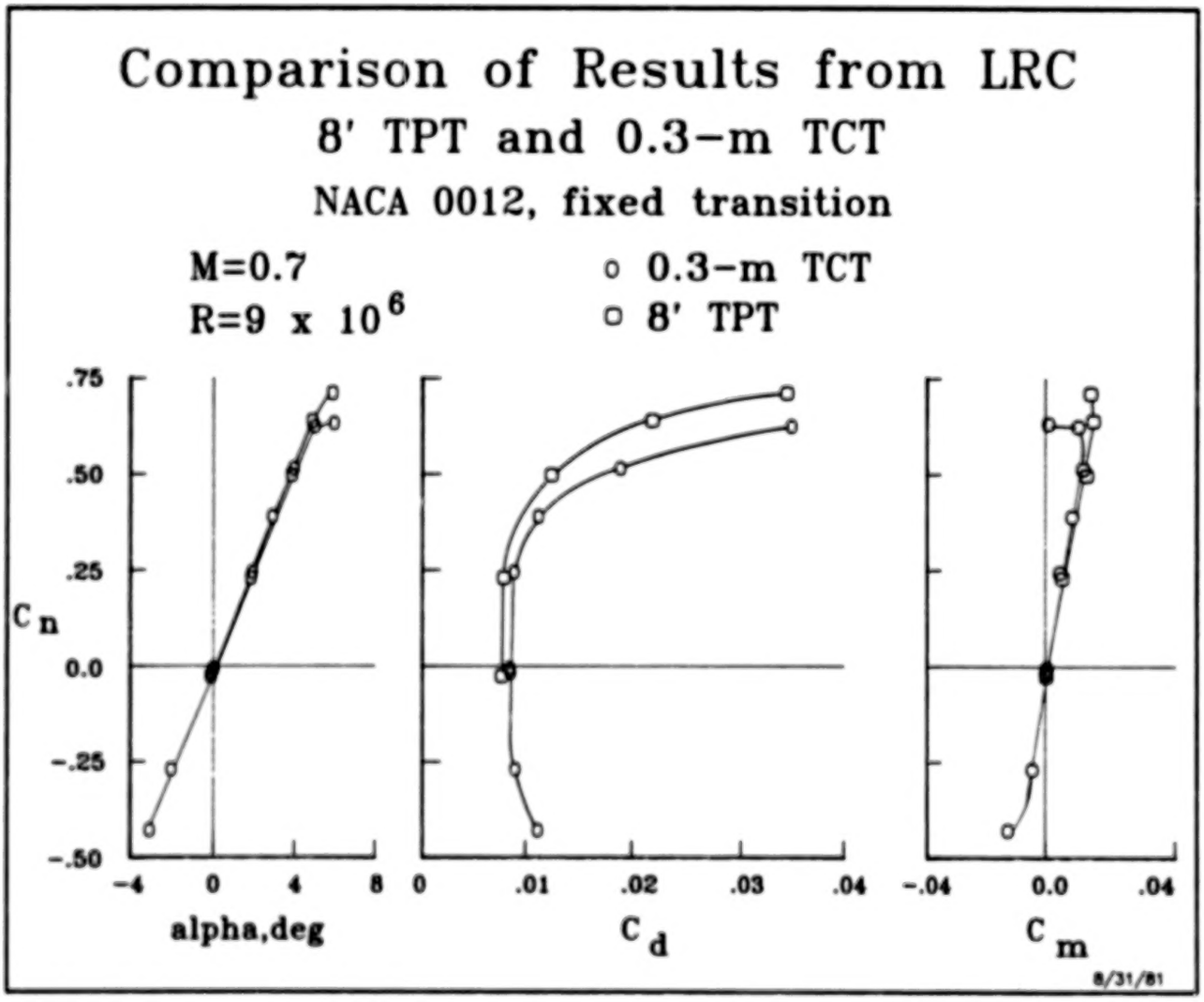

Figure 9

COMPARISON WITH THEORY

Methods for correction of experimental data are currently being improved and expanded at LRC. One method for determining angle of attack and Mach number correction based on tunnel wall measurements has been developed and is discussed in reference 7. The effects of model influence on tunnel sidewall boundary layer have also been investigated and these effects on Mach number are discussed in references 8 and 9. An example of application of these corrections to the experimental data and a comparison with the Grumfoil theory is presented in figure 10.

On the left-hand side of the figure, uncorrected experimental data are compared with theory for the same Mach number and normal force coefficient. Although the general agreement is good, there are areas where sizeable differences in pressure coefficient exist and the shock position is not predicted accurately. When the experimental data are corrected for wall effects and again compared with theory at the same Mach number and normal force coefficient, the agreement is improved greatly. These comparisons, to date, have been for only a limited number of data points. The effects of variables such as Mach number, normal-force coefficient, and airfoil shape have yet to be determined, but research is underway.

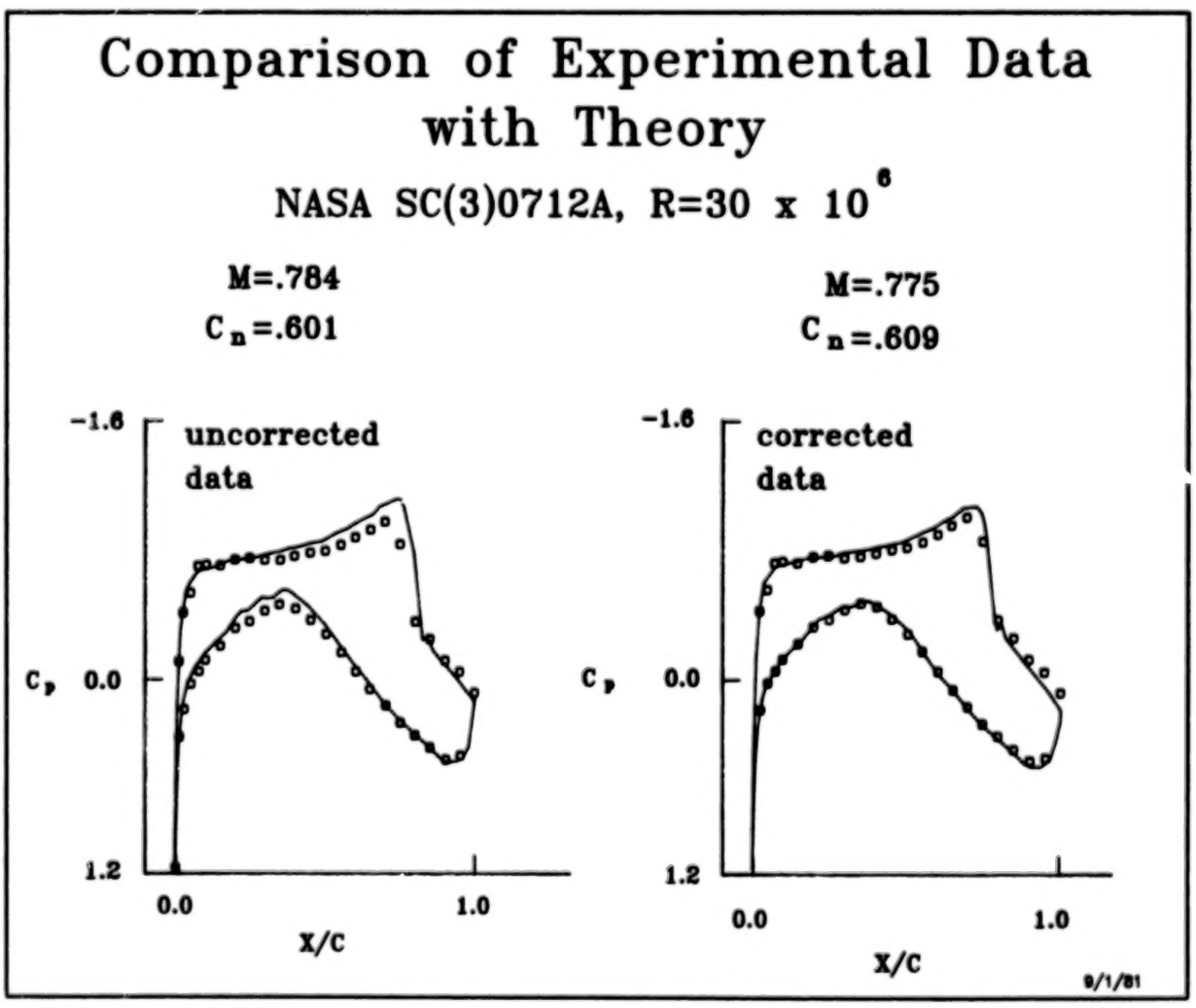

Figure 10

EFFECTS OF REYNOLDS NUMBER ON NORMAL FORCE COEFFICIENT

The effects of Reynolds number on several aerodynamic parameters are presented in figures 11 through 13. Data are shown at lifting conditions for three airfoils: the NACA 0012, the NASA SC(3)0712A, and the BAC 1 airfoils. Data for the NACA 0012 are shown for a normal force coefficient of 0.4; whereas, the remaining airfoils are for 0.6 since the high normal force is above drag rise for this airfoil. The BAC 1 airfoil is about 10 percent thick and would be expected to have different characteristics than the thick airfoils shown.

Plots of normal force coefficient as a function of angle of attack are presented in figure 11 for a Mach number of 0.76. There are no appreciable effects of Reynolds number on the lift curve slope noted for any of the airfoils at this Mach number. However, the two advanced airfoils do exhibit an increase in normal force coefficient as the Reynolds number is increased from the minimum value to 30×10^6. A further increase to about 40×10^6 has only little effect.

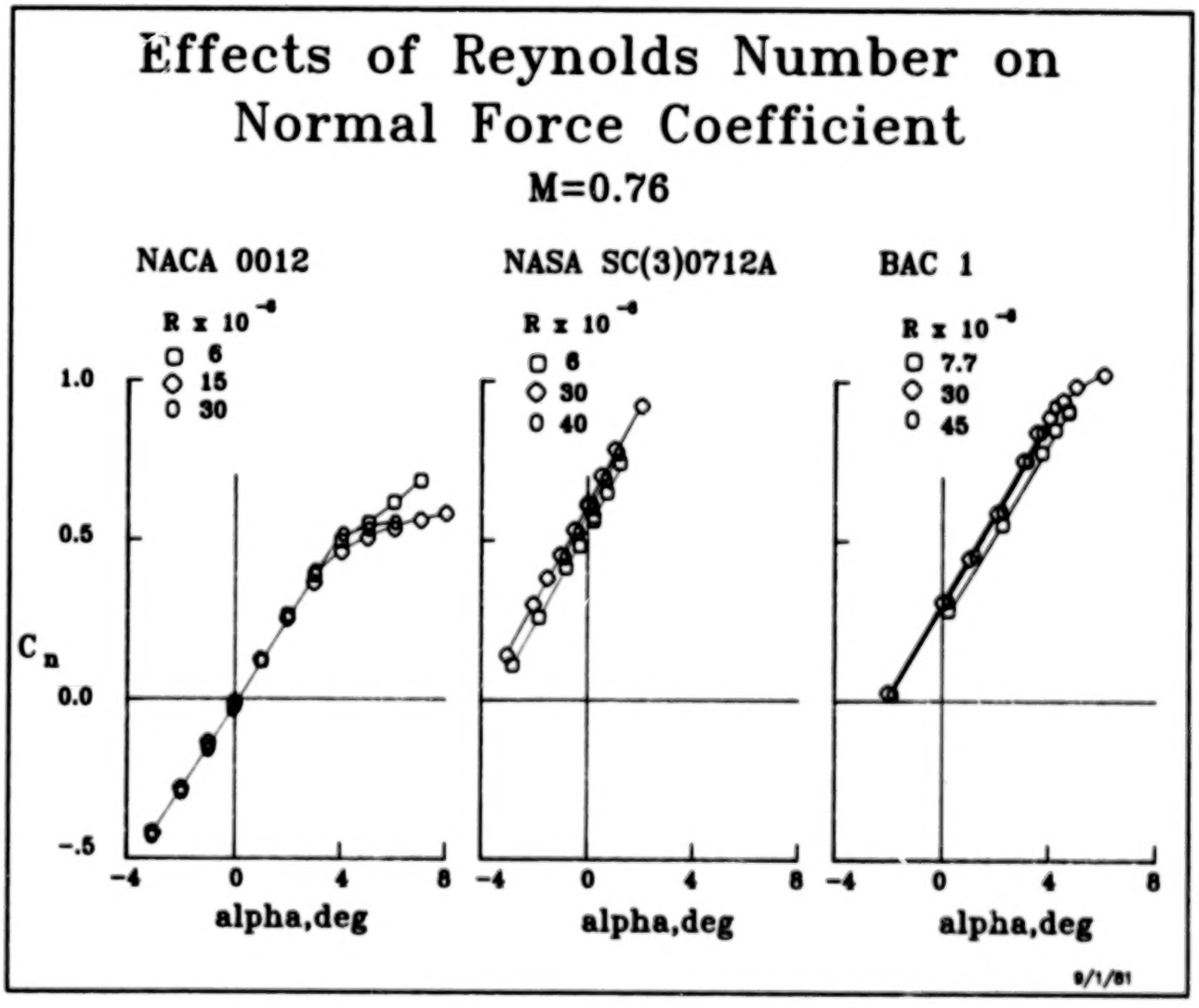

Figure 11

EFFECTS OF REYNOLDS NUMBER ON CENTER OF PRESSURE

The effects of Reynolds number on the variation of longitudinal location of center of pressure with Mach number is shown in figure 12 for the same three airfoil shapes as in figure 11. The NACA 0012 airfoil shows essentially no effect of Reynolds number, whereas, the two advanced airfoil shapes indicate a rearward movement with increasing Reynolds number. The effects of increasing R_c from 30 to about 40 x 10^6 are very slight, however. Other than the slight rearward shift (about 4 percent chord at the higher Mach number), no effects of R_c are observed for these test conditions.

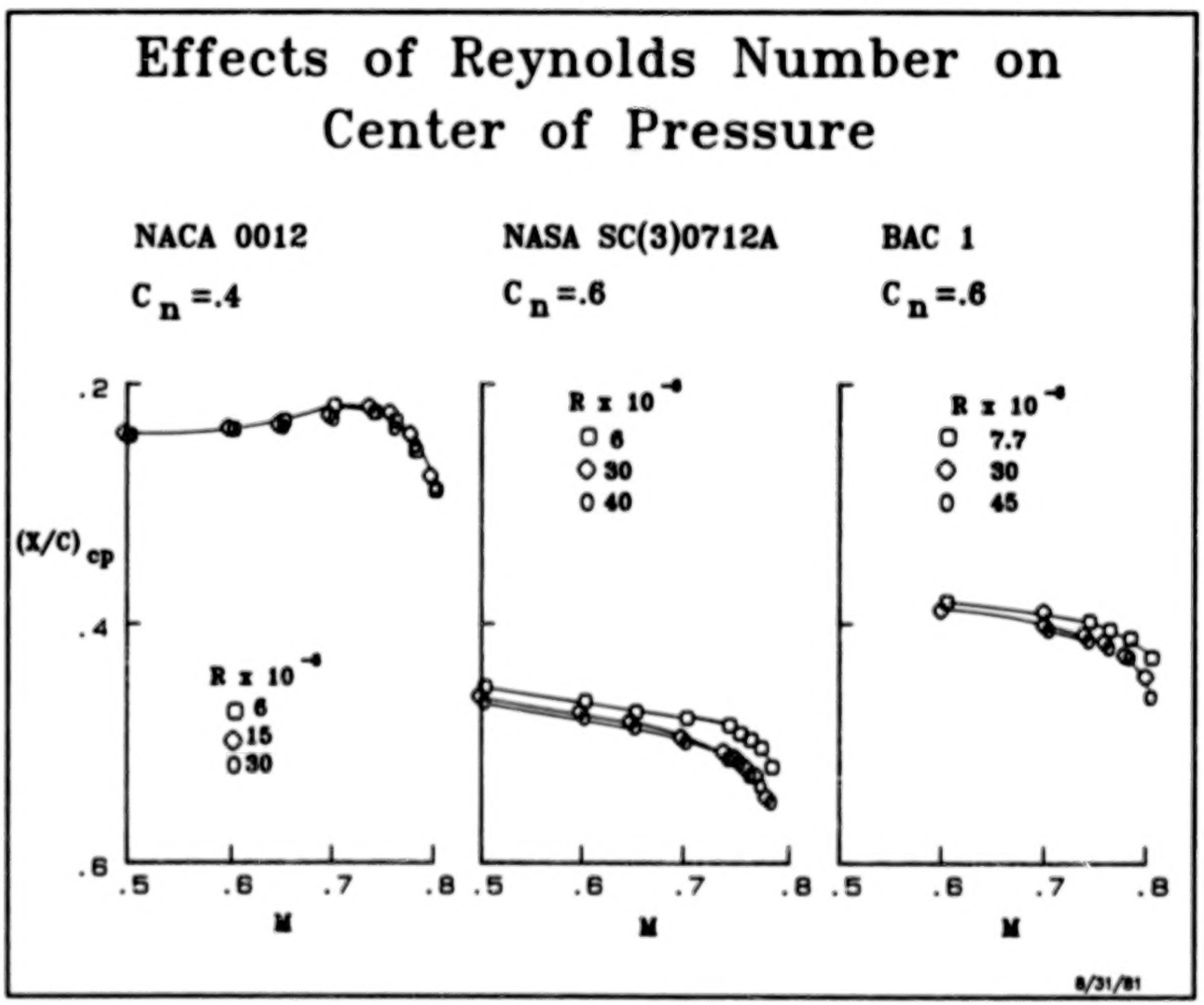

Figure 12

EFFECTS OF REYNOLDS NUMBER ON DRAG COEFFICIENT

The variations in drag coefficient with Mach number and Reynolds number for the three airfoil shapes are shown in figure 13. At the lower Mach number, the drag is constant with Mach number for the NACA 0012, whereas, the SC(3)0712A shows a continual gradual rise. This rise (or drag creep) is also evident for the BAC 1 at the lower Reynolds number, but tends to decrease with increasing Reynolds number. There is very little effect of Reynolds number on the drag rise Mach number for the two advanced technology airfoils.

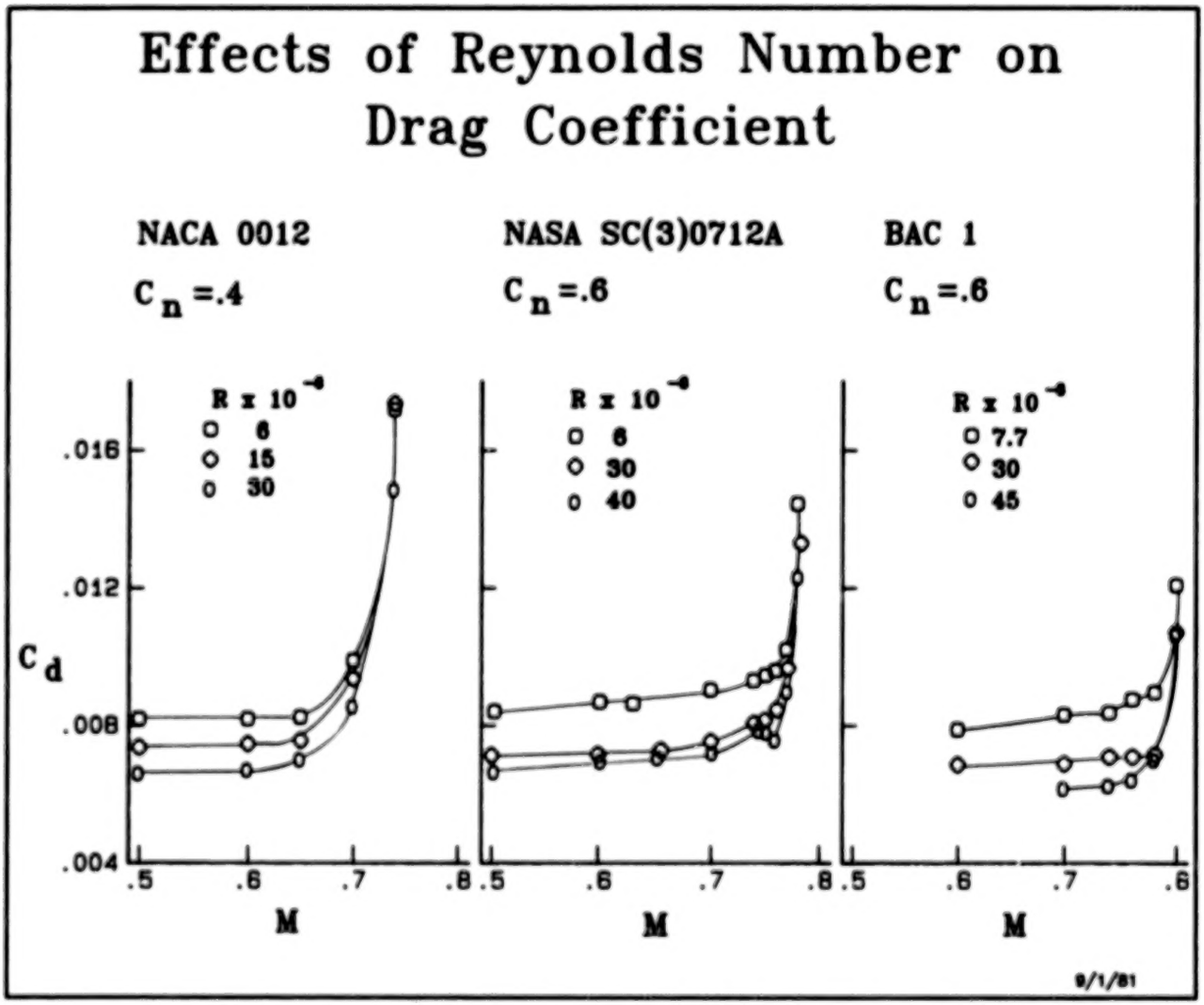

Figure 13

SUMMARY

Formal airfoil testing programs with both U.S. industry and the DFVLR have been established. Construction for all models to be tested in the program is well underway and the test program is nearing 50 percent completion. The test results, comparisons with other facilities, and comparison with theory have provided a valuable high R_c addition to the airfoil technology base and will undoubtedly be further enhanced with continued analysis and correlation of the data. The cooperative test program is scheduled to be completed during the summer of 1982 and all basic data are expected to be released for public dissemination by the end of that year.

Summary

+ **Formal Cooperative Programs with U.S. Industry and DFVLR established**
+ **Model construction problems and solutions identified; all models either under construction or complete**
+ **Test program in progress and results to date appear satisfactory**
+ **Test program should be complete in about one year and all basic data published by Jan. 1983**

REFERENCES

1. Kilgore, Robert A.: Design Features and Operational Characteristics of the Langley 0.3-Meter Transonic Cryogenic Tunnel. NASA TN D-8304, 1976.

2. Ray, Edward J.; Ladson, Charles L.; Adcock, Jerry B.; Lawing, Pierce L.; and Hall, Robert M.: Review of Design and Operational Characteristics of the 0.3-Meter Transonic Cryogenic Tunnel. NASA TM-80123, 1979.

3. Ladson, Charles L. and Kilgore, Robert A.: Instrumentation for Calibration and Control of a Continuous - Flow Cryogenic Tunnel. NASA TM-81825, 1980.

4. Kilgore, Robert A.: Model Design and Instrumentation Experiences With Continuous - Flow Cryogenic Tunnels. AGARD LS-111m 1980.

5. Harris, Charles D.: Two-Dimensional Aerodynamic Characteristics of the NACA 0012 Airfoil in the Langley 8-Foot Transonic Pressure Tunnel. NASA TM-81927, 1981.

6. Barnwell, Richard W.: Design and Performance Evaluation of Slotted Walls for Two-Dimensional Wind Tunnels. NASA TM-78648, 1978.

7. Kemp, William B., Jr.: Transonic Assessment of Two-Dimensional Wind Tunnel Wall Interference Using Measured Wall Pressures. NASA Conference Publication 2045, March 1978, pp. 473-486.

8. Barnwell, Richard W.: Similarity Rule for Sidewall Boundary-Layer Effect in Two-Dimensional Wind Tunnels. AIAA Journal, Vol. 18, No. 9, September 1980, pp. 1149-1151.

9. Sewall, William G.: The Effects of the Sidewall Boundary Layers on Two-Dimensional Subsonic and Transonic Wind Tunnels. AIAA Fourteenth Fluid and Plasma Dynamic Conference, 1981.

LANGLEY HIGH-LIFT RESEARCH ON A HIGH-ASPECT-RATIO SUPERCRITICAL WING CONFIGURATION

Harry L. Morgan, Jr., and Scott O. Kjelgaard
NASA Langley Research Center

Abstract

To determine the low-speed performance characteristics of a representative high-aspect-ratio supercritical wing, two low-speed jet transport models were fabricated. A 12-ft. span model was used for low Reynolds number tests in the Langley 4- by 7-Meter Tunnel and the second, a 7.5-ft. span model, was used for high Reynolds number tests in the Ames 12-Foot Pressure Tunnel. A brief summary of the results of the tests of these two models is presented and comparisons are made between the data obtained on these two models and other similar models. Follow-on two- and three-dimensional research efforts related to the EET high-lift configurations are also presented and discussed.

INTRODUCTION

The rapid worldwide increase in the consumption and price of crude oil in recent years has generated a renewed interest by many government and private research organizations in ways of improving the energy efficiency of vehicles that use fuels distilled from crude oil. In particular, NASA has been actively involved in an aeronautical research project to improve the energy efficiency of modern wide-body jet transport aircraft. The Aircraft Energy Efficiency (ACEE) project was formulated to stimulate research efforts by both industry and NASA. One element of the ACEE project is the Energy Efficient Transport (EET) program which is concerned primarily with the development of advanced aerodynamic and active-controls technology for application to derivative or next-generation transport aircraft. One part of the EET program has been the aerodynamic development, by NASA Langley Research Center (LaRC) personnel, of advanced supercritical wings with greater section thickness-chord ratios, higher aspect ratios, higher cruise lift coefficients, and lower sweepback than the conventional wings on current transports. These advanced supercritical wings have been tested extensively in the LaRC wind tunnels to determine their high-speed cruise performance characteristics (ref. 1 and 2). Because of their high cruise lift coefficients and high aspect ratios, these wings could be smaller and more fuel efficient than conventional wings, provided the low-speed, high-lift performance requirements could be met.

To determine the low-speed performance characteristics of a representative high-aspect-ratio supercritical wing, two low-speed jet transport models were fabricated, one for low Reynolds number tests in the Langley 4- by 7-Meter Tunnel and the other, smaller model, for high Reynolds number tests in the Ames 12-Foot Pressure Tunnel. The data presented represent some of the highlights from the low-speed tests of these two models. Presented also are current plans for research efforts following the determination of the present EET programs. The follow-on efforts consist of the low-speed two- and three-dimensional research being proposed by personnel of both the Transonic Aerodynamics Division and the Low-Speed Aerodynamics Division.

12-FOOT-SPAN EET HIGH-LIFT MODEL

The first model tested to determine the low-speed characteristics of a representative high-aspect-ratio supercritical wing was a 3.66-meter (12-foot) span low-speed transport model. This model was equipped with conventionally sized part- and full-span, double-slotted trailing-edge flap systems, full-span leading-edge slat, low- and high-speed ailerons, spoilers, and interchangeable aspect-ratio-12 and aspect-ratio-10 wing tips. Wind-tunnel tests were conducted in the Langley 4- by 7-Meter Tunnel at free-stream conditions corresponding to Reynolds numbers (based on the mean geometric chord) of 0.97 to 1.63 x 10^6 and corresponding Mach numbers of 0.12 to 0.20, through an angle-of-attack range of -4^o to 24^o and a side-slip-angle range of -10^o to 5^o. The results of these tests are presented in detail in references 3 and 4. Presented in figure 1 are photographs of the part- and full-span configurations mounted on an aft-support sting system in the Langley 4- by 7-Meter Tunnel (formerly V/STOL).

PART-SPAN TWO-SEGMENT FLAPS

FULL-SPAN FLAPS

MODEL MOUNTED IN V/STOL TUNNEL

Figure 1

L-78-7523

DESCRIPTION OF EET HIGH-LIFT MODEL

The leading-edge slat, trailing-edge flap, and spoiler and aileron control surface areas were sized and positioned spanwise on the basis of a comparative analysis of several existing designs for aspect-ratio-6 to aspect-ratio-8 transport wings. The basic planform details of the part-span trailing-edge flap configuration are presented in figure 2. The trailing-edge flap was a double-slotted design that consisted of an advanced-design, large-vane and small-aft-flap combination in comparison with the more conventional, small-vane and large-aft-flap combinations. The model was fabricated with aluminum wings and empennage and glass-fiber fuselage. The empennage consisted of movable horizontal tails without elevators and a fixed vertical fin without a rudder. The horizontal tails were mounted on the model with a geared, pivoting bracket that allowed for incidence angles from -15° to 15° in 5° increments. The model was also equipped with two, wing-mounted, flow-through nacelles with scaled external dimensions similar to those of a typical high-bypass-ratio (approximately 6) turbofan engine. The model was also equipped with simulated landing gear and doors. The basic cruise-wing dimensions are the same as those of the SCW-2a wing reported in reference 1. This wing had a 27° quarter-chord sweep; an inboard trailing-edge extension that increased the root chord by 40 percent; and streamwise supercritical sections with maximum thickness-chord ratios of 0.144 at the side-of-body station, 0.120 at the trailing-edge-break station, and 0.100 at the wing tip (aspect-ratio-12).

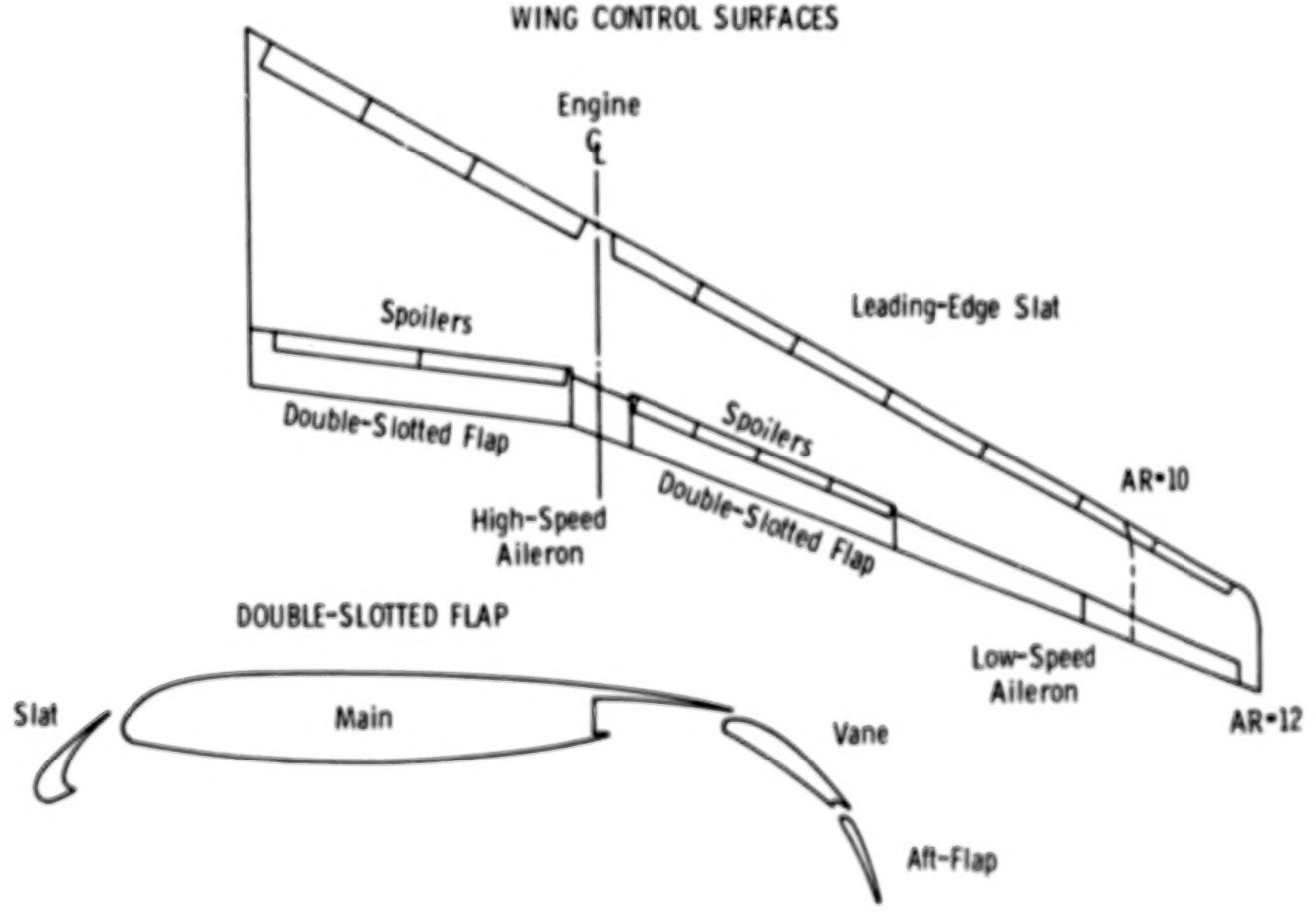

Figure 2

WING CONFIGURATIONS FOR 12-FOOT-SPAN EET MODEL

The EET High-Lift Model was fabricated with removable leading- and trailing-edge segments. The cruise-wing segments could be removed easily and replaced with a leading-edge slat and trailing-edge spoiler/flap and aileron segments. Although many wing configurations were possible, six basic wing configurations were tested: (1) cruise (slats and flaps nested); (2) climb (slats deflected and flaps nested); (3) part-span flaps; (4) full-span flaps; (5) full-span flaps with low-speed ailerons; and (6) full-span flaps with high-speed ailerons. A sketch of the basic planform of each wing configuration is presented in figure 3. Each of the four flapped-wing configurations was tested with the full-span leading-edge slat and the trailing-edge flap segments deflected to settings representative of both take-off and landing conditions. The leading-edge slat was deflected to -50^{0} for climb, take-off, and landing conditions and the trailing-edge flaps were deflected to 30^{0} for take-off and 60^{0} for landing. The wing was also instrumented with chordwise rows of surface static-pressure taps at three spanwise stations. The pressure data obtained during the tests in the Langley 4- by 7-Meter Tunnel are presented in references 5, 6, and 7.

WING CONFIGURATIONS FOR 12-FOOT-SPAN EET MODEL

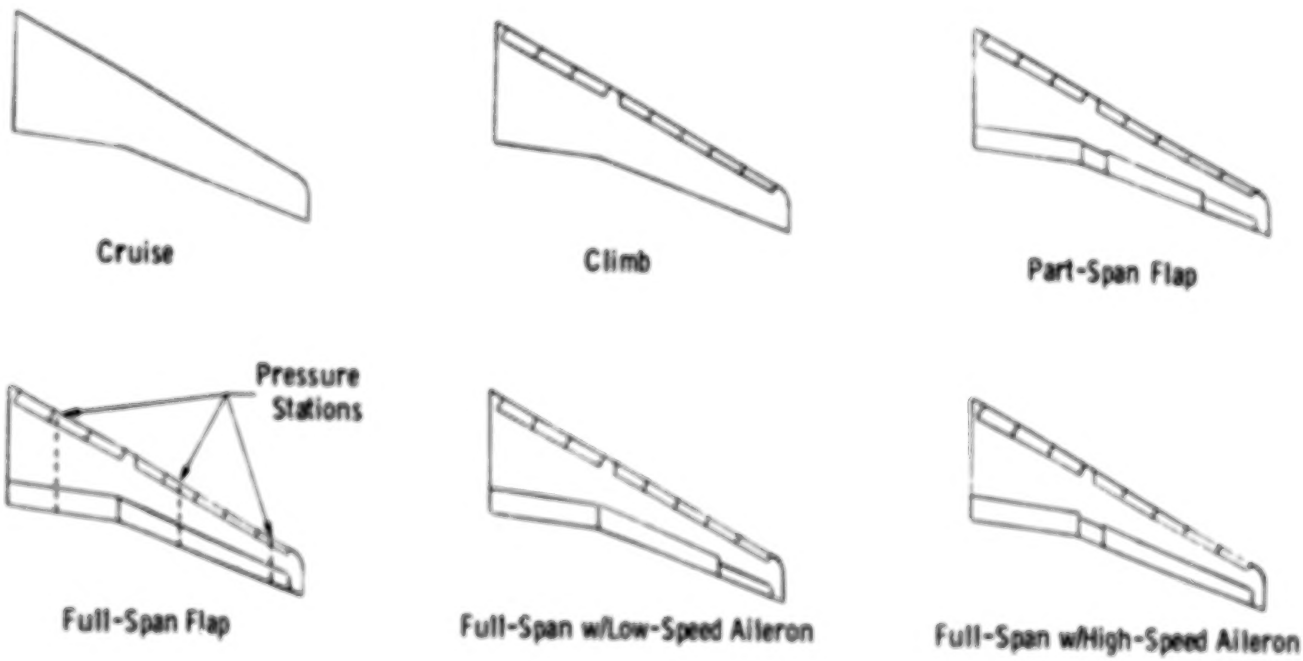

Figure 3

$C_{L,max}$ PERFORMANCE OF 12-FOOT-SPAN EET MODEL IN 4- BY 7-METER TUNNEL

A summary of the $C_{L,max}$ performance of the 12-foot-span, EET high-lift model from tests in the Langley 4- by 7-Meter Tunnel are presented in figure 4. The data presented show a comparison between the trimmed (tail-on) and untrimmed (tail-off) $C_{L,max}$ characteristic of the six basic wing configurations tested. The leading-edge slat was deflected -50° for the climb and flapped-wing configurations and the trailing-edge flaps were deflected to 60° (landing) for the flapped-wing configurations. Each of the six wing configurations show the expected result of a loss in $C_{L,max}$ due to the negative horizontal-tail loads required to trim the model. Both wing configurations, full-span flaps and full-span flaps with high-speed ailerons, had higher untrimmed $C_{L,max}$ capabilities than the wing configurations with part-span flaps and with full-span flaps with low-speed ailerons. However, the trim load requirements reduced the trimmed $C_{L,max}$ capability of the four flapped-wing configurations to about the same level. In fact, the wing configuration having full-span flaps with low-speed ailerons had a slightly higher $C_{L,max}$ than the other three flapped-wing configurations.

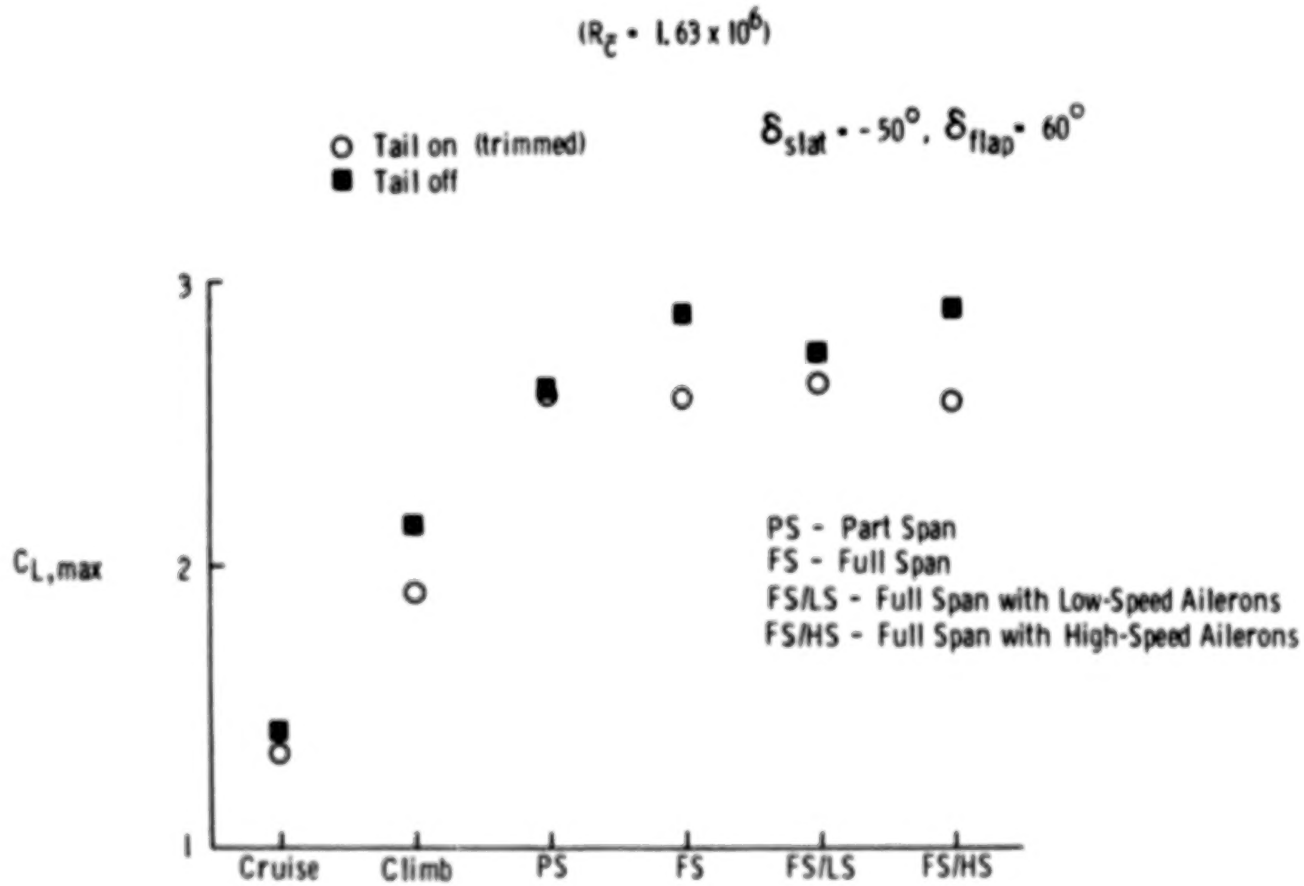

Figure 4

7.5-FOOT-SPAN EET HIGH-LIFT MODEL

Prior research by both industry and NASA on high-lift models similar to the EET configuration has indicated that Reynolds number often has tremendous effects on the performance of high-lift systems. The highest Reynolds number, based on mean aerodynamic chord, obtained for the 12-foot span EET high-lift model in the Langley 4- by 7-Meter Tunnel was 1.63×10^6. In order to obtain higher Reynolds-number data, a 2.29-meter (7.5-foot) span model with identical 0.625-scaled dimensions of the 3.66-meter (12-foot) span model was built for tests in the Ames 12-Foot Pressure Tunnel. The Ames tunnel has a maximum Reynolds number of 6×10^6 per foot at a Mach number of 0.20 which represents a maximum Reynolds number, based on mean aerodynamic chord, of 4.2×10^5 for the 7.5-foot-span model. This model was fabricated with steel wings, aluminum empennage, and glass-fiber fuselage. This smaller model only had a part-span trailing-edge flap system, but two additional flap deflections of 15^o take-off and 45^o landing were available. The full-span leading-edge slat had additional deflections of -30^o, -40^o, and -60^o. The horizontal tails were mounted to a remotely controlled gear-drive system.

The Ames model support system consisted of a tandem strut support system. The model was pitched about the main strut pivot point and was powered by the aft pitch strut. This strut system caused an acceleration of the flow on the lower surfaces of the model which produced interference loads. In order to determine the magnitude of these interference loads, tests were conducted in the Langley 4- by 7-Meter Tunnel with the 7.5-foot-span model mounted to the Ames strut support system and the LaRC aft-support sting system. Additional tests were also conducted with the model mounted to the newly constructed LaRC telescoping strut support. A photograph of this new telescoping strut and the sting-mounted model is shown in figure 5.

Figure 5 L-80-9085

EFFECTS OF STRUT ON PERFORMANCE OF EET HIGH-LIFT MODEL IN LANGLEY 4- BY 7-METER TUNNEL

A sample of the results of the tests to determine the strut interference loads is presented in figure 6. These results show the expected positive increments in the lift and pitching-moment coefficients due to the acceleration of the flow on the lower surface of the model. The strut appears to have very little effect on the drag coefficient; however, it is believed that the drag increments were within the error band of the particular strain-gage balance used during the initial tests. The balance was sized primarily for the tests in the Ames tunnel at dynamic pressure conditions five times greater than those in the LaRC tunnel. A more properly sized, smaller load balance was used during the second tests with the model mounted on the LaRC telescoping strut; however, the drag increments still appear to be very small. Additional tests are planned to further examine the interference effects of the strut with particular attention to drag interference.

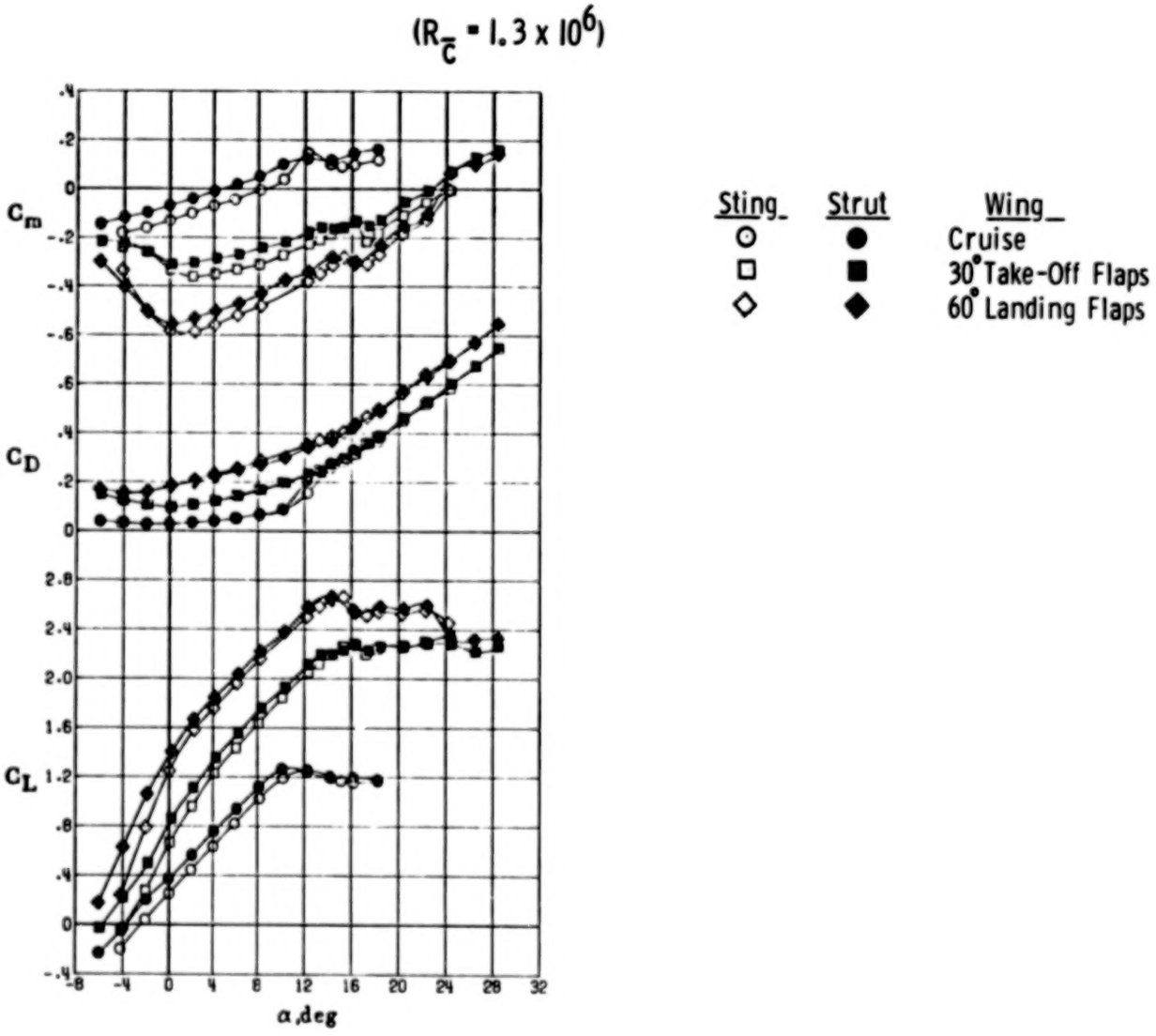

Figure 6

PERFORMANCE COMPARISON OF 7.5- AND 12-FOOT-SPAN MODELS FROM TESTS IN LANGLEY 4- BY 7-METER TUNNEL

A comparison of the performance of the 7.5- and 12-foot span EET high-lift models from tests in the Langley 4- by 7-Meter Tunnel are presented in figures 7 and 8. Both models were sting mounted and the horizontal tails were off. The data for the two models are in excellent agreement at angles of attack below stall. At angles at attack above stall, there are considerable differences between the data for the two models with the climb, 30° take-off, and 60° landing wing configurations. The 7.5- foot span model consistently stalled at angles of attack from 4° to 5° lower than those for the 12-foot span model. It was initially believed that this premature stall was due to some type of balance fouling; however, this was ruled out when identical stall trends occurred with the model mounted on the strut support system. The increase in negative pitching moment after the premature stall indicates an inboard separation of the flow either on the leading-edge slat or the trailing-edge flap. An analysis of the very limited pressure data obtained did not indicate where the inboard separation occurred. For some unexplained reason, this stall tendency did not occur during the tests of the 7.5-foot span model in the Ames tunnel. The stall angles that occurred during the Ames tests are in close agreement with those for the 12-foot span model.

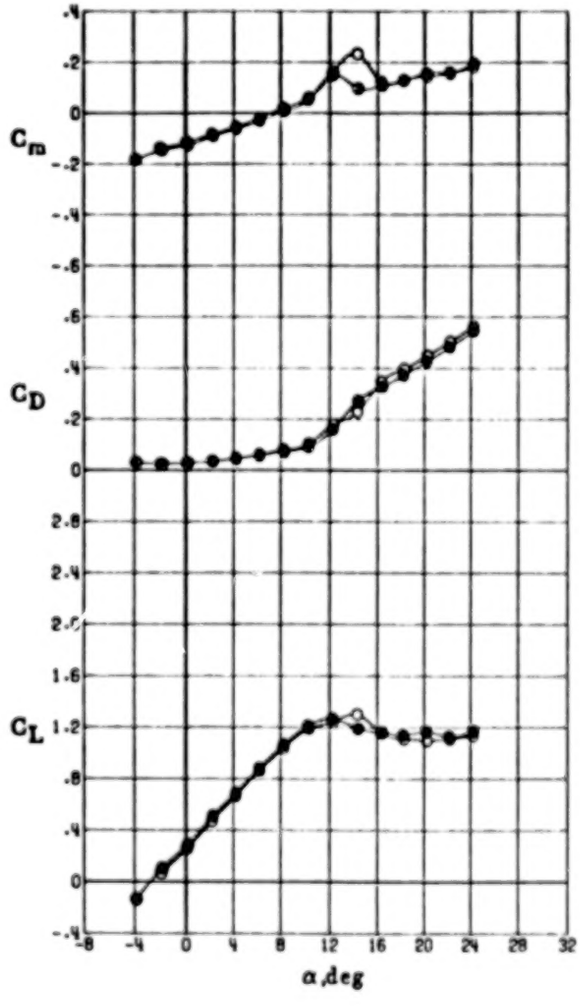

Sting Mount

12-Ft	7.5-Ft	Wing
○	●	Cruise

($R_{\bar{c}} = 1.3 \times 10^6$)

Figure 7

PERFORMANCE COMPARISON OF 7.5- AND 12-FOOT-SPAN MODELS
FROM TESTS IN LANGLEY 4- BY 7-METER TUNNEL

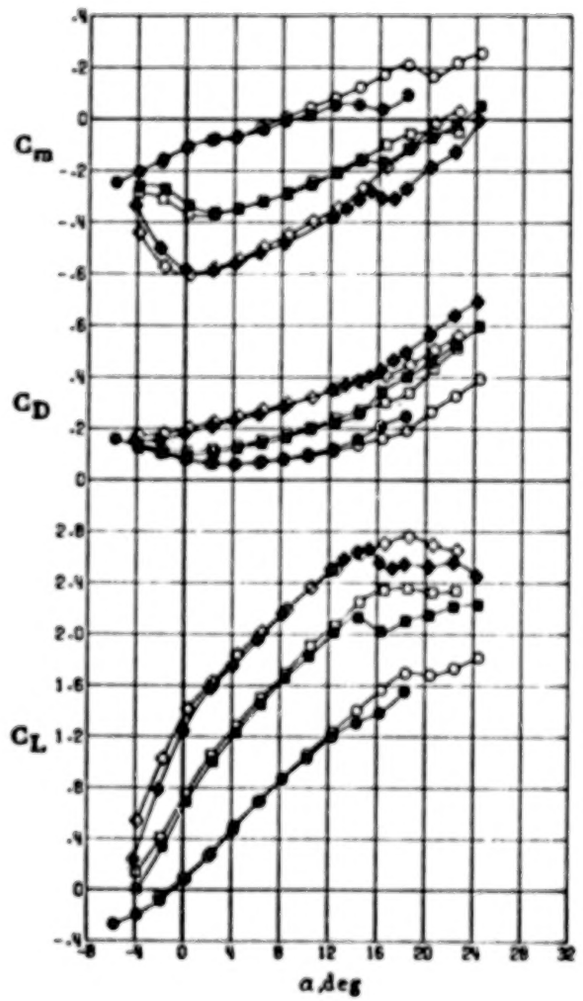

Sting Mount

12-Ft	7.5-Ft	Wing
○	●	Climb
□	■	30° Flaps
◇	◆	60° Flaps

($R_{\bar{c}} = 1.3 \times 10^6$)

Figure 8

SUMMARY OF EET HIGH-LIFT MODEL PERFORMANCE FROM TESTS IN AMES 12-FOOT TUNNEL

Following the tests of the 7.5-foot span model in the Langley 4- by 7-Meter Tunnel, tests were conducted in the Ames 12-Foot Pressure Tunnel. A photograph of the model mounted on the strut support system in the Ames tunnel is presented in figure 9. The tests were conducted in the Ames tunnel at total pressures from 1 to 5 atmospheres with a free-stream Mach number of 0.20 which corresponds to a Reynolds-number range of 1.3 to 6.0 x 10^6 per foot (0.9 to 4.2 x 10^6 based on mean aerodynamic chord).

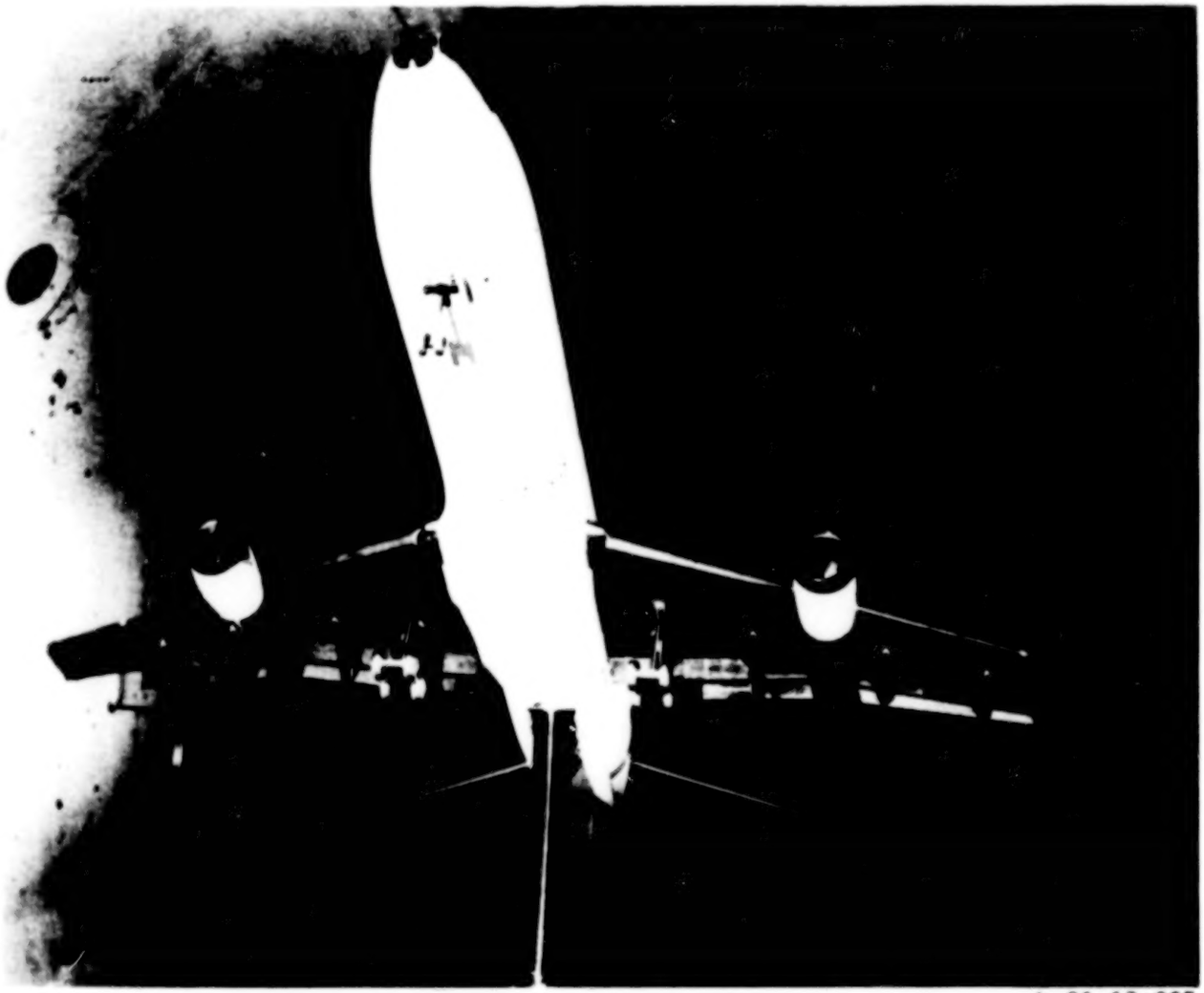

L-81-10,365

Figure 9

SUMMARY OF EET HIGH-LIFT MODEL PERFORMANCE FROM TESTS IN AMES 12-FOOT TUNNEL

A summary of the tail-off performance of the configurations tested is presented in figure 10. These data show the expected increase in lift, drag, and negative pitching-moment coefficients with an increase in flap deflection. The value of the incremental increase in performance also decreased with an increase in flap deflection. In fact, an increase in the flap deflection from 45° to 60° produced only about one half the increment in performance obtained by an increase in deflection from 30° to 45° and only a very small increase in $C_{L,max}$ was obtained above that for 45° deflection. The rapid increase in drag coefficient and a positive shift in pitching-moment coefficient and angle of attack above 16° for the 60° flap deflection indicates a loss of lift near the wing tips and, therefore, an undersirable loss in $C_{L,max}$.

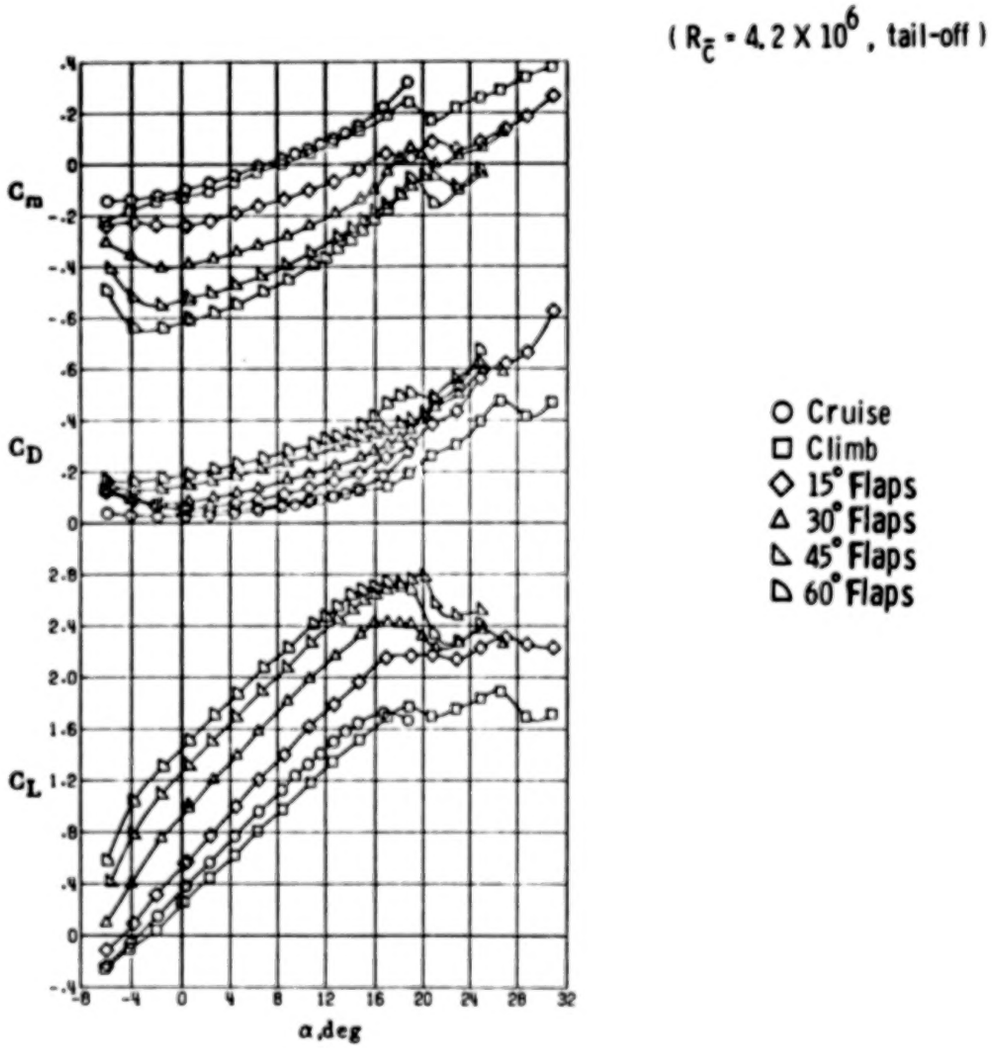

Figure 10

EFFECT OF REYNOLDS NUMBER ON $C_{L,max}$ PERFORMANCE

The effects of an increase in Reynolds number of the tail-off $C_{L,max}$ capabilities of the six wing configurations tested are presented in figure 11. These data show a rather large increase in $C_{L,max}$ for the cruise-wing configuration and small increases in $C_{L,max}$ for the climb and four flapped-wing configurations. The climb and four flapped-wing configurations had almost no increase in $C_{L,max}$ for Reynolds number above 4×10^6 per foot. In contrast, the Douglas Advanced Commercial Aircraft (ACA), which has a similar wing planform and leading-edge slat and trailing-edge flap system, had a rather large increase in $C_{L,max}$ over the same Reynolds-number range as reported in reference 8. This difference in the effects of Reynolds number on the performance of these two apparently similar models cannot be fully explained at this time; however, some small differences do exist between the planforms of the two models and the positions and deflections of the ACA have been optimized for maximum performance. This difference in performance further enhances the problem of reliably predicting the influence of Reynolds number on high-lift system performance.

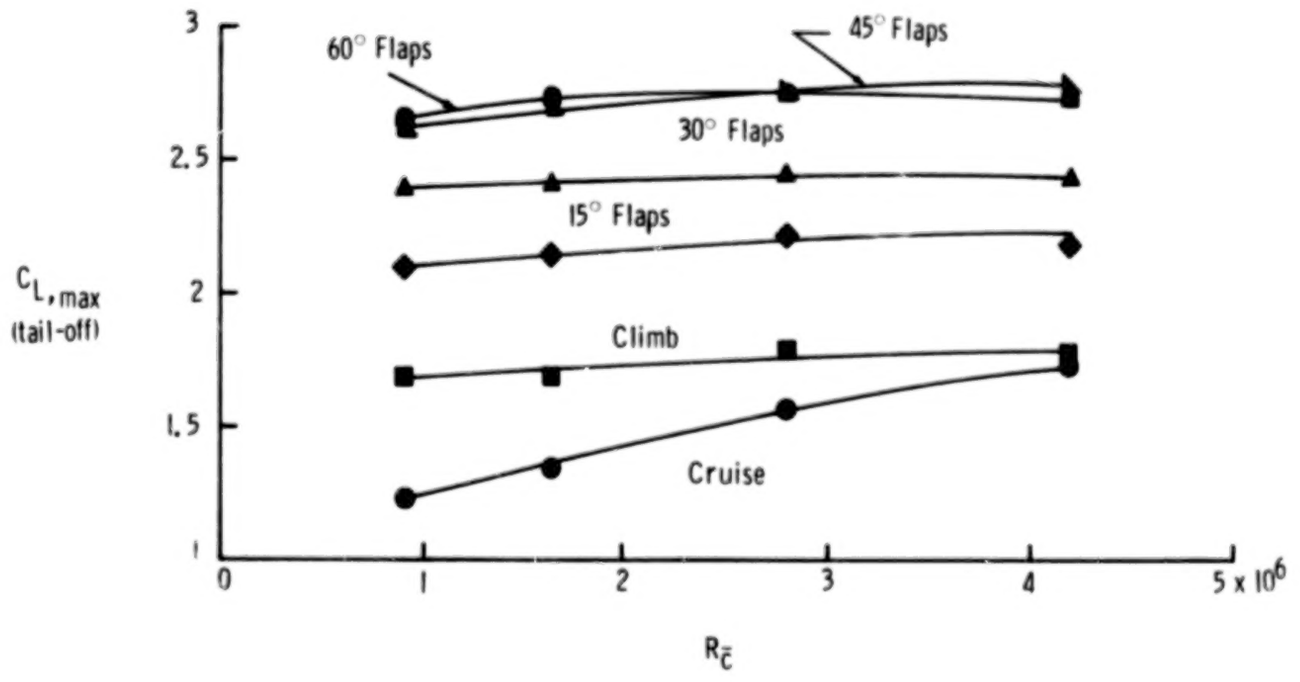

Figure 11

COMPARISON OF 7.5-FOOT-SPAN EET HIGH-LIFT MODEL PERFORMANCE FROM TESTS IN LANGLEY 4- BY 7-METER TUNNEL AND AMES 12-FOOT PRESSURE TUNNEL

Comparisons between the data obtained from tests of the 7.5-foot span model in the Langley 4- by 7-Meter Tunnel and the Ames 12-Foot Pressure Tunnel at atmospheric conditions are presented in figures 12 and 13. The data obtained with the model mounted on the Ames and LaRC telescoping struts are presented from the Langley 4- by 7-meter tests. As shown in figure 12, the data for the cruise-wing configurations are in excellent agreement from the tests in the two different facilities. The data presented in figure 13 for the 45^{o} landing flaps configurations show good agreement at angles of attack below 12^{o}; however, data from the Langley 4- by 7-Meter Tunnel show a considerable loss in lift coefficient at angles of attack greater than 12^{o}. As previously discussed, this difference appears to be due to an unexplained separation of the flow on the inboard part of the wing during the LaRC tests. Because the LaRC data with the model mounted on the Ames and LaRC struts and the LaRC sting support (fig. 8) show the very same premature stall characteristic, the difference between the Ames and LaRC data is probably not due to the model support system. The other major difference that exists between the two facilities, other than size, is the turbulence levels of the tunnel flows. The Ames facility is well noted for its very low free-stream turbulence and, in contrast, the LaRC facility has a moderate turbulence level. This difference in turbulence levels may be adversely affecting the development of the turbulence boundary layers on the inboard portion of the wing, thereby, causing premature separation and wing stall.

$(R_{\bar{c}} = 1.3 \times 10^{6})$

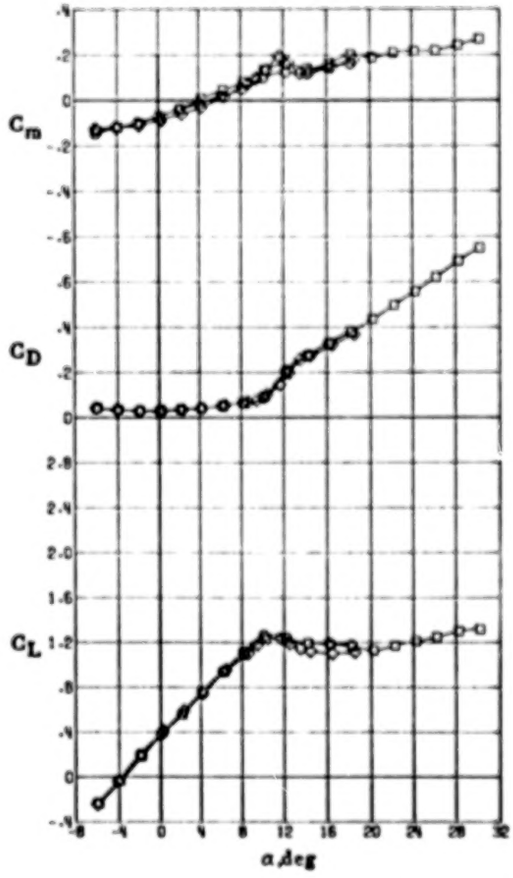

	Tunnel	Strut
○	4 x 7	Ames
□	4 x 7	LaRC
◇	Ames	Ames

Figure 12

COMPARISON OF 7.5-FOOT-SPAN EET HIGH-LIFT MODEL PERFORMANCE FROM TESTS IN LANGLEY 4- BY 7-METER TUNNEL AND AMES 12-FOOT PRESSURE TUNNEL

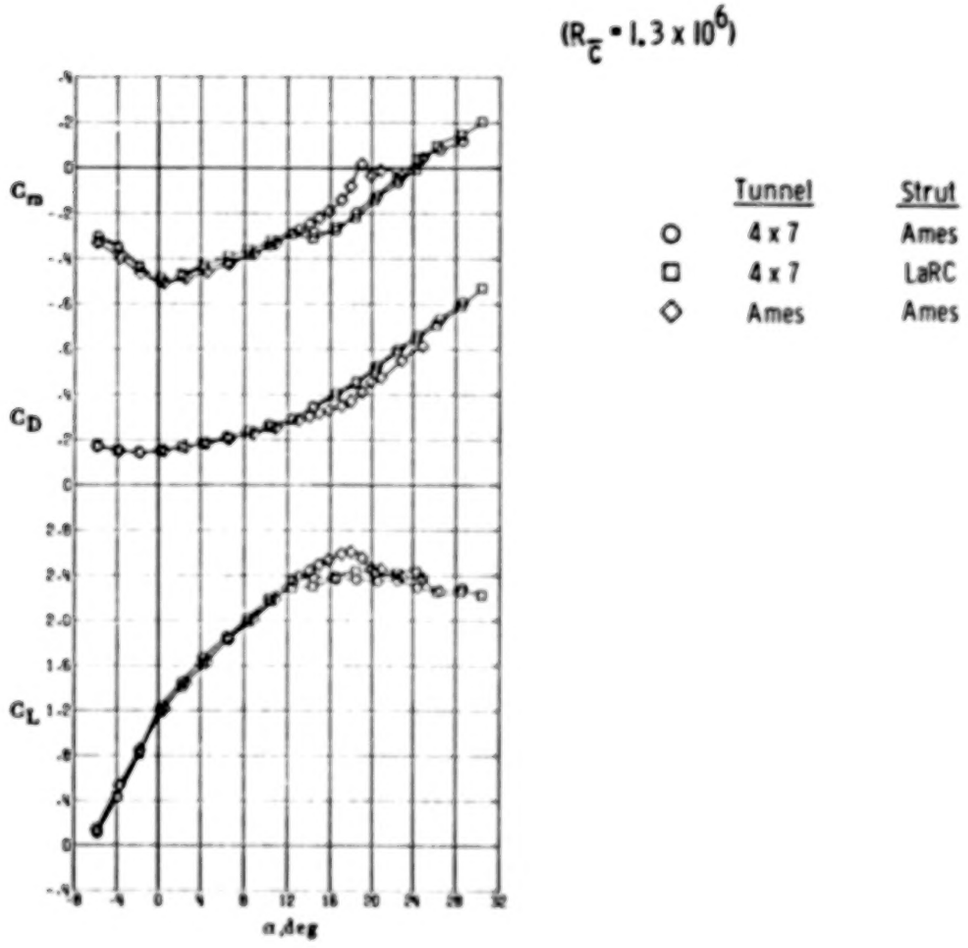

Figure 13

PERFORMANCE OF DOUGLAS ACA, DC-10, AND LANGLEY EET HIGH-LIFT MODELS

The performance of the Douglas Advanced Commercial Aircraft, DC-10 and Langley EET high-lift models are presented in figure 14 in the form of $C_{L,max}$ versus effective flap deflection. The effective flap deflection is defined as the vane deflection plus one half of the aft-flap deflection. Results from the Ames 12-Foot Pressure Tunnel show that the Langley EET has better $C_{L,max}$ performance than the DC-10 and that the Douglas ACA has a substantial $C_{L,max}$ increment over the EET. The primary reason for this $C_{L,max}$ difference is that the ACA had an optimized wing while the EET had a standard gap and overlap. Other possible reasons for the difference are that the ACA has a deflector flaperon and that the ACA has an inboard leading-edge extension.

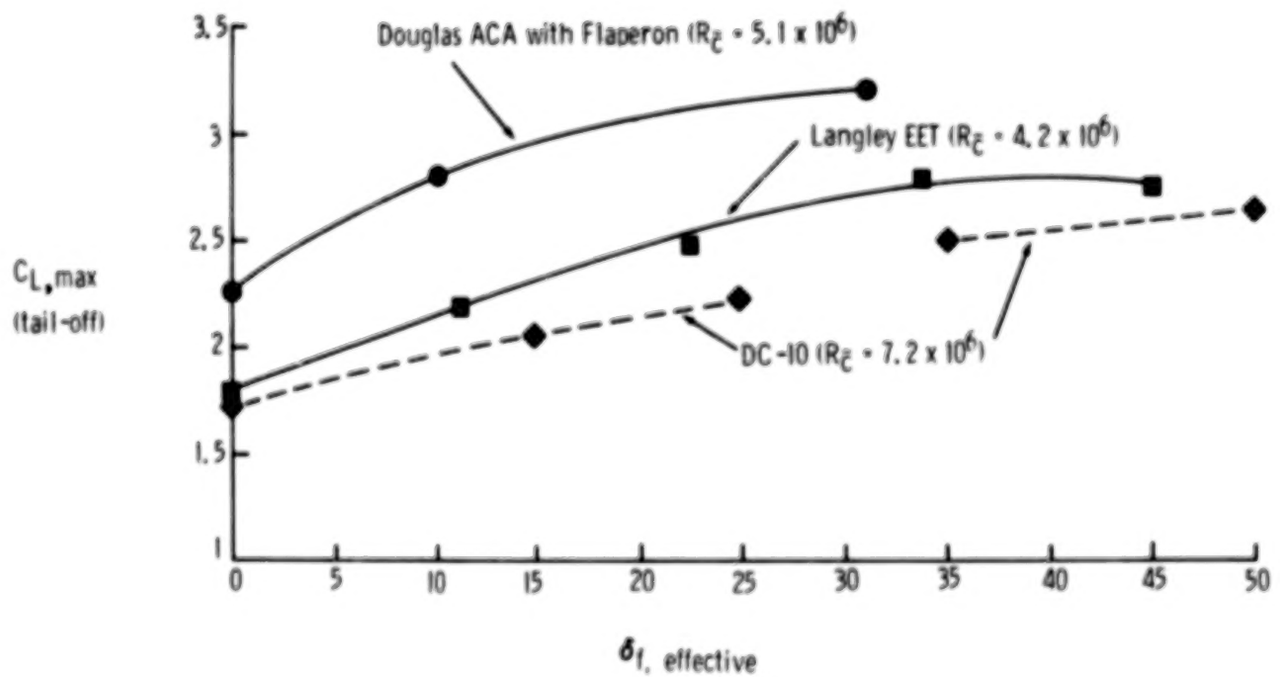

Figure 14

PLANFORM OF DOUGLAS ACA AND LANGLEY EET HIGH-LIFT MODELS

Planforms of the ACA and EET are presented in figure 15. $C_{L,max}$ data presented for the ACA and DC-10 were taken from reference 8.

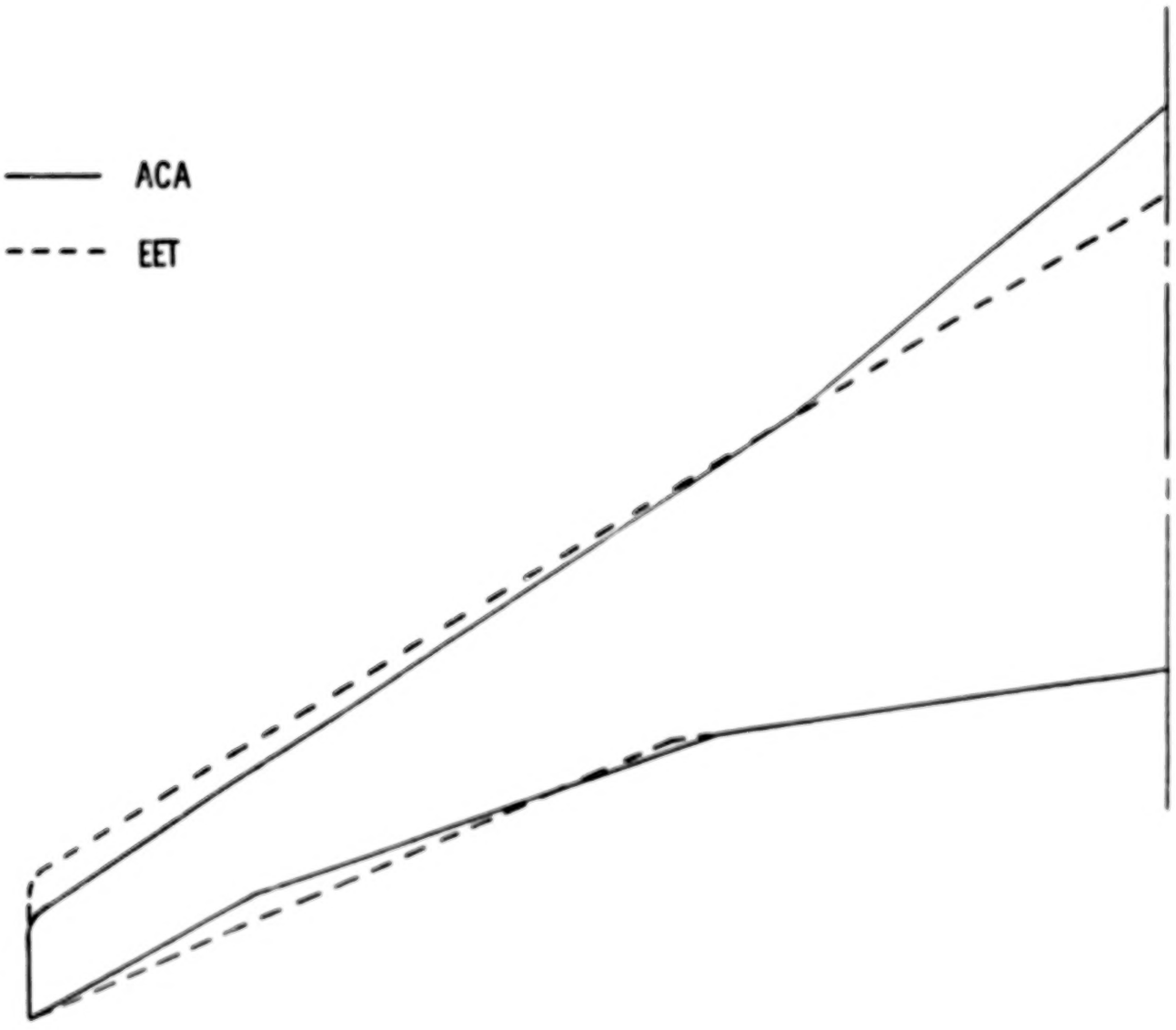

Figure 15

LTPT MODEL SUPPORT AND BALANCE SYSTEM

As part of the follow-on, EET high-lift research effort, two-dimensional high-lift airfoil tests are being proposed to complement the three-dimensional configuration tests. These 2-D tests will be conducted in the Langley Low-Turbulence Pressure Tunnel (LTPT) which is currently nearing completion of major modifications to provide a capability to test high-lift airfoils. A sketch of one of the major modifications to the facility, a new model support and high-lift balance system, is presented in figure 16. Other major modifications include the installation of new screens and an internal heat-exchange radiator to improve the tunnel flow quality and the installation of a new computer system and downstream wake survey device to improve the data acquisition process. The LTPT facility is a unique 2-D facility which is capable of obtaining a Reynolds number as high as 18×10^6 per foot at a total pressure of 10 atmospheres and a free-stream Mach number of 0.22. The tunnel has a 0.91- by 2.29-meter (3- by 7.5-foot) test section and a maximum free-stream Mach number capability of approximately 0.4. The new model support system consists of mounting the model between two sidewall inner drums which are held in place by an outer drum and yoke arm support system. This yoke support system is mounted on a very large 3-component strain gage balance which is, in turn, connected to the tunnel through a balance platform. This new balance has load ranges of 80 kN (18 000 lb) normal force, 2.45 kN (550 lb) axial force, and 16.27 kJ (12 000 ft-lb) pitching moment. Boundary-layer separation on each sidewall can be controlled by the placement of up to six tangential blowing boxes at positions perpendicular to the airfoil upper or lower surfaces. The attitude of the model is controlled by a motor-driven, externally mounted pitch mechanism which rotates the bearing-mounted inner drums. A multipath labyrinth seal is used to prevent the flow of air from the test section into the outer plenum.

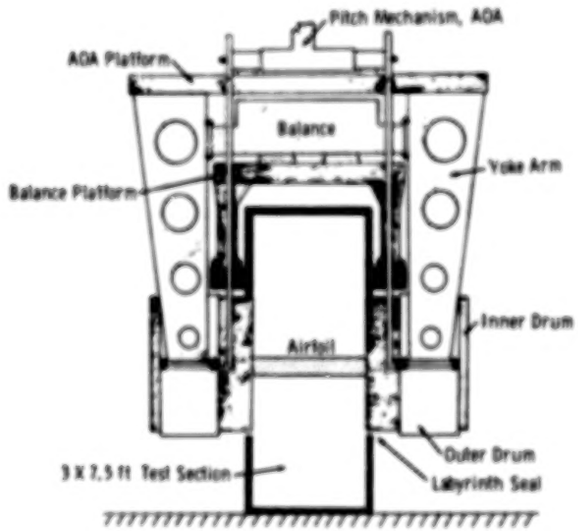

Figure 16

EET 2-D HIGH-LIFT AIRFOIL CONFIGURATIONS FOR LTPT

The EET 2-D high-lift airfoil configurations being proposed for tests in the LTPT are illustrated in figure 17. The basic cruise section is a supercritical airfoil with 12 percent thickness-chord ratio and coordinates identical to those of the airfoil at the trailing-edge-break station of the 12-foot span EET high-lift model. The 2-D model, like the corresponding 3-D model, will be fabricated with removable leading- and trailing-edge segments. The model will be equipped with a leading-edge slat and trailing-edge double-slotted flap system with coordinates identical to those on the 3-D model. Various slat and flap deflections, gaps, and overlaps will be investigated over a wide range of Reynolds numbers. In addition to balance forces and moments, detailed chordwise and spanwise airfoil static and downstream wake pressures will be obtained. Future tests are also being planned to investigate the benefits of using both leading- and trailing-edge tangential blowing slots (boundary-layer control (BLC)) to control the boundary-layer separation; thereby, improving the maximum lift and lift-drag ratio of the basic high-lift section. Tests are also planned to examine the feasibility of replacing the leading-edge slat with a leading-edge BLC system for a possible application to the natural laminar flow (NLF) wings.

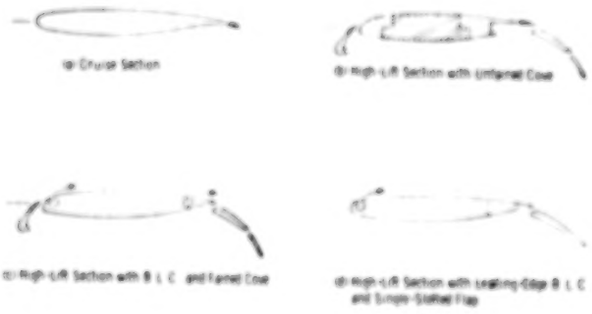

Figure 17

FOLLOW-ON EET HIGH-LIFT STUDIES

Research efforts with the EET high-lift models are continuing with various wing and tail configurations, as illustrated in figures 18 and 19. On the 12-foot span EET high-lift model a boundary-layer control (BLC) system is currently being fabricated. This BLC system will employ a modest amount of blowing to augment the flow over the various wing elements. The BLC system has been designed with a full-span leading-edge blowing slot and an inboard trailing-edge blowing slot. The leading-edge slot is located at 3 percent and two positions for inboard aft blowing are located at 55 percent and 65 percent of the local chords.

On the 7.5-foot span EET high lift model, an inboard variable-camber Krueger (VCK) device is being fabricated. A Krueger configuration is beneficial because of a weight savings and an improved $C_{L,max}$ over a conventional slat configuration.

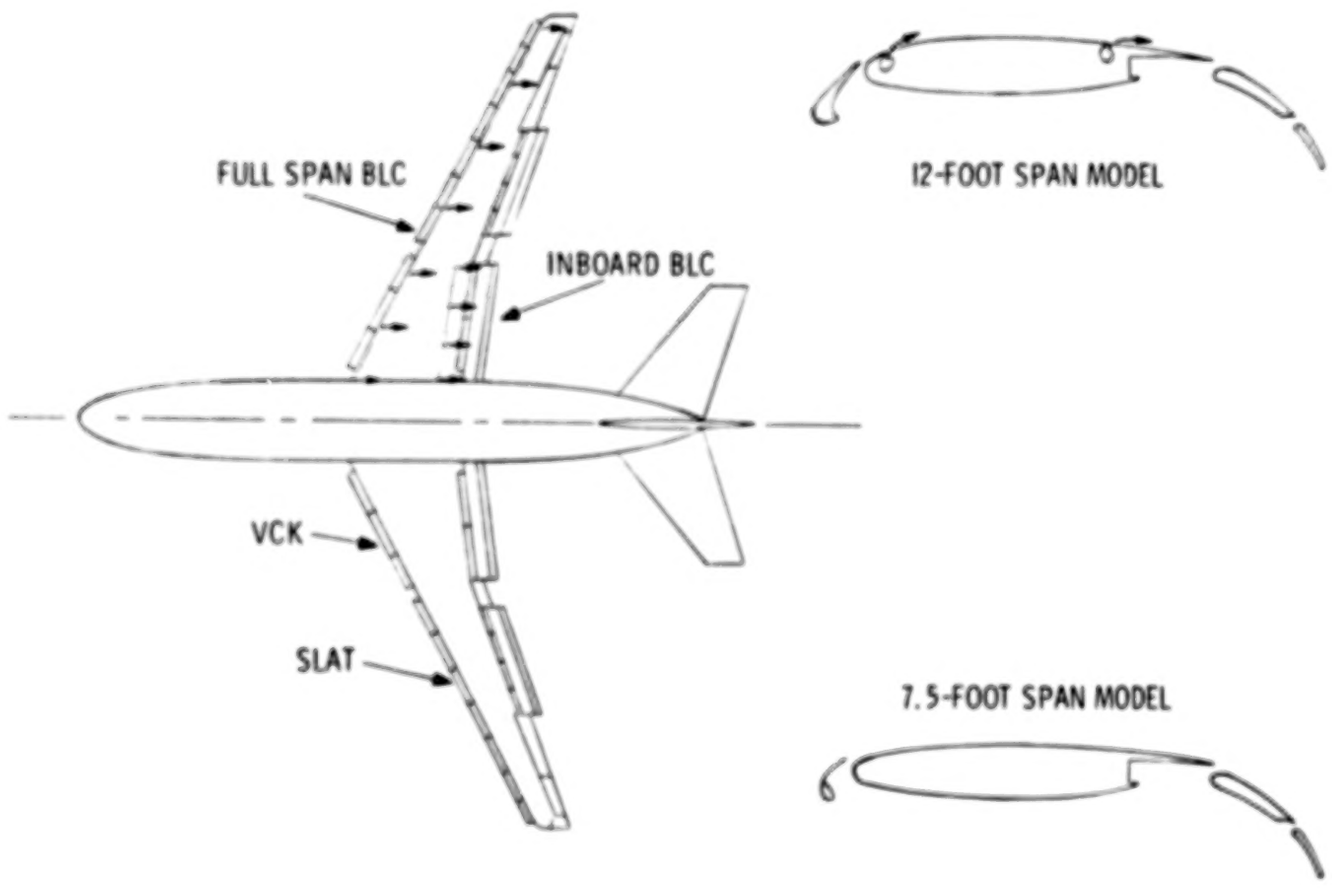

Figure 18

FOLLOW-ON EET HIGH-LIFT STUDIES

Another area of interest with the EET high-lift model is the empennage configuration. The conventional low-tail configuration with two additional empennage configurations are presented in figure 19. The T-tail configuration is being examined to complement earlier high-speed tests conducted in the Langley 8-Foot Transonic Pressure Tunnel. Results from those tests showed a reduced pitch-up characteristic with the T-tail configuration. A T-tail configuration has been fabricated for the 12-foot span EET model and will be tested in the near future in the Langley 4- by 7-Meter Tunnel. Another configuration of interest is the canard with small tail. The small horizontal tail is favorable due to drag savings at cruise; however, the small tail cannot produce the nose-up pitching moment needed for rotation. To achieve the necessary pitching moment a forward-mounted canard has been added to augment the small horizontal tail.

LOW-TAIL

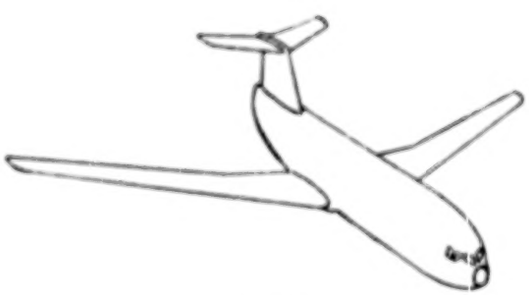

T-TAIL

SMALL TAIL AND CANARD

Figure 19

HIGH-TECHNOLOGY SMALL TRANSPORT

With the increased interest in fuel savings, a high-technology small transport aircraft is being examined. This aircraft, as shown in figure 20, will carry 60 to 90 passengers at Mach numbers of 0.7 for 500 nautical miles. At this point, a twin, aft-mounted turboprop configuration is a favorable candidate. To determine both powered and unpowered aerodynamic characteristics of a high-technology small transport aircraft, the following modifications will be made to the 12-foot-span EET high-lift model: (1) unsweeping the wing to 7.5^{0} at the quarter chord; (2) adding wing tips to increase the aspect ratio to 13; (3) adding pylons and nacelles to the aft fuselage; (4) adding fore and aft plugs to lengthen the fuselage; and (5) replacing the trailing-edge, double-slotted flap system with a full-span, single-slotted flap system. The model empennage will have six basic configurations as follows: (1) pusher low tail; (2) tractor low tail; (3) pusher T-tail; (4) tractor T-tail; (5) pusher V-Tail; and (6) tractor V-tail. The model will also be equipped with five-component strain-gage engine balances and two types of propeller drive systems - a 30-HP electric powered system and a 50-HP air drive system. The tests will be conducted with the model both in and out of ground proximity.

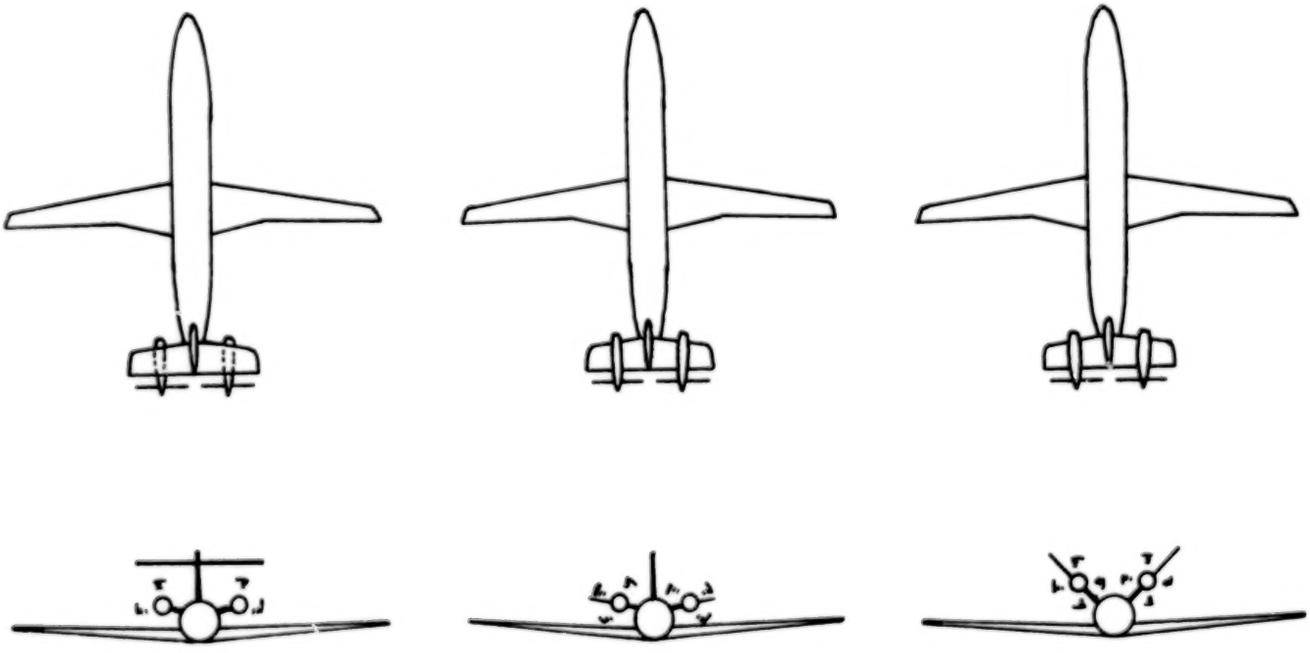

Figure 20

REFERENCES

1. Bartlett, Dennis W.: Wind-Tunnel Investigation of Several High-Aspect-Ratio Supercritical Wing Configurations on a Wide-Body-Type Fuselage. NASA TM X-71996, 1977.

2. Bartlett, Dennis W.; and Patterson, James C., Jr.: NASA Supercritical-Wing Technology. NASA TM-78731, 1978.

3. Morgan, Harry L., Jr.; and Paulson, John W., Jr.: Low-Speed Aerodynamic Performance of a High-Aspect-Ratio Supercritical-Wing Transport Model Equipped With Full-Span Slat and Part-Span Double-Slotted Flaps. NASA TP-1580, 1979.

4. Morgan, Harry L., Jr.: Low-Speed Aerodynamic Performance of an Aspect-Ratio-10 Supercritical-Wing Transport Model Equipped With a Full-Span Slat and Part-Span and Full-Span Double-Slotted Flaps. NASA TP-1805, 1981.

5. Morgan, Harry, L., Jr.: Model Geometry Description and Pressure Distribution Data From Tests of EET High-Lift Research Model Equipped With Full-Span Slat and Part-Span Flaps. NASA TM-80048, 1979.

6. Morgan, Harry L., Jr.: Supplemental Pressure Distribution Data From Tests of EET High-Lift Research Model Equipped With Full-Span Slat and Part-Span Flaps. NASA TM-80049, 1979.

7. Howard, Jenny M.; and Morgan, Harry L., Jr.: Pressure Distribution Data From Tests of Aspect-Ratio-10 EET High-Lift Research Model Equipped With Part- and Full-Span Flaps. NASA TM-80082, 1979.

8. Oliver, Wayne R.: Results of Design Studies and Wind Tunnel Tests of an Advanced High Lift System for an Energy-Efficient Transport. NASA CR-159389, 1980.

EET THEORETICAL DESIGN TECHNIQUES

Douglas L. Dwoyer
NASA Langley Research Center

EXPANDED ABSTRACT

As a part of the EET aerodynamics program, the Theoretical Aerodynamics Branch of the NASA Langley Research Center developed and monitored an out-of-house program to provide theoretical procedures useful in the design of transport aircraft. The focus of the effort was to provide tools valid in the nonlinear transonic speed range. The effort was divided into two basic areas, inviscid configuration analysis and design procedures and viscous correction procedures.

The major component of the inviscid portion of the work was the development, over the last 6 years, of the well-known Boppe embedded-grid transonic small-disturbance codes. Early versions of the code are discussed in references 1-3. The culmination of this effort is the Wing-Body-Pod-Pylon Winglet code (WBPPW) (ref. 4) which is capable of analyzing the flow past fairly complete transport configurations. During the next fiscal year, work on the WBPPW code is expected to be completed with the addition of the capability to analyze swept, canted, cambered pylons. In addition to direct support for the development of the WBPPW code, an effort was supported to extensively validate this code and its predecessor, the Transonic Wing-Body Code (WIBCO). The WIBCO validation is now complete and has been published in reference 3. The validation of the WBPPW code is now under way. In the course of this paper, the status of the WBPPW code will be summarized.

Another active area of work in the inviscid area has been in the development of wing-design codes; i.e., inverse solvers in which surface pressure is input and wing shape is output. Two efforts are currently underway in this area, one at New York University (NYU) under the direction of Dr. Paul Garabedian and the other at Rockwell Science Center under the direction of Dr. Vijaya Shankar. Results from the NYU effort will be summarized in this paper. During the next fiscal year, the NYU code will be modified to include a pylon/nacelle combination on the wing. The Rockwell effort is not sufficiently advanced to warrent discussion.

In the viscous correction area, the largest effort has been in the development of a method for predicting the turbulent viscous flow in wing/fuselage junctions. This project is nearing completion, with validation of the theory against experimental data now under way. This project will be summarized in a forthcoming NASA contractor report.

The second major result to be reported in this area is the development of a transonic viscous/inviscid interaction procedure for wing-body combinations (ref. 5). This program, which includes wing-wake viscous effects, has proven very accurate in predicting wing loading without recourse to lift matching.

The final effort in the viscous flow area is just now beginning. In this effort, a group at Grumman under the direction of Dr. Robert Melnik will attempt to develop a model for the strong viscous/inviscid interaction at wing trailing edges. This effort is expected to last 3 years.

TRANSONIC WING-BODY CODE (WIBCO)

The Transonic Wing-Body Code (WIBCO) was developed by Mr. Charles Boppe of the Grumman Aerospace Corporation for the analysis of complex wing-body configurations at transonic speeds (ref. 2). The code solves the transonic small-disturbance equation using a finite-difference procedure in combination with the embedded-grid concept (ref. 1). This concept, developed at NASA Langley during Mr. Boppe's stay as an Industry/Research Associate, combined with the simplicity of the small-disturbance boundary condition allows for a great deal of geometric complexity with a minimum number of field grid points and coordinate-system complexity.

The program was extensively validated against the EET data base by Mr. Ed Waggoner of Vought Corporation (ref. 3). In addition to the validation, Mr. Waggoner is currently upgrading the wing boundary-layer procedure to include a 3-dimensional (3-D) integral method in regions of attached flow and a 2-dimensional (2-D) strip integral method in regions of separated flow.

The WIBCO program is currently available through COSMIC with a FEDD restriction (ref. 6).

- DEVELOPED EMBEDDED GRID WING ANALYSIS CODE (WIGET) AS NASA/INDUSTRY RESEARCH ASSOCIATE AT LANGLEY, 1975/1976 (AIAA PAPER 77-207)
- EXTENDED TO WING-BODY CASE (WIBCO) UNDER NASA CONTRACT, 1977 (AIAA PAPER 78-104)
- WIBCO TO COSMIC, 1979 (FEDD RESTRICTION)
- CODE DOCUMENTATION PUBLISHED, NASA CR-3243, 1980
- WAGGONER/VOUGHT VALIDATION AND EXTENSION
  - o VALIDATION ON NASA-EET DESIGN MODS., 1979 (AIAA PAPER 80-124)
  - o ADDITION OF STREETT/DORNIER 3-D BOUNDARY-LAYER METHOD, 1981
  - o ADDITION OF 2-D STRIP SEPARATION MODEL, 1981

Figure 1

TRANSONIC WING-BODY-POD-PYLON-WINGLET CODE (WBPPW)

The Wing-Body-Pod-Pylon-Winglet code (WBPPW)(ref. 4) is an extension of WIBCO to the more complete configuration as given by its title. This extension was due to Mr. Charles Boppe of Grumman Aerospace Corporation. Again, Mr. Ed Waggoner of Vought Corporation is validating the code against the EET data base and enhancing the existing boundary-layer capability.

Preliminary versions of the code and its documentation have been provided to several users for comment. The delivered code (developed on an IBM 370) has now been debugged for use on CDC computers, and this version of the code will be sent to COSMIC during the fall of 1981 with final user documentation available in early 1982.

In addition to the WBPPW version of the code, other versions have been developed to treat the Space Shuttle launch configuration and canard/swept-forward-wing fighters.

- PRELIMINARY CODE DOCUMENTATION PREPARED, 1980
- VOUGHT VALIDATION ON NASA-EET DESIGN MODS. STARTED, 1980
- PRELIMINARY CODE PROVIDED TO SEVERAL USERS FOR FEEDBACK, 1980
- CODE TO COSMIC, 1981 (FEDD RESTRICTION)
- VOUGHT MODS. FOR 3-D B.L., 2-D STRIP SEPARATION, 1981
- OTHER CONFIGURATION APPLICATIONS
  - o Space Shuttle Orbiter/Tank/Booster Combination (NASA sponsored)
  - o Fuji Fighter Studies (In-House)
  - o Canard, Swept Forward Fighter Studies (Air Force Sponsored)

Figure 2

PREDICTION OF C-141 WING PRESSURE WITH WBPPW

Figure 3 shows a comparison of the prediction of the WBPPW code and experimental data for the wing surface pressure at the $\eta = 0.19$ span station of a C-141. Of particular interest in this case is the influence of the landing-gear fairing on the lower-surface pressure distribution at this station. This effect is illustrated by comparing the wing-alone calculation with the wing-body calculation.

$M = 0.82 \quad \alpha = -0.3^{0} \quad R = 36 \times 10^{6} \quad \eta = 0.19$

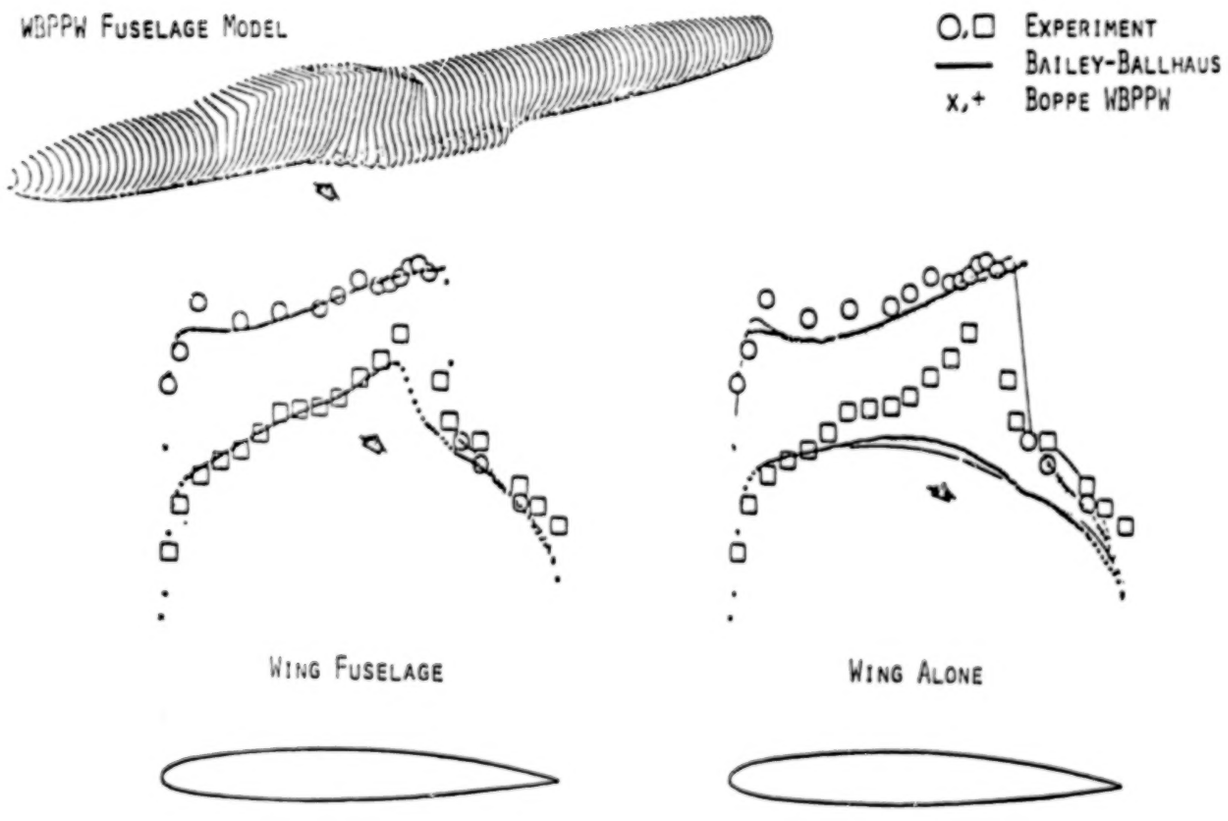

Figure 3

PREDICTION OF WING AND WINGLET PRESSURE ON MODIFIED KC-135 USING WBPPW

Figure 4 snows a comparison of the prediction of the WBPPW code and experimental data for a KC-135 with winglets. Both the wing surface pressure and winglet surface pressure are compared at three span stations. Agreement is seen to be good on the wing including the near-tip station of $\eta_w = 0.93$ and the winglet including the near-root section of $\eta_{w/t} = 0.16$. Since the WBPPW code calculates the boundary layer only on the wing, the good winglet agreement was obtained without viscous correction.

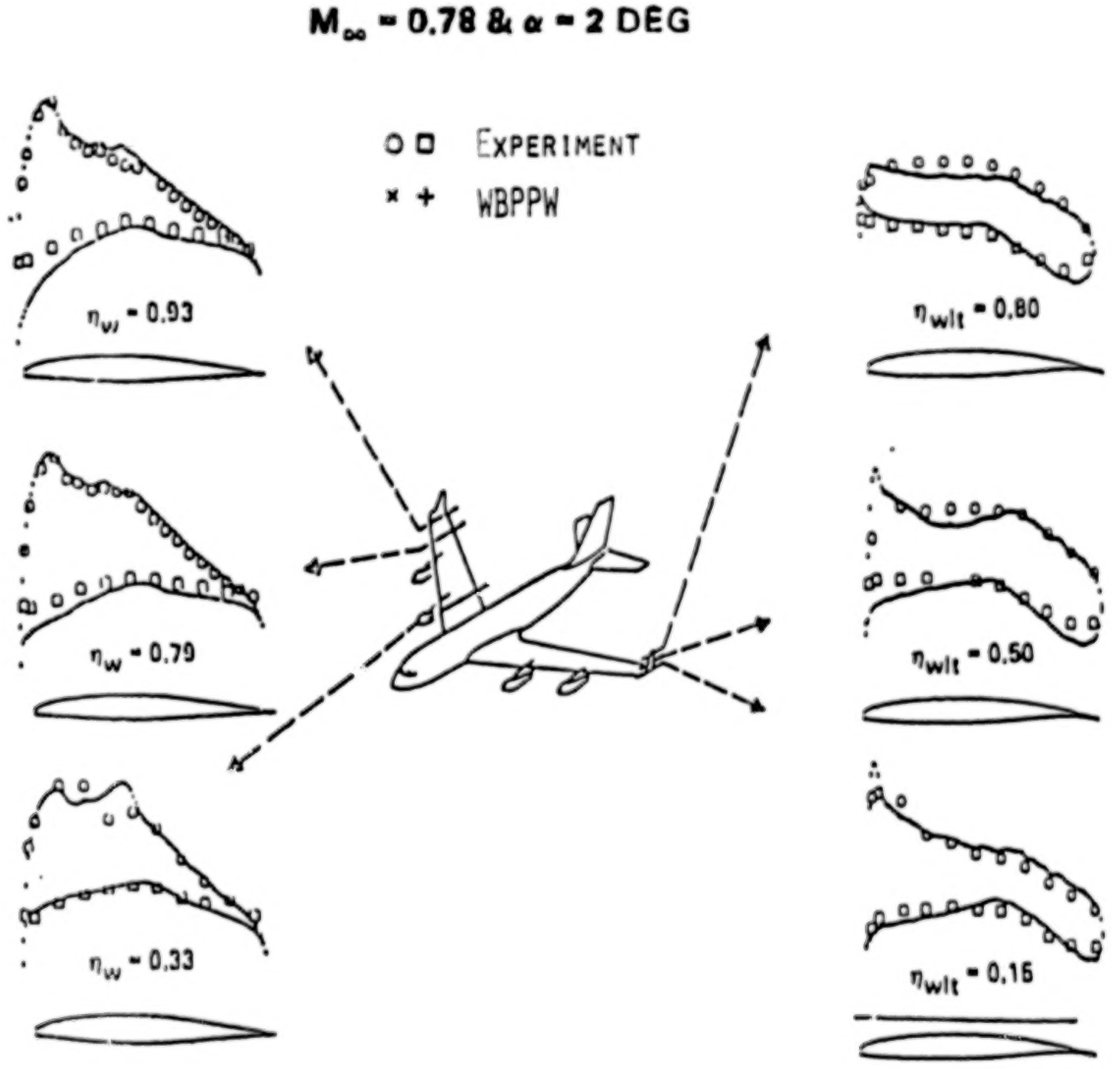

Figure 4

SPACE SHUTTLE LAUNCH CONFIGURATION

An interesting test of the range of validity of transonic small-disturbance theory to relatively nonslender configurations is the predictions of a special version of the WBPPW code of the Space Shuttle launch-configuration surface pressure. The analysis model of the launch configuration treated by the code is shown in figure 5. For the prediction of pressure on the external tank, a fine grid was used on the tank and coarse grids on the orbiter and solid rocket boosters. For prediction of orbiter pressures, the coarse grids were on the tank and boosters while the orbiter itself was treated with a fine grid.

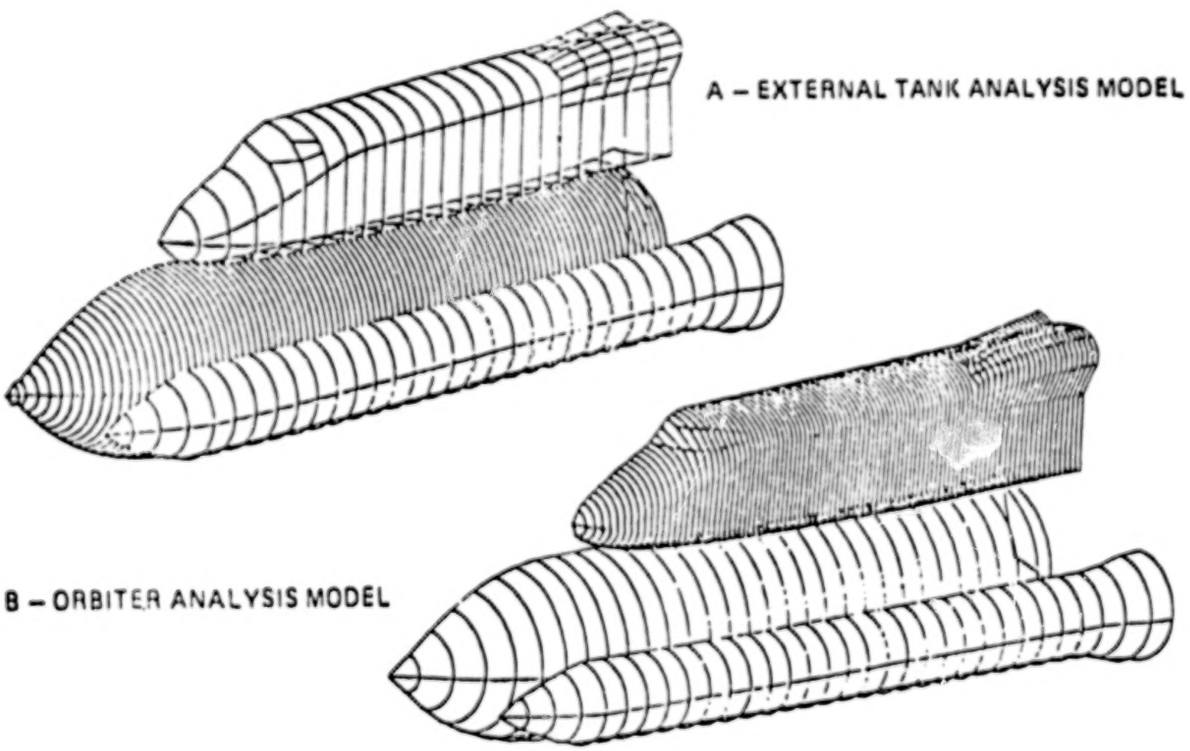

Figure 5

PREDICTION OF SPACE SHUTTLE ORBITER PRESSURE DISTRIBUTION FOR SPACE SHUTTLE LAUNCH CONFIGURATION USING MODIFIED WBPPW CODE

A comparison of measured and WBPPW-predicted orbiter surface pressures is shown in figure 6 for free-stream Mach numbers of 0.9 and 1.1. Note the generally good agreement around the fuselage, including the narrow slot between the orbiter and tank. Deviations on the lower fuselage surface near the rear of the external tank are attributed to the absence of modeling the struts which attach the tank to the orbiter. Calculations such as these were used in the evaluation of aerodynamic loads on individual tiles of the orbiter's thermal protection system.

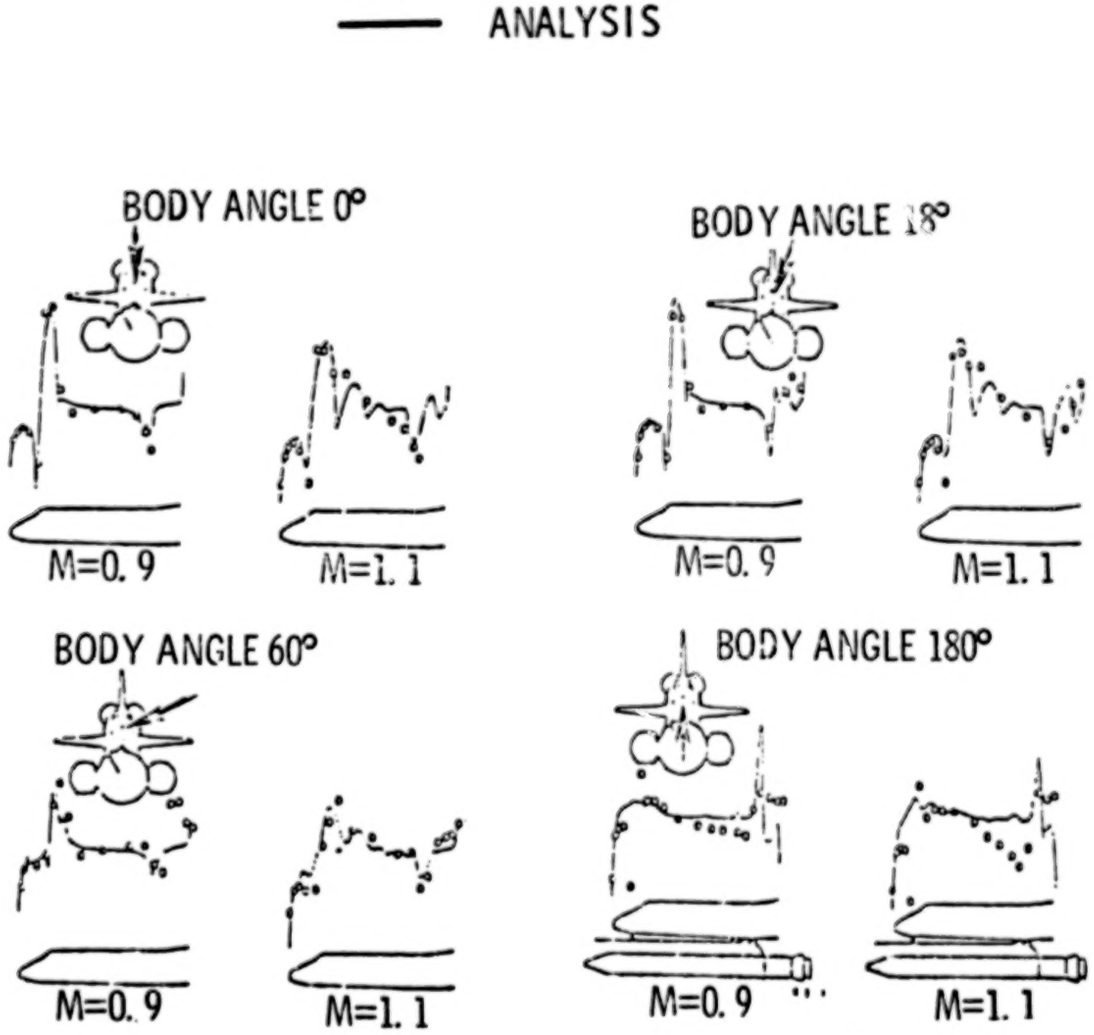

Figure 6

REDESIGN OF TRANSONIC WING USING NYU TRANSONIC-WING DESIGN PROCEDURE

Under a continuing grant with New York University, a research group led by Dr. Paul Garabedian is developing a design-mode transonic full-potential wing code. In this mode, the user can specify a portion of the wing surface-pressure distribution and have the wing shape returned. The procedure is based on the FLO-22 non-conservative code and features automatic trailing-edge closure and a constraining box inside the wing which the outer-wing surface is not allowed to cross.

Figure 7 compares the predicted surface pressures and shocks on an original wing and the same wing with the shock supressed through the design calculation. In the figure, the "blobs" appearing over the inner portion of the wing are computer graphic shock diagrams. The rear boundary of the "blob" represents the shock location while the thickness of the "blob" represents the shock strength. As can be seen, the redesigned wing has a greatly reduced shock strength which is reflected in the reduction in wave drag.

It is planned to enhance this code by including pylon/nacelle combinations in the analysis during the next year.

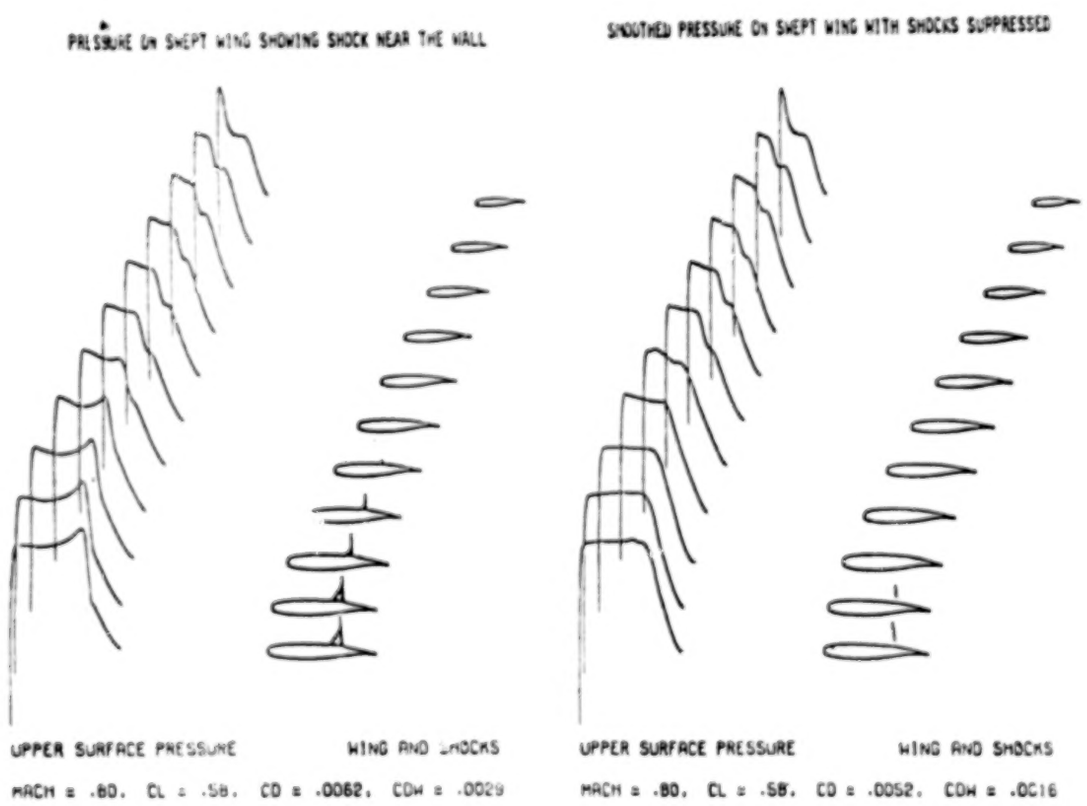

Figure 7

VISCOUS/INVISCID INTERACTION FOR TRANSONIC FLOW PAST WING-BODY CONFIGURATIONS

Under partial funding from the EET project, Mr. Craig L. Streett of the NASA Langley Research Center has developed a viscous/inviscid interaction procedure for transonic flow past wing-body combinations (ref. 5). Modern supercritical wing sections have substantial spanwise flow in the lower-surface cove region, requiring a three-dimensional boundary-layer calculation. In addition, for the case of transonic airfoils, it has been found that inclusion of wake-curvature and thickness effects are crucial for proper prediction of shock location and lift (ref. 7). The procedure developed by Streett uses a 3-D boundary-layer method and includes a viscous wake model in order to account for all of the weak interaction effects on the wing.

- MODERN TRANSONIC POTENTIAL FLOW CODES CAPABLE OF CALCULATING FLOW PAST WING-BODY COMBINATIONS
  - o α , M_∞ ADJUSTMENTS REQUIRED TO OBTAIN AGREEMENT WITH EXPERIMENT
- IMPROVED AGREEMENT WITH EXPERIMENT SHOWN BY INTERACTING 3-D POTENTIAL CODES WITH 2-D STRIP BOUNDARY LAYER
  - o SUBSTANTIAL SPANWISE FLOW EXISTS IN COVE REGION OF SUPERCRITICAL WINGS REQUIRING 3-D BOUNDARY-LAYER METHOD
- INCLUSION OF EFFECTS OF WAKE CURVATURE AND THICKNESS FOUND IMPORTANT IN TRANSONIC 2-D AIRFOIL CASE
- SEVERAL 3-D POTENTIAL FLOW/3-D WING BOUNDARY-LAYER INTERACTION METHODS INTRODUCED IN PAST 3 YEARS - SUMMARIZED ON NEXT SLIDE

Figure 8

COMPARISON OF AVAILABLE TRANSONIC WING-BODY VISCOUS-INVISCID INTERACTION METHODS

Figure 9 summarizes three published transonic wing and wing-body viscous interaction methods. Note that two of the procedures use integral boundary-layer methods and one is based on a finite-difference procedure. The Streett procedure makes use of a highly modified version of the Dornier wing boundary-layer code (which uses the P. D. Smith method for turbulent flow and a method developed by Stock for laminar flow).

All three procedures use different methods for calculating the outer potential flow, the Streett procedure being the most complete in that it uses the full-potential, conservative, wing-body code FLO-30. In both the Streett and McLean methods, the boundary-layer and potential flows are coupled using the displacement-thickness concept while Firmin uses the wall-blowing method. Finally, note that the Streett and Firmin procedures include wake effects and none of the procedures include any strong interaction effects.

METHOD			WEAK INTERACTION			STRONG INTERACTION	
			DISPLACEMENT EFFECT		WAKE CURVATURE	SHOCK	TRAILING EDGE
	INVISCID FLOW	B.L.	WING	WAKE			
McLEAN (BOEING)	FC (No Body)	FINITE DIFF.	δ^*	No	No	No	No
FIRMIN (RAE)	NCSD (Body)	P.D. SMITH (INTEGRAL)	V_w	$[\![V_w]\!]$	Yes	No	No
STREETT (NASA LaRC)	FC (Body)	P.D. SMITH (INTEGRAL)	δ^*	δ^*	Yes	No	No

Figure 9

PREDICTION OF WING LOADING ON MODERN TRANSPORT CONFIGURATION USING PROCEDURE OF REFERENCE 5

Figure 10 shows a comparison between the predicted and measured span load distribution on the NASA Langley EET transport configuration. The configuration features a moderately-swept, high-aspect-ratio, supercritical wing; low-mounted on a wide body. The predictions were made by the Streett viscous/inviscid interaction procedure run at the experimental Mach number, angle of attack, and Reynolds number. No lift matching was used to obtain these results. The comparison of the inviscid and interacted loads indicate strong viscous effects for the test conditions of $M_\infty = 0.78$ and $Re_\infty = 2.4 \times 10^6$. The predicted overall lift coefficient for the complete configuration was predicted to be 0.431 while a value of 0.432 was measured.

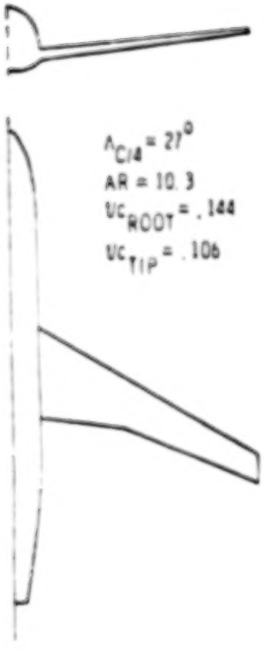

TEST CONFIGURATION

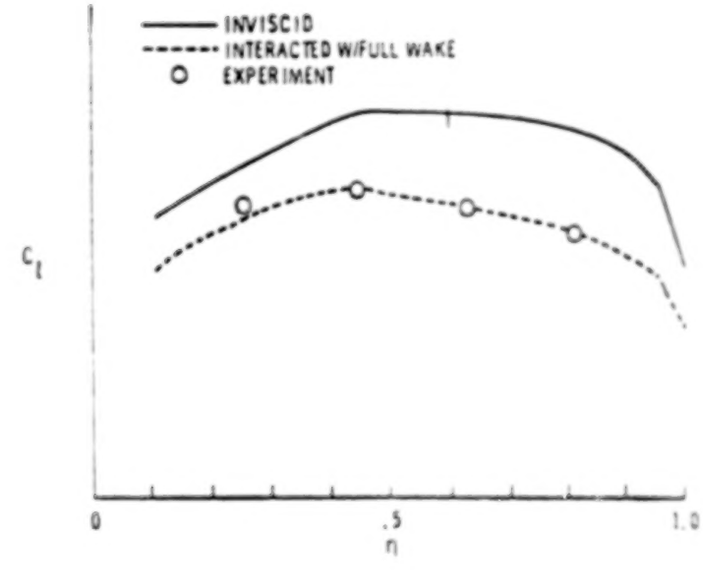

SPANWISE LIFT DISTRIBUTION

Figure 10

METHOD FOR PREDICTION OF TURBULENT WING/FUSELAGE JUNCTURE FLOWS

The viscous effects on several areas of a typical transport configuration are not amenable to analysis by conventional boundary-layer methods. One such region is the junction between the wing and the fuselage. COMCO, Inc., under the direction of A. J. Baker, is developing a method for predicting the juncture region flow. The method is designed to permit sufficient geometric flexibility to allow the study of junction geometry changes on such phenomena as vortex roll-up and will be reported in a forthcoming NASA Contractor Report.

The heart of the procedure is the COMOC program, a finite-element solution of the partially parabolized Navier-Stokes equation. The approximate governing equations are derived by splitting the pressure into three contributions, an inviscid contribution, a contribution due to the turbulent viscous flow on the wall, and a contribution arising from the conservation of mass. A complex second-order Reynolds stress model is used to close the system.

The inviscid pressure is calculated from a potential-flow code; the contribution from the turbulent viscous flow comes from a marching solution of the parabolized momentum equations and the continuity equation solution provides the mass-balance contribution.

The method is currently operational on the NASA Langley CYBER 175 computer and is being converted to the Langley CYBER 203. Calculations on the CYBER 203 will allow sufficient grid resolution to make direct comparison with experiment.

It is felt that, with little modification, the COMOC program can also be used to analyze wing-tip flows.

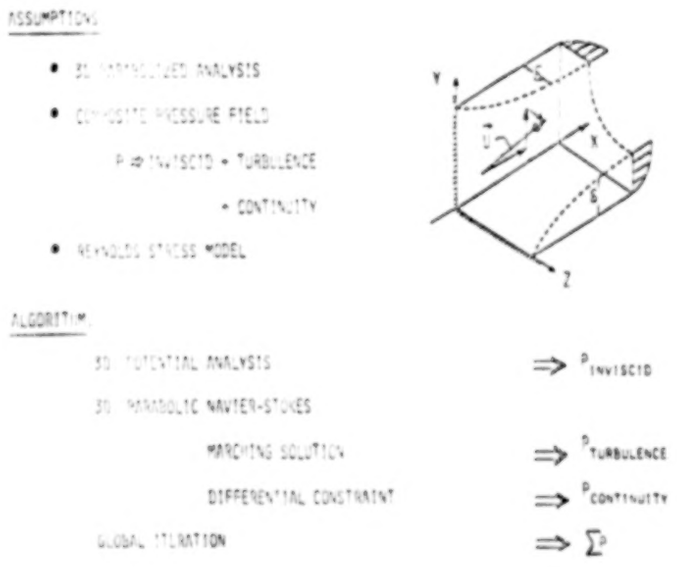

Figure 11

C - 2

PREDICTION OF TURBULENT DUCT FLOW USING COMOC CODE

Figure 12 contains a qualitative comparison of the prediction of the COMOC program and the measurements of Melling and Whitelaw (ref. 10) of the cross-flow velocity field in a turbulent square-duct flow. The COMOC predictions are made with a conventional first-order turbulence model and the full, Baker, second-order model. Note the excellent qualitative agreement between the second-order calculation and the measured flow and the dramatic change between the first- and second-order prediction. These results indicate the importance of a valid turbulence model if one is to accurately predict the effect of corner-vortex roll-up.

EXPERIMENT
(MELLING & WHITELAW, x/D = 37)

1ST-ORDER REYNOLDS STRESS
(x/D = 30)

2ND-ORDER REYNOLDS STRESS
(x/D = 30)

Figure 12

EXPERIMENTAL ARRANGEMENT FOR JUNCTURE FLOW MEASUREMENTS

Due to the dominant role the turbulence model plays in the prediction of corner-vortex roll-up, the need was felt for complete and accurate measurements of Reynolds stresses in a typical juncture flow. Under a grant, Professor Howard McMahon has made such measurements using the model illustrated in figure 13. The model consists of a blunt-nosed flat-plate "wing" mounted on a flat-plate "fuselage." Complete Reynolds stress measurements were made in two planes normal to the free-stream flow located approximately 15 cm and 46 cm from the leading edge. These data will be used in the validation of the COMOC-juncture-region computer program and will be published in a forthcoming NASA Contractor Report. The program will be terminated due to lack of money before the effects of fillets on the corner flow can be measured.

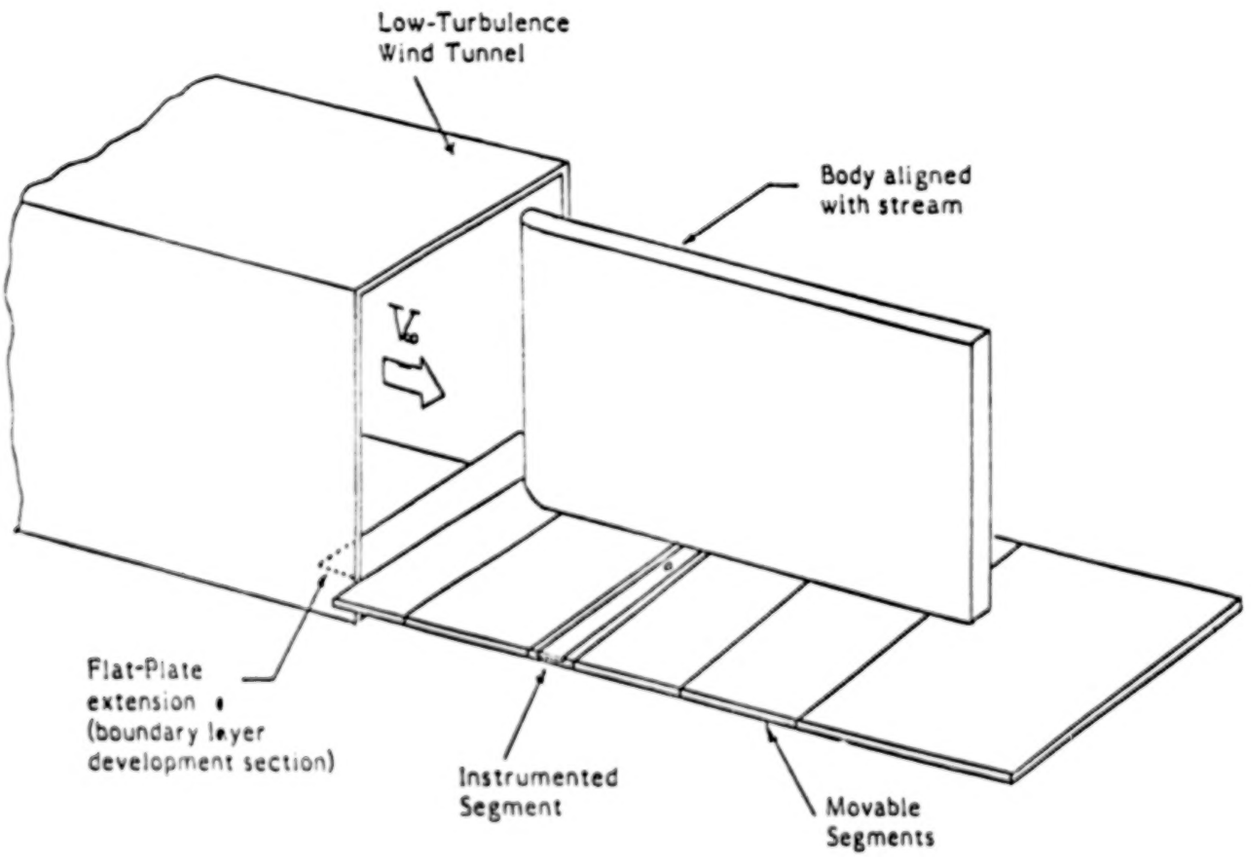

Figure 13

SUMMARY

The program reported in the present paper represents a fairly mature program with many of its major components nearing completion. Under the auspices of the program, the WBPPW program for analyzing fairly complete transport configurations has been developed and is about to be released. In addition, with the development of the CCMOC-juncture flow code, the 3-D boundary-layer interaction code, and with the future completion of the trailing-edge analysis, all the components will be available to develop a complete viscous/inviscid wing/body code for the transonic speed range.

REFERENCES

1. Boppe, C. W.: Calculation of Transonic Wing Flows by Grid Embedding. AIAA Paper 77-207, Jan. 1977.

2. Boppe, C. W.: Computational Transonic Flow About Realistic Aircraft Configurations. AIAA Paper 78-104, Jan. 1978.

3. Waggoner, E. G.: Computational Transonic Analysis for a Supercritical Transport Wing-Body Configuration. AIAA Paper 80-129, Jan. 1980.

4. Boppe, C. W.; and Stern, M. A.: Simulated Transonic Flow for Aircraft With Nacelles, Pylons, and Winglets. AIAA Paper 80-130, Jan. 1980.

5. Streett, C. L.: Viscous-Inviscid Interaction for Transonic Wing-Body Configurations Including Wake Effects. AIAA Paper 81-1266, June 1981.

6. Boppe, C. W.: Transonic Flow Field Analysis of Wing-Fuselage Configurations. NASA CR-3243, 1980.

7. Melnik, R. E.: Turbulent Interactions on Airfoils at Transonic Speeds - Recent Developments. Paper No. 10, AGARD CP-291, 1981.

8. McLean, J. D.; and Randall, J. L.: Computer Program to Calculate Three-Dimensional Boundary-Layer Flows Over Wings With Wall Mass Transfer. NASA CR-3123, 1979.

9. Firmin, M. C. P.: Calculations of Transonic Flow Over Wing/Body Combinations With an Allowance for Viscous Effects. Paper No. 8, AGARD CP-291, 1981.

10. Melling, A.; and Whitelaw, J. G.: Turbulent Flow in a Rectangular Duct. J. Fld. Mech., vol. 78, pt. 2, 1976, pp. 289-315.

~~END DATE~~

~~FEB. 11, 1982~~